UNIVERSITÄT
PADERBORN

Coherent Control Schemes for Semiconductor Quantum Systems

Der Naturwissenschaftlichen Fakultät
der Universität Paderborn
zur Erlangung des akademischen Grades
Doktor der Naturwissenschaften (Dr. rer. nat.)
vorgelegte

Dissertation

von

Eva Schöll

Paderborn, den 03.04.2024

"I would rather have questions that can't be answered
than answers that can't be questioned."
– Richard Feynman

Abstract

Advances in quantum technology applications, such as quantum computing, also require quantum networks. Single photons are the only flying qubits that carry information in such networks, making ideal single-photon sources inevitable. These sources must meet stringent criteria, including high single-photon purity, indistinguishability, brightness, and entanglement fidelity, while allowing tunability of certain properties and integrability into quantum photonic circuits. Semiconductor quantum dots (QDs) are good candidates, already fulfilling many requirements, but also quantum emitters in 2D materials show promising results, especially in terms of integrability. The measurements performed here were based on four different types of quantum emitters, namely GaAs, InGaAs, and InAsP nanowire QDs, and quantum emitters in a WSe_2 monolayer. The focus of this thesis is to gain a deeper understanding of quantum level schemes and the impact of different excitation methods on the emitted photons. Therefore, we have studied QDs under s-shell resonant excitation and two-photon excitation (TPE), revealing intrinsic limits for photon indistinguishability from a radiative cascade. A novel excitation technique based on TPE and stimulation of the first transition can overcome this limit. In addition, we have investigated growth, fabrication, and optically controlled methods to tune the wavelength, integrate quantum emitters into quantum photonic circuits, and increase the extraction efficiency.

Kurzfassung

Fortschritte in Quantentechnologien erfordern auch Quantennetzwerke. In diesen sind Photonen die einzigen fliegenden Qubits, was ideale Einzelphotonenquellen notwendig macht. Diese müssen hohe Anforderungen erfüllen, wie hohe Reinheit, Ununterscheidbarkeit, Helligkeit und Verschränkung, sowie die Manipulation bestimmter Eigenschaften und die Integration in photonische Schaltkreise ermöglichen. Halbleiter-Quantenpunkte (QPs) erfüllen viele der Anforderungen, aber auch Quantenemitter in 2D Materialien zeigen vielversprechende Ergebnisse, insbesondere hinsichtlich der Integrierbarkeit. Die hier durchgeführten Messungen basierten auf verschiedenen Emittern, nämlich GaAs, InGaAs, InAsP Nanodraht QPs und Emittern in WSe_2 Monolagen. Der Fokus dieser Arbeit lag auf einem grundlegenden Verständnis der Quanten-Energieniveau-Schemata und dem Einfluss verschiedener Anregungsmethoden auf die Eigenschaften der emittierten Photonen. Zu diesem Zweck haben wir QPs unter s-Schalen resonanter Anregung und Zwei-Photonen-Anregung (ZPA) untersucht und eine intrinsische Grenze für die Photonen Ununterscheidbarkeit aus einer Strahlungskaskade aufgezeigt. Mit einer neuen Anregungsmethode, die auf ZPA und Stimulation des ersten Übergangs basiert, kann diese Grenze überwunden werden. Außerdem haben wir Wachstums, Fabrikations und optisch kontrollierte Methoden untersucht, um die Wellenlänge abzustimmen, Quantenemitter in photonische Schaltkreise zu integrieren und die Extraktionseffizienz zu erhöhen.

Preface

This thesis deals with states of lights emitted by semiconductor quantum light sources with a focus on epitaxial GaAs and InGaAs quantum dots emitting in the near-infrared spectral range. Stringent requirements have to be met to make them usable in quantum technology applications such as long distance quantum networks. Different coherent excitation processes are investigated and analyzed in terms of single-photon purity and indistinguishability of the emitted photons. In addition, the integration of quantum dots into tunable and efficiency-enhancing structures and the integration of InAsP nanowire quantum dots and emitters in two-dimensional WSe_2 into quantum photonic integrated circuits have been demonstrated. Efforts have also been made to push the emission wavelength of InAsP nanowire quantum dots into the telecom spectral range to enable long-distance transmission in fibers.

Paper 1. S. Haffouz, K. D. Zeuner, D. Dalacu, P. J. Poole, J. Lapointe, D. Poitras, K. Mnaymneh, X. Wu, M. Couillard, M. Korkusinski, E. Schöll, K. D. Jöns, V. Zwiller, R. L. Williams, *Bright Single InAsP Quantum Dots at Telecom Wavelengths in Position-Controlled InP Nanowires: The Role of the Photonic Waveguide*, Nano Letters **18**, 3047–3052 (2018)

Paper 2. A. W. Elshaari, E. Büyüközer, I. E. Zadeh, T. Lettner, P. Zhao, E. Schöll, S. Gyger, M. E. Reimer, D. Dalacu, P. J. Poole, K. D. Jöns, V. Zwiller, *Strain-Tunable Quantum Integrated Photonics*, Nano Letters **18**, 7969–7976 (2018)

Paper 3. E. Schöll†, L. Hanschke†, L. Schweickert†, K. D. Zeuner, M. Reindl, S. F. Covre da Silva, T. Lettner, R. Trotta, J. J. Finley, K. Müller, A. Rastelli, V. Zwiller, K. D. Jöns, *Resonance Fluorescence of GaAs Quantum Dots with Near-Unity Photon Indistinguishability*, Nano Letters **19**, 2404–2410 (2019)

Paper 4. T. Lettner, K. D. Zeuner, E. Schöll, H. Huang, S. Scharmer, S. F. Covre Da Silva, S. Gyger, L. Schweickert, A. Rastelli, K. D. Jöns, V. Zwiller, *GaAs Quantum Dot in a Parabolic Microcavity Tuned to* ^{87}*Rb* D_1, ACS Photonics **7**, 29–35 (2020)

Paper 5. L. Hanschke†, L. Schweickert†, J. C. L. Carreño†, E. Schöll, K. D. Zeuner, T. Lettner, E. Z. Casalengua, M. Reindl, S. F. Covre da Silva, R. Trotta, J. J. Finley, A. Rastelli, E. del Valle, F. P. Laussy, V. Zwiller, K. Müller, K. D. Jöns, *Origin of Antibunching in Resonance Fluorescence*, Physical Review Letters **125**, 170 402 (2020)

Paper 6. E. Schöll†, L. Schweickert†, L. Hanschke, K. D. Zeuner, F. Sbresny, T. Lettner, R. Trivedi, M. Reindl, S. F. Covre da Silva, R. Trotta, J. J. Finley, J. Vučković, K. Müller, A. Rastelli, V. Zwiller, K. D. Jöns, *The Crux of Using the Cascaded Emission of a 3-Level Quantum Ladder System to Generate Indistinguishable Photons*, Physical Review Letters **125**, 233 605 (2020)

Paper 7. C. Errando-Herranz†, E. Schöll†, R. Picard, M. Laini, S. Gyger, A. W. Elshaari, A. Branny, U. Wennberg, S. Barbat, T. Renaud, M. Sartison, M. Brotons-Gisbert, C. Bonato, B. D. Gerardot, V. Zwiller, K. D. Jöns, *Resonance Fluorescence from Waveguide-Coupled, Strain-Localized, Two-Dimensional Quantum Emitters*, ACS Photonics **8**, 1069–1076 (2021)

Paper 8. F. Sbresny[†], L. Hanschke[†], E. Schöll, W. Rauhaus, B. Scaparra, K. Boos, E. Z. Casalengua, H. Riedl, E. del Valle, J. J. Finley, K. Jöns, K. Müller, *Stimulated Generation of Indistinguishable Single Photons from a Quantum Ladder System*, Physical Review Letters **128**, 093 603 (2021)

Paper 9. B. Jonas, D. Heinze, E. Schöll, P. Kallert, T. Langer, S. Krehs, A. Widhalm, K. D. Jöns, D. Reuter, S. Schumacher, A. Zrenner, *Nonlinear Down-Conversion in a Single Quantum Dot*, Nature Communications **13**, 1387 (2022)

Author contributions

The main advisor for the projects are Prof. Dr. K. D. Jöns and Prof. Dr. V. Zwiller.

Paper 1 Participation in sample characterization.

Paper 2 Participation in building the optical setup, performing the experiment and analyzing the data. Input to the manuscript.

Paper 3 Building the setup, performing the experiment and data analysis. Preparation of the manuscript.

Paper 4 Building the setup, performing the experiment and data analysis. Preparation of the manuscript.

Paper 5 Building the setup, performing the experiment and data analysis. Input to the manuscript.

Paper 6 Building the setup, performing the experiment and data analysis. Preparation of the manuscript.

Paper 7 Building the setup, performing the experiment and data analysis. Preparation of the manuscript.

Paper 8 Participation in performing the experiment. Input to the manuscript.

Paper 9 Performing the experiment and contribution in the data analysis. Input to the manuscript.

[†]These authors contributed equally to the paper

Other publications

The following paper, although related, is not included in this thesis.
K. D. Zeuner, K. D. Jöns, L. Schweickert, C. R. Hedlund, C. N. Lobato, T. Lettner, K. Wang, S. Gyger, E. Schöll, S. Steinhauer, M. Hammar, V. Zwiller, *On-Demand Generation of Entangled Photon Pairs in the Telecom C-Band with InAs Quantum Dots*, ACS Photonics **8**, 2337–2344 (2021)

Conferences

Part of the work in this thesis has been presented in international conferences, schools and workshops.

Oral contributions

E. Schöll, L. Hanschke, L. Schweickert, K. D. Zeuner, M. Reindl, S. F. Covre da Silva, T. Lettner, R. Trotta, J. J. Finley, K. Müller, A. Rastelli, V. Zwiller, and K. D. Jöns, *Resonance fluorescence of GaAs/AlGaAs quantum dots with near-unity photon indistinguishability.* 2. International Symposium on Single Photon based Quantum Technologies. Berlin, Germany, 2019.

E. Schöll, L. Hanschke, L. Schweickert, K. D. Zeuner, M. Reindl, S. F. Covre da Silva, T. Lettner, R. Trotta, J. J. Finley, K. Müller, A. Rastelli, V. Zwiller, and K. D. Jöns, *Resonance fluorescence of GaAs/AlGaAs quantum dots with near-unity photon indistinguishability.* 14th IEEE Nanotechnology Materials and Devices Conference. Stockholm, Sweden, 2019.

E. Schöll, C. Errando-Herranz, M. Laini, S. Gyger, A. W. Elshaari, U. Wennberg, S. Barbat, T. Renaud, M. Sartison, M. Brotons-Gisbert, A. Branny, C. Bonato, V. Zwiller, B. D. Gerardot, and K. D. Jöns, *Resonance fluorescence from waveguide-coupled strain-localized two-dimensional quantum emitters.* OECS 17 International Conference Optics of Excitons in Confined Systems. Online (Dortmund, Germany), 2021.

E. Schöll, C. Errando-Herranz, M. Laini, S. Gyger, A. W. Elshaari, U. Wennberg, S. Barbat, T. Renaud, M. Sartison, M. Brotons-Gisbert, A. Branny, C. Bonato, V. Zwiller, B. D. Gerardot, and K. D. Jöns, *Resonance fluorescence from waveguide-coupled strain-localized two-dimensional quantum emitters.* MRS Spring Meeting & Exhibit. Honolulu, USA, 2022.

E. Schöll, *Communication meets the Quantum world.* Humboldt meets Leibnitz. Hannover, Germany, 2022.

E. Schöll, L. Schweickert, L. Hanschke, K. D. Zeuner, F. Sbresny, T. Lettner, R. Trivedi, M. Reindl, S. F. Covre da Silva, R. Trotta, J. J. Finley, J. Vučković, K. Müller, A. Rastelli, V. Zwiller, and K. D. Jöns, *Crux of Using the Cascaded Emission of a Three-Level Quantum Ladder System to Generate Indistinguishable Photons.* DPG Meeting of the Condensed Matter Section. Regensburg, Germany, 2022. *invited talk*

Poster contributions

S. Haffouz, K.D. Zeuner, D. Dalacu, P.J. Poole, J. Lapointe, D. Poitras, K. Mnaymneh, X. Wu, M. Couillard, M. Korkusinski, E. Schöll, K.D. Jöns, V. Zwiller, and R.L. Williams, *Bright Single InAsP Quantum Dots at Telecom Wavelengths in Position-Controlled InP Nanowires.* Bad Honnef Physics School on Quantum Technologies. Bad Honnef, Germany, 2018.

S. Haffouz, K.D. Zeuner, D. Dalacu, P.J. Poole, J. Lapointe, D. Poitras, K. Mnaymneh, X. Wu, M. Couillard, M. Korkusinski, E. Schöll, K.D. Jöns, V. Zwiller, and R.L. Williams, *Bright Single InAsP Quantum Dots at Telecom Wavelengths in Position-Controlled InP Nanowires.* 6th international workshop "Engineering of Quantum Emitter Properties". Rome, Italy, 2018.

E. Schöll, L. Hanschke, L. Schweickert, K. D. Zeuner, M. Reindl, S. F. Covre da Silva, T. Lettner, R. Trotta, J. J. Finley, K. Müller, A. Rastelli, V. Zwiller, and K. D. Jöns, *Resonance fluorescence of GaAs/AlGaAs quantum dots with near-unity photon indistinguishability.* Summerschool on Quantum devices for non-classical light generation and manipulation. Erice, Italy, 2019.

E. Schöll, C. Errando-Herranz, M. Laini, S. Gyger, A. W. Elshaari, U. Wennberg, S. Barbat, T. Renaud, M. Brotons-Gisbert, A. Branny, C. Bonato, V. Zwiller, B. D. Gerardot, and K. D. Jöns, *Single photon emission from a two-dimensional semiconductor quantum emitter coupled into a photonic waveguide.* 7th international workshop "Engineering of Quantum Emitter Properties". Berlin, Germany, 2019.

E. Schöll, C. Errando-Herranz, M. Laini, S. Gyger, A. W. Elshaari, U. Wennberg, S. Barbat, T. Renaud, M. Brotons-Gisbert, A. Branny, C. Bonato, V. Zwiller, B. D. Gerardot, and K. D. Jöns, *Single photon emission from a two-dimensional semiconductor quantum emitter coupled into a photonic waveguide.* 21st International Winterschool on New Developments in Solid State Physics. Mauterndorf, Austria, 2020.

E. Schöll, C. Errando-Herranz, M. Laini, S. Gyger, A. W. Elshaari, U. Wennberg, S. Barbat, T. Renaud, M. Brotons-Gisbert, A. Branny, C. Bonato, V. Zwiller, B. D. Gerardot, and K. D. Jöns, *Single photon emission from a two-dimensional semiconductor quantum emitter coupled into a photonic waveguide.* QTech 2020 Quantum technologies international conference. Online (Barcelona, Spain), 2020.

E. Schöll, C. Errando-Herranz, M. Laini, S. Gyger, A. W. Elshaari, U. Wennberg, S. Barbat, T. Renaud, M. Brotons-Gisbert, A. Branny, C. Bonato, V. Zwiller, B. D. Gerardot, and K. D. Jöns, *Single photon emission from a two-dimensional semiconductor quantum emitter coupled into a photonic waveguide.* QD 2020 11th International Conference on Quantum Dots. Online (Munich, Germany), 2020. *Awarded as one of four best posters*

E. Schöll, C. Errando-Herranz, M. Laini, S. Gyger, A. W. Elshaari, U. Wennberg, S. Barbat, T. Renaud, M. Sartison, M. Brotons-Gisbert, A. Branny, C. Bonato, V. Zwiller, B. D. Gerardot, and K. D. Jöns, *Resonance fluorescence from waveguide-coupled strain-localized two-dimensional quantum emitters.* 716. WE-Heraeus-Seminar 2D Materials for Photonic Quantum Technologies. Online (Bad Honnef, Germany), 2021. *Awarded with a poster prize*

E. Schöll, L. Schweickert, L. Hanschke, K. D. Zeuner, F. Sbresny, T. Lettner, R. Trivedi, M. Reindl, S. F. Covre da Silva, R. Trotta, J. J. Finley, J. Vučković, K. Müller, A. Rastelli, V. Zwiller, and K. D. Jöns, *Crux of Using the Cascaded Emission of a Three-Level Quantum Ladder System to Generate Indistinguishable Photons.* 764. WE-Heraeus-Seminar Photonic Quantum Technologies – A Revolution in Communication, Sensing, and Metrology. Bad Honnef, Germany, 2022.

E. Schöll, B. Jonas, D. Heinze, P. Kallert, T. Langer, S. Krehs, A. Widhalm, K.D. Jöns, D. Reuter, S. Schumacher, and A. Zrenner, *Optical Control of Single Photons Emitted by a Quantum Dot.* 22st International Winterschool on New Developments in Solid State Physics. Mauterndorf, Austria, 2023.

E. Schöll, L. Hanschke, M. Peter, A. Garcia Jr., P. Kallert, F. Salusti, S. F. Covre da Silva, S. Manna, A. Rastelli, and K. D. Jöns, *Near Fourier-Transform Limited Blinking Free Quantum Dots.* DPG Meeting of the Condensed Matter Section. Dresden, Germany, 2023.

E. Schöll, L. Hanschke , F. Sbresny, L. Schweickert, K. D. Zeuner, W. Rauhaus, B. Scaparra, K. Boos, H. Riedl, T. Lettner, R. Trivedi, M. Reindl, S. F. Covre da Silva, E. Zubizarreta Casalengua, R. Trotta, E. del Valle, J. J. Finley, J. Vučković, K. Müller, A. Rastelli, V. Zwiller, and K. D. Jöns, *Indistinguishable single photons from a quantum ladder system.* Summerschool on Quantum technology from fundamental science to real world applications. Erice, Italy, 2023.

Contents

Part I

Overview and summary

List of Abbreviations

1L	monolayer
2L	bilayer
Al	aluminum
AlAs	aluminum arsenide
AlGaAs	aluminum gallium arsenide
As	arsenic
AsH_3	arsine
Au	gold
BD	beam dump
BS	beamsplitter
CB	conduction band
CCD	charge-coupled device
CMOS	complementary metal–oxide–semiconductor
Ctrl	control
DAC	digital-to-analogue converter
DBR	distributed Bragg reflector
DM	dichroic mirror
e	electron
FDTD	Finite difference time domain
FSS	fine-structure splitting
GaAs	gallium arsenide
GaP	gallium phosphide
H	horizontal(ly polarized)
h	hole
hBN	hexagonal boron nitride

HBT	Hanbury-Brown and Twiss
HF	hydrofluoric
hh	heavy hole
HOM	Hong-Ou-Mandel
HWP	half-wave plate
In	indium
InAs	indium arsenide
InAsP	indium arsenide phosphide
InGaAs	indium gallium arsenide
InP	indium phosphide
IR	infrared
L	left (circularly polarized)
LED	light emitting diode
lh	light hole
lin. pol.	linear polarizer
$LiNbO_3$	lithium niobate
LP	longpass filter
MEMS	micro-electromechanical systems
MoS_2	molybdenum disulfide
NA	numerical aperture
NIR	near-infrared
NW	nanowire
P	phosphine
PBS	polarizing beamsplitter
PDMS	polydimethylsiloxane
PH_3	phosphine
piezo	piezoelectric
PM	power meter
PMN-PT	lead magnesium niobate-lead titanate ($Pb(Mg_{1/3}Nb_{2/3})O_3$-$PbTiO_3$)
PS	pulse shaper
qubit	quantum bit
QD	quantum dot
QWP	quarter-wave plate
R	right (circularly polarized)

RF	resonance fluorescence
SDC	spontaneous down-conversion
Se	selenium
SIL	solid immersion lens
SiN, Si_3N_4	silicon nitride
SiO_2	silicon dioxide, silica
SPDC	spontaneous parametric down-conversion
Stim.	stimulation
TDC	time-to-digital converter
TMD, TMDC	transition metal dichalcogenide
TPE	two-photon excitation
V	vertical(ly polarized)
VB	valence band
X, X^0	exciton
$X^{\pm,*}$	positively/ negatively/ unknown charged exciton
2X	biexciton
TMD	transition metal dichalcogenides
VOA	variable optical attenuator
W	tungsten
WG	waveguide
WP	wave plate
WSe_2	tungsten diselenide

Chapter 1

Introduction

The discovery of quantum physics in the 20th century marks an inception of a scientific revolution as it fundamentally changes our understanding of matter and energy. Key findings such as the wave-particle duality, quantization of energy levels and the probabilistic nature of quantum states led to the development of technologies in the 1950s which use quantum mechanical principles. Among the most famous examples are lasers, transistors and atomic clocks. These devices are sometimes attributed to the first quantum revolution. As the first quantum revolution unfolded, a deeper understanding emerged, setting the stage for the second quantum revolution [Mil97]. Now the focuses lays on the active manipulation of quantum states and explores applications across three pillars: quantum metrology, sensing, and imaging; quantum computing; and quantum communication. The first pillar promises breakthroughs in precision measurements, surpassing classical sensor limits, often using sensing with N00N states [Lee02, Mül17]. It finds applications in geophysics, navigation systems, and medical diagnostics. One renowned example is the LIGO experiment [LIG16], detecting gravitational waves and affirming Einstein's theory of relativity.
Quantum computing [Fey82, Pre12, DiV95, Kni01] promises quantum supremacy [Aru19, Zho20] with computational capabilities far beyond the reach of classical computers. Harnessing the principles of superposition and entanglement, quantum

computers hold the key to solving complex problems in cryptography, optimization, and machine learning. A prominent example is solving problems of the non-polynomial complexity class such as prime number factorizing. Applying the Shor algorithm [Sho97], the number of operations scales polynominally with the number of digits with a quantum processor instead of exponentially with a classical processor. This in turns will be a thread for today's encryption protocols as they are often based on the complexity of prime number factorizing or other complex mathematical algorithms.

Quantum communication secures and enhances communication channels and provides links between quantum computers to build quantum networks or a quantum internet [Kim77]. The no-cloning theorem in quantum mechanics prevents copying of a quantum state and therefore makes unnoticed eavesdropping impossible with different protocols for quantum key distribution [Ben14, Eke91]. Similar to a classical bit, the quantum mechanical counterpart for the fundamental unit of information, the quantum bit (qubit), encounters losses. But the no-cloning theorem makes classical amplification of the signal impossible and quantum repeaters (i.e. based on the scheme from Lloyd et al. [Llo01]), are a prerequisite for bridging long distances in quantum communication channels. Single photons serve as the sole but excellent flying qubits in such networks, traveling at the speed of light and having only a small interaction cross-section. Therefore, sources that emit single photons are required. An ideal quantum light source must exhibit several key characteristics to meet the stringent requirements of quantum technology applications. First, it should emit pure single-photons without background or multi-photon emissions. Additionally, deterministic and on-demand photon generation is essential for precise control in quantum systems. Furthermore, it must ensure the emission of highly indistinguishable photons even when subjected to long time delays, therefore it should feature Fourier-transform limited linewidths. A short lifetime will on the one hand enable high qubit rates and will on the other hand reduce the interaction time with the environment, which increases the coherence of the system. Moreover, the source should facilitate the emission of entangled photon pairs, a fundamental requirement for various quantum information and communication protocols. The ability to tune the emission wavelength, enhances the versatility of the source and enabling specific quantum technology applications such as coupling to an atomic

transition to realize a quantum memory or tune it into resonance with another source, which is both required for example to realize a quantum repeater. Furthermore, for practical integration into quantum systems, the quantum light source should offer integrability into quantum integrated photonic circuits, photonic cavities, or other photonic structures. This enables scaling up of complex quantum architectures and enhances the extraction efficiency of photons. Emitting in the telecom C-band at 1550 nm is preferred for long-distance applications in quantum communication, as conventional optical glass fibers exhibit minimal absorption in that range.
In the course of the past decades, different quantum light sources have been realized. For a long time sources based on spontaneous parametric down-conversion processes have been the working horse in the field [Gho87, Pan98, DR03, Yin20, Neu22]. The major drawback of those sources is that the probabilistic process prevents on-demand generation of entangled photon pairs and they have to obey a trade off between efficiency and purity. Sources based on single emitters, including single trapped atoms and ions [Hig16, Deb16], molecules [Rez19], defects in crystals [Doh13, Bec20], semiconductor quantum dots [Sch18b, Zha22], and emitters hosted by two-dimensional materials [Cha19b], inherently overcome this limitation. This is due to their quantum mechanical level scheme and a characteristic time, known as the excited state lifetime, that must elapse before a successive photon can be emitted. Advances in the growth and nanofabrication in the past years and decades enhanced the quality and tailorability of semiconductor quantum dots significantly. Particularly noteworthy are Al droplet etched GaAs quantum dots [daS21, Gur19] which have caught attention in the past years as they quickly surpassed the more established InGaAs quantum dots, grown with the Stranski-Krastanow method, in many properties. Especially the strain-free lattice matched growth results e.g. in a low fine structure splitting [Huo13], short lifetimes and a narrow wavelength distribution. Furthermore the GaAs quantum dots are emitting in the near-infrared spectral range around $780-800$ nm holding the potential to be tuned in resonance with the atomic rubidium ^{87}Rb D_1 and D_2 lines [Ako11, Hua17]. Another type of quantum dots are InAsP quantum dots in nanowires with good optical properties [Jön17]. They especially show potential for integration into quantum photonic circuits [Zad16]. But also the relatively newly emerging emitters in two-dimensional materials show potential especially in terms of integrability and scalability.

This thesis aims to achieve a fundamentally deeper understanding of quantum level schemes and explores the influence of different excitation methods. Furthermore, efforts are being made to address properties of the aforementioned ideal quantum light source in terms of increasing the extraction efficiency, tuning the wavelength, and integrating it into photonic circuits.

Thesis structure In part I of this thesis I introduce the basics to understand the papers in part II. In **chapter 2**, I discuss different types of quantum emitters. The main focus is on three different types of semiconductor quantum dots and key properties of each type. Additionally I introduce quantum emitters hosted in TMD monolayers. **Chapter 3** covers cryogenic micro-photoluminescence spectroscopy. I focus here on different excitation methods, outlining the advantages and limitations of each technique. I also describe how the experimental setup has been adjusted to accommodate these different excitation methods. Moving on to **chapter 4**, I introduce three types of light sources based on the photon number statistic. Furthermore, I explain the second-order correlation function and an experiment to measure it, which is an important tool to characterize our quantum emitters in terms of single-photon purity and excited state lifetime. **Chapter 5** focuses on the concept of indistinguishability. I explain two-photon interference and its significance for applications in quantum technologies. I also describe an experiment designed to measure the indistinguishability of photons and explain the resulting histogram. Lastly, in **chapter 6**, I briefly cover different methods for tailoring quantum emitter properties. I specifically focus on tuning methods, such as strain tuning and electric field tuning, to adjust the emission energy, various photonic structures and microcavities that enhance the extraction efficiency, and quantum photonic integrated circuits.
Part II of this thesis includes the following papers:
In **paper 1** we study the emission wavelength of InAsP quantum dots in InP nanowires, which shifts from the near-infrared spectral range at approximately 900 nm to the telecom C-band at 1550 nm depending on the As content. By adjusting the nanowire diameter, the overlap between the emitted photons and the fundamental waveguide mode of the nanowire can be restored and bright single photons in the telecom spectral range can be observed. In **paper 2** we deterministically integrate an above mentioned near-infrared emitting nanowire quantum dot into a SiN quantum photonic integrated circuit using a pick-and-place tech-

nique. The photonic circuit is fabricated directly on a piezoelectric substrate using a novel method that allows better strain transfer. We show reversible strain tuning of an integrated optical resonator and quantum emitter, as well as single photon emission. **Paper 3** presents highly indistinguishable photons with visibilities up to $V_{\mathrm{HOM}} = 95^{+5.0}_{-6.1}$ % from both a neutral and a charged exciton transition in a GaAs quantum dot without the need for Purcell enhancement. We achieved this due to short excited state lifetimes, s-shell resonant excitation, and polarization suppression of the scattered laser. In **paper 4** we present a novel photonic structure, a microparaboloid with a GaAs quantum dot at the focus of the structure, with broadband collection efficiency enhancement and Gaussian emission modes. We measure collection efficiencies of 12 % (63 % with finite difference time domain simulations), single-photon emission, and cascaded emission under two-photon excitation. In addition, the structure is combined with a piezoelectric substrate to allow wavelength tuning of the emission energy. In **paper 5** we investigate a two-level system in the Rayleigh regime, where most of the signal comes from coherently scattered photons from the laser. We independently demonstrate antibunching and subnatural linewidth of a GaAs quantum dot under weak continuous-wave s-shell resonant excitation. The origin of the antibunching is explained by the interference between the narrow coherently scattered, and the broad incoherent signal in a skewed squeezed state. As a result, the antibunching dip disappears for narrowing filter widths, as we prove experimentally. In **paper 6** we show that the indistinguishability of the two cascaded photons from any three-level quantum ladder system is intrinsically limited by the lifetime ratio. The finite linewidth of the intermediate state introduces an energy jitter to the excited state emission, while the finite excited state lifetime adds a timing jitter to the intermediate state decay, both of which reduce the indistinguishability of the respective transition. We prove this by measuring the indistinguishability of biexciton and exciton photons emitted from a GaAs quantum dot under two-photon excitation and find good agreement with quantum optical simulations. Furthermore, we measure excellent single-photon purity, as the cascaded emission protects the system from re-excitation. Additionally, we compare these results with a two-level system (e.g. the exciton transition of the same quantum dot under s-shell resonant excitation). While it dominates in terms of indistinguishability (as also shown in paper 3), the single-photon purity is limited by the re-excitation

process. In **paper 7** we couple strain-localized quantum emitters hosted by a WSe_2 monolayer to a SiN waveguide. We demonstrate single-photon propagation in the waveguide by coupling a lensed fiber to the cleaved waveguide facet and measure the single-photon purity of the waveguide-coupled signal. We also demonstrate on-chip resonant continuous wave excitation of a quantum emitter. To suppress the excitation laser, we combine out-of-plane detection and polarization filtering. **Paper 8** proposes a new coherent excitation scheme based on two-photon excitation and subsequent stimulation of the biexciton-exciton transition. This method can overcome the limited indistinguishability of the exciton transition revealed in paper 6 by reducing the timing jitter stemming from the biexciton lifetime. We demonstrate this by comparing the indistinguishability of an exciton transition in an InGaAs quantum dot under this new excitation method, two-photon excitation, and s-shell resonant excitation. Furthermore, the polarization of the exciton photons can be controlled by the polarization of the stimulation laser, resulting in nearly twice the brightness compared to s-shell resonant excitation with polarization suppression, and high single-photon purity of the cascaded emission is maintained, since the transition is still protected from re-excitation. In **paper 9** we demonstrate the all-optical control of single-photon properties. We start from the biexciton state in an InGaAs quantum dot under two-photon excitation. An additional laser, energetically close to one of the cascaded decay transitions, provides a virtual state for a stimulated down-conversion process. We show single-photon emission, as well as laser-controlled energy tuning and polarization control of the signal.

Chapter 2

Semiconductor quantum light sources

Contents

Quantum light sources emit light with non-classical properties, particularly showing single-photon emission. Other key attributes include deterministic and on-demand generation of single photons with Fourier-transform limited linewidths, short lifetimes, and high degrees of indistinguishability. Furthermore, these sources should facilitate the generation of entangled photon pairs. The first experimental demonstration of a single-photon source was in 1974, where a cascaded transition in a mercury atom emitting two photons at different frequencies was exploited to use one photon to herald the other after spectral filtering [Cla74]. The first demonstration not based

on heralding was in 1977 with sodium atoms [Kim77]. Since then, a whole zoo of different single-photon sources with varying key characteristics have been discovered. They can be broadly classified into three families: heralded photons, single atoms, ions and molecules, and solid state sources.

Most heralded photon sources are based on a nonlinear process. Pumping a nonlinear crystal with a significant second-order susceptibility $\chi^{(2)}$ at high power can lead to pairs of entangled photons by spontaneous parametric down conversion, first demonstrated by Ou and Mandel in 1988 [Ou88]. To reduce the probability of double-pair formation, the pump power is kept low, which also limits the probability for single-pair formation to a few percent, thereby inherently limiting the source brightness and preventing on-demand generation. Periodic poling of a nonlinear crystal increases the down conversion probability significantly and can be optimized for a desired wavelength [Ram13, Her13, Mon17]. Despite the limited brightness, excellent single-photon purity of 0.09 [Kan16] and Hong-Ou-Mandel indistinguishability of 92 % [Wan16] have been demonstrated. Furthermore, entanglement distribution and quantum key distribution has been shown over large distances in field experiments [Yin20, Neu22].

Quantum light sources based on single molecules, atoms or, ions rely on quantum level schemes. A quantum system is in its energy ground state when all electrons are in the lowest possible shells. By absorbing a photon, an electron can be lifted to a higher shell, meaning that the atom is in an excited state. After a characteristic time, the lifetime of the excited state, the atom spontaneously relaxes back to the ground state by emitting a single photon. This inherently prevents multi-photon emission and a single-photon purity of $g^{(2)}(0) = (3 \pm 1.5) \cdot 10^{-4}$ has been demonstrated [Hig16]. Experimentally, a single atom or ion is isolated in a magneto-optical trap and cooled to cryogenic temperatures to reach this energy ground state and to isolate the system from the environment. This leads to very long spin coherence times of up to 0.5 s [Deb16], making them suitable as stationary qubits. Although the complex trapping setup makes it difficult to scale up for quantum technology applications, atoms are predestined for experiments to gain a deeper fundamental understanding of quantum mechanics and as a platform for first quantum information processing applications. A small atom-based processor has been built that demonstrates Shor factorization [Deb16]. Single organic molecules (e.g. dibenzanthanthrene

or dibenzoterrylene) are often embedded in an anthracene or naphthalene crystal to improve the optical properties. Those sources are mostly studied in context of biology, physical chemistry and spectroscopy and less as quantum system. But also with molecules e.g., single-photon emission [Paz18] and polarization entangled photon pair generation [Rez19] could be demonstrated. An alternative atom-based single-photon source in an atomic vapor is based on the Rydberg blockade. It also shows good indistinguishability [Pad21] and single-photon purity [Dud12], even at room temperature [Rip18]. Another alternative source is based on four wave mixing providing impressive entangled pair generation rates compatible with the telecom infrastructure and atomic systems [Cra24].

The family of solid state single-photon sources exhibits the widest variety of different sources, including fluorescent defects in crystals, carbon nanotubes, epitaxial and colloidal quantum dots, and quantum emitters hosted by two-dimensional materials [Aha16]. For brevity, carbon nanotubes and colloidal quantum dots will be excluded from this brief overview. Their primary applications lie in classical photonics, such as display technology, due to dephasing, bleaching, and blinking.

Foreign atoms or vacancies in a crystal can form point-like defects that locally change the potential to create quantized energy levels. Among the most studied defects are color centers in diamond such as nitrogen vacancies [Doh13] and silicon vacancies [Bec20]. These emitters offer advantages such as room temperature operation, near Fourier-transform limited linewidths [Bar13], and long spin coherence times of up to 0.6 s [Bar13], making them suitable for quantum memory applications, although not all desired properties are simultaneously present in one defect type. Unfortunately, single-photon purity [Kur00, Sch11b] does not show excellent properties, but ongoing research continues to explore new defects [Zai00].

Throughout my thesis, my primary focus was on epitaxial semiconductor quantum dots (hereafter referred to as quantum dots) with some involvement with recently discovered emitters in transition metal dichalcogenide monolayers. In the following sections, I will provide a more detailed introduction to these emitters.

2.1 Quantum Dots

Quantum dots (QDs) are small nanometer sized semiconductor crystals, typically consisting of a few ten to a hundred thousand atoms, providing a three-dimensional confinement for charge carriers. This confinement is achieved by incorporating a low band gap semiconductor into a high band gap semiconductor material, such as GaAs ($E_{\mathrm{g,\ GaAs}} = 1.52\,\mathrm{eV}$) embedded in AlGaAs ($E_{\mathrm{g,\ AlGaAs}} = 2.03\,\mathrm{eV}$ at $4\,\mathrm{K}$) for the case of the quantum dots in Sec. 2.1.4. Arakawa and Sakaki first presented this three-dimensional confinement concept in 1982 [Ara82], and Reed later introduced the term "quantum dots" in 1986 [Ree86]. Back then, the quantum dots were obtained using a top-down approach involving electron beam lithography and reactive ion etching of a multi quantum well structure. Nowadays, most semiconductor quantum dots are directly grown in an epitaxial growth process [Gol85]. The statistical or self-assembled growth process leads to a random distribution over the sample, varying sizes, and shapes of quantum dots. Additionally, each quantum dot is influenced by its semiconductor environment, including phonons and charge traps, leading to slightly different optical properties for each quantum dot on a sample. Due to the high refractive index of the solid state host matrix, most of the emission is trapped inside the sample, resulting in a low extraction efficiency. However, the solid state bulk material allows for relatively easy integration of the quantum dots into structures, boosting the extraction efficiency or enabling wavelength tuning (see Ch. 6). Nowadays, quantum dots exhibit the best overall performance among all single-photon sources, with the highest single-photon purity [Sch18b] and near unity indistinguishability [Zha22]. Different growth methods are discussed in Secs. 2.1.3, 2.1.4 and 2.1.5.

2.1.1 Band structure

In semiconductors at low temperatures, the most electrons occupy the valence band. They can be excited to the conduction band through optical, thermal, or electrical excitation, leaving behind a positively charged hole in the valence band, thus forming an electron-hole pair. A trapped electron-hole pair inside a quantum dot is called an exciton (X or X^0) and is more favorable compared to an electron-hole pair in the bulk semiconductor due to a larger overlap of the wave functions and Coulomb interaction. The recombination of the electron back to the valence band results in the emission

of a photon with the energy given by the band gap, called photoluminescence. If the confinement of the small band gap material is on the order of the de Broglie wavelength of the electrons or holes

$$\lambda_{\mathrm{dB}} \leq \frac{h}{\sqrt{3m^*_{\mathrm{e,h}}k_{\mathrm{B}}T}}, \tag{2.1}$$

with the Planck constant h, the effective mass of electrons and holes $m^*_{\mathrm{e,h}}$, and the thermal energy $k_{\mathrm{B}}T$, the density of states becomes delta-like. As a result, the number of states is substantially reduced to only a few discrete states, resembling the energy levels in an atom. For this reason, quantum dots are sometimes referred to as artificial atoms. Self-assembled quantum dots typically have a diameter of a few tens of nanometers and a height of only a few nanometers [Leo94, Huo13]. The small height leads to a strong confinement in z (growth direction) and results in only the lowest energy state being populated. Consequently, higher states in z are not considered, and the quantum dot can be quantum mechanically described as an in-plane two-dimensional harmonic oscillator. For rotationally symmetric quantum dots, the Hamiltonian becomes

$$\hat{\mathcal{H}} = \frac{\hat{\mathbf{p}}^2}{2m^*_{\mathrm{e,h}}} + \frac{1}{2}m^*_{\mathrm{e,h}}\omega_0^2\hat{\mathbf{x}}^2 \tag{2.2}$$

with the momentum operator $\hat{\mathbf{p}}$, the angular frequency ω_0 and the position operator $\hat{\mathbf{x}}$. Solving the Schrödinger equation, as first done by Fock and Darwin [Foc28, Dar31], leads to the following energy eigenvalues

$$E_{n,l} = \hbar\omega_0\left(2n + |l| + 1\right), \tag{2.3}$$

where $n = 0, 1, 2, ...$ is the principal quantum number, and $l = 0, \pm1, \pm2, ...$ is the angular momentum. The shells with index $s = 2n + |l| + 1 = 0, 1, 2, ...$ are often called s- p- d-, ... shells like in atoms. Accounting for the spin and the Pauli exclusion principle, the shell degeneracy is given by $2\left(s + 1\right) = 2, 4, 6, ...$ Since electron-hole pairs tend to relax into the lowest energy state (the s-shell), only recombination from this shell is considered here. While the upper limit for the quantum dot diameter is determined by the de Broglie wavelength, the minimum in-plane diameter is dictated by the smallest size at which bound single-carrier states exist, depending on the

effective masses and the potential depth.
Energy bands in semiconductors are described as s-like, p-like, etc., according to the respective atomic orbitals. The materials used in this work have an s-like conduction band and a p-like valence band, resulting in an orbital angular momentum $L_\mathrm{e} = 0$ for the electrons and $L_\mathrm{h} = 1$ for the holes. Both electron and hole spins are $S_\mathrm{e,h} = \frac{1}{2}$, i.e. up or down. Due to the two spin configurations with projection in the growth direction $S_z = \pm\frac{1}{2}$, the conduction band is twofold degenerate. For the valence band, the spin-orbit coupling must be taken into account, with the consequence that the orbital angular momentum L_h and the spin S_h are not conserved, but only the total angular momentum $J_\mathrm{h} = L_\mathrm{h} \pm S_\mathrm{h}$. This results in three different bands: Heavy holes (hh) with $J_\mathrm{hh} = \frac{3}{2}$ and the projection $J_{\mathrm{hh},z} = \pm\frac{3}{2}$, light holes (lh) with $J_\mathrm{lh} = \frac{3}{2}$ and $J_{\mathrm{lh},z} = \pm\frac{1}{2}$, and split-off (so) holes with $J_\mathrm{so} = \frac{1}{2}$ and $J_{\mathrm{so},z} = \pm\frac{1}{2}$. Confinement in quantum dots leads to an energy splitting of the heavy and light holes, with the heavy holes in the highest band [Kor13]. In InGaAs (Sec. 2.1.3) and GaAs (Sec. 2.1.4) quantum dots, the mixing of both states can be neglected [Cor01, Hub17, Huo14]. In InAsP nanowire quantum dots (Sec. 2.1.5), heavy hole-light hole mixing is possible and becomes even stronger for quantum dots emitting at telecom wavelengths. However, the photons resulting from a recombinations with light holes are unable to couple to the guiding mode of the nanowire [Jea17]. Since all quantum dots used in this work are dominated by heavy hole recombination, only these will be considered here. However, heavy hole-light hole mixing in quantum dots is influenced by applying strain to the sample and was studied e.g., in [Plu13].

2.1.2 Excitonic states

Considering an electron with $S_{\mathrm{e},z} = \pm\frac{1}{2}$ and a heavy hole with $J_{\mathrm{hh},z} = \pm\frac{3}{2}$ leads to four possible excitonic states which are characterized by their angular momentum projection $M = S_{\mathrm{e},z} + J_{\mathrm{hh},z} = \pm1, \pm2$. Only states with $M = \pm1$, which means that the charge carriers have opposite spins, (see Fig. 2.1a) satisfy the dipole selection rules $M = 0, \pm 1$ and couple to the light field. Hence these are called bright excitons (X or X^0). The states with $M = \pm2$ cannot couple to the light field and are called dark excitons. These spin configurations are shown in Fig. 2.1b and will not be considered further in this work. After the generation of a bright exciton, it recombines to the ground state after a characteristic lifetime, which is in the range of a few hundred

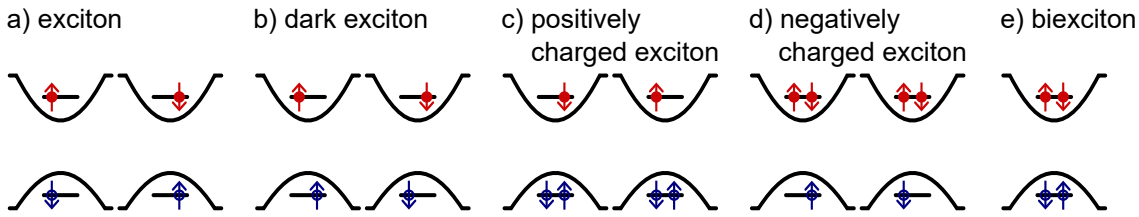

Figure 2.1 | Excitonic states in a quantum dot **a**, exciton **b**, dark exciton **c**, positively charged exciton **d**, negatively charged exciton **e**, biexciton. Electrons are represented with red dots, holes in blue. The arrows denote the spin of the charge carrier up or down.

picoseconds to a few nanoseconds depending on the semiconductor material and the environment of the single emitter. Upon recombination, a single photon is emitted with an energy E_X given by the energy difference between the electron and hole states. The quantum dots studied here are emitting in the near-infrared and infrared wavelength range.

If an additional hole (electron) is trapped inside the quantum dot, a positively (negatively) charged exciton ($\mathrm{X}^{\pm}$) is generated. These states also appear with two spin configurations each, as shown in Fig. 2.1c,d. Charged excitons are sometimes also called trions ($\mathrm{T}^{\pm}$). If the charge is not known, they are labeled X^* or T^*. The extra charge carrier gives rise to additional Coulomb interaction terms, leading to slightly different energies compared to the neutral exciton.

Due to Pauli's exclusion principle, up to two charge carriers with opposite spin can occupy the lowest energy state in the quantum dot, namely two electrons in the conduction band and two holes in the heavy hole band of the valence band (see Fig. 2.1e). This configuration is called a biexciton (2X or XX). The biexciton binding energy $E_\mathrm{B} = 2E_\mathrm{X} - E_\mathrm{2X}$ can be both positive and negative depending on the additional Coulomb interaction terms, but only biexcitons with $E_\mathrm{B} > 0$ are considered here, since the others cannot be resonantly excited under two-photon excitation [Jus20] (see Sec. 3.2.3). Due to optical selection rules, a biexciton cannot recombine directly to the ground state. Rather, it decays in a cascaded emission called a biexciton-exciton cascade, as experimentally demonstrated by crosscorrelation measurements in 2001 [Mor01]. First, one electron-hole pair recombines by emitting a photon of energy E_2X. In the second step, the remaining exciton recombines by emitting a photon with energy E_X. This cascaded emission is shown in an energy level scheme and the corresponding spectrum in Fig. 2.2a. The polarization of the

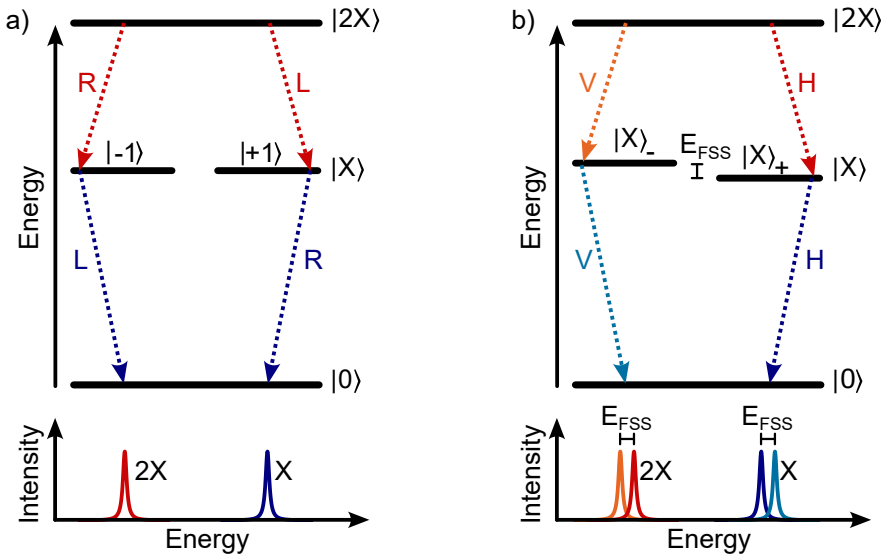

Figure 2.2 | Biexciton-exciton cascade a, without fine structure splitting (FSS) and **b**, with fine structure splitting. The biexciton state (2X) decays via two possible decay paths with the intermediate exciton (X) state to the ground state (0). Due to the biexciton binding energy, the biexciton line appears at lower energy than the exciton line in the spectrum (bottom panels). In the case of zero fine structure splitting, the two possible exciton states are determined by angular momentum ($M = \pm 1$) and the emitted photons are circularly polarized (R, L). With fine structure splitting E_{FSS}, the exciton states are not degenerate anymore and hybridize into two linear combinations $|X\rangle_{\pm}$ and the emitted photons are linearly polarized (H, V).

emitted biexciton photon is right (R) or left (L) circularly polarized, depending on whether the final state is the $M = -1$ or $+1$ exciton. The subsequent exciton photon has the opposite circular polarization. Due to the degeneracy of the intermediate states, both decay channels of the cascade are in a superposition and the states are polarization entangled:

$$|\Phi^{+}\rangle = \frac{1}{\sqrt{2}}\left(|\mathrm{RL}\rangle + |\mathrm{LR}\rangle\right) = \frac{1}{\sqrt{2}}\left(|\mathrm{HH}\rangle + |\mathrm{VV}\rangle\right). \tag{2.4}$$

The first letter in the ket refers to the polarization of the biexciton photon, the last to the polarization of the subsequent exciton photon. Since the rectilinear basis with horizontal (H) and vertical (V) polarization can be expressed as a linear combination of the circular basis ($|\mathrm{L}\rangle = \frac{1}{\sqrt{2}}\left(|\mathrm{H}\rangle + i\,|\mathrm{V}\rangle\right)$, $|\mathrm{R}\rangle = \frac{1}{\sqrt{2}}\left(|\mathrm{H}\rangle - i\,|\mathrm{V}\rangle\right)$), the entangled state can be written in different bases. As already proposed in 2000, quantum dots

can emit polarization entangled photon pairs on-demand [Ben00].
So far, the exchange interaction between electrons and holes has not been considered, which leads to the so called fine structure splitting (FSS) of the energy levels of the four excitonic spin states with $M = \pm 1, \pm 2$. The corresponding Hamiltonian is given by [van90]:

$$\hat{\mathcal{H}}_{\mathrm{ex}} = -\sum_{i=x,y,z} \left(a_i \hat{J}_{\mathrm{h},i} \hat{S}_{\mathrm{e},i} + b_i \hat{J}^3_{\mathrm{h},i} \hat{S}_{\mathrm{e},i} \right). \tag{2.5}$$

Where a_i and b_i are the spin-spin coupling constants along the respective axis i, and $\hat{J}_{\mathrm{h},i}$ and $\hat{S}_{\mathrm{e},i}$ are the spin operators for the holes and electrons, respectively. The interaction depends on the crystal structure, the dominant hole type (heavy holes in our cases), the potential symmetry and the strain in the material. Writing the Hamiltonian in the basis of the two bright $|\pm 1\rangle$ and dark $|\pm 2\rangle$ exciton states leads to [Bay02]

$$\hat{\mathcal{H}}_{\mathrm{ex}} = \frac{1}{2} \begin{pmatrix} +E_0 & E_1 & 0 & 0 \\ E_1 & +E_0 & 0 & 0 \\ 0 & 0 & -E_0 & E_2 \\ 0 & 0 & E_2 & -E_0 \end{pmatrix}. \tag{2.6}$$

E_i are splittings of the different states. $E_0 = \frac{3}{2}\left(a_z + \frac{9}{4} b_z\right)$ is the splitting between the bright and dark states, and $E_1 = \frac{3}{4}(b_x - b_y)$ and $E_2 = \frac{3}{4}(b_x + b_y)$ are the splittings of the bright and dark exciton doublets, respectively. In the case of vanishing exchange interaction $\hat{\mathcal{H}}_{\mathrm{ex}} = 0$, all four excitonic states are degenerate. For $\hat{\mathcal{H}}_{\mathrm{ex}} \neq 0$ the degeneracy between the bright and dark exciton states is broken and the states $|\pm 1\rangle$ and $|\pm 2\rangle$ are split with the electron hole exchange energy E_0. In the case of a rotationally symmetric confinement potential ($b_x = b_y$, $E_1 = 0$), the two dark exciton states hybridize with an energy splitting E_2. If the rotation symmetry is broken the bright exciton states $|\pm 1\rangle$ are no longer eigenstates of the exchange interaction Hamiltonian and the states hybridize into new symmetric and antisymmetric linear combinations $|X\rangle_{\pm} = \frac{1}{\sqrt{2}}(|+1\rangle \pm |-1\rangle)$ with the splitting E_1. The photoluminescence from these transitions is linearly cross-polarized (H and V) along the main symmetry axis of the quantum dot. Since only bright excitonic states are investigated in this thesis, we refer to their splitting as E_{FSS} instead of E_1 for simplification hereafter. The splitting is typically between a few and a few tens of micro electronvolts in unoptimized quantum dots. This is usually below

the resolution limit of spectrometers and can only be measured with the use of polarization resolved photoluminescence spectroscopy (see Sec. 3.1), time correlated single-photon spectroscopy (see Sec. 4.3) or scanning Fabry-Pérot interferometers. A positively (negatively) charged exciton can be seen as a single electron (hole) interacting with the two holes (electrons) forming a spin-singlet, leading to a vanishing exchange energy and thus no fine structure splitting [Bay02]. The same applies to the biexciton. Nevertheless, the emission from the biexciton state shows the same splitting as the exciton, since the exciton is the final state for that recombination process, as shown in the energy level scheme and spectrum in Fig. 2.2b. The biexciton-exciton cascade thus has two non-degenerate linearly cross-polarized decay channels. The intermediate state receives a time-dependent phase $\mathrm{e}^{i\frac{E_{\mathrm{FSS}}}{\hbar}t}$. The initial exciton state is determined by the polarization of the biexciton photon and thus the decay path and starts to precess on the Poincaré sphere with the frequency $\frac{E_{\mathrm{FSS}}}{\hbar}$. As a consequence, the exciton photon has a different polarization depending on the emission time [Ste08b]. The entangled state of the radiative cascade in Eq. (2.4) becomes $|\Psi\rangle = \frac{1}{\sqrt{2}}\left(|\mathrm{HH}\rangle + \mathrm{e}^{i\frac{E_{\mathrm{FSS}}}{\hbar}t}|\mathrm{VV}\rangle\right)$ and the time-averaged entanglement degrades as a function of the splitting E_{FSS} [Hud07]. But in fact the state oscillates between the two Bell states $|\Phi^+\rangle = \frac{1}{\sqrt{2}}(|\mathrm{HH}\rangle + |\mathrm{VV}\rangle)$ and $|\Phi^-\rangle = \frac{1}{\sqrt{2}}(|\mathrm{HH}\rangle - |\mathrm{VV}\rangle)$ and thus remains maximally entangled. In practice, this can only be measured if the temporal resolution of the setup is high enough to resolve the oscillation, which is on the order of a few hundred picoseconds, and if the two emitted photons are synchronized, which was first demonstrated by Winik et al. [Win17] and also shown by us [Zeu21]. However, in most quantum-engineering applications, a time-invariant entangled state is desired to overcome the more stringent setup requirements. Therefore, various methods have been exploited to obtain a quantum dot without fine structure splitting ($E_{\mathrm{FSS}} \approx 0\,\mu\mathrm{eV}$). They range from samples that have been carefully characterized to find a quantum dot without fine structure splitting [Haf07], growth methods that have been developed to grow quantum dots with very small average fine structure splitting (see. Secs. 2.1.4 and 2.1.5) and thermal annealing [Lan04, Tar04] to post-growth techniques for fine structure tuning based on a magnetic field [Ste06b], strain field [Sei06, Tro15], electric field [Gha12] and optical Stark effect [Mul09a]. The manipulation of the fine structure splitting is discussed in more detail in Sec. 6.1.

2.1.3 Stranski-Krastanow grown quantum dots

The first epitaxial quantum dots were based on Stranski-Krastanow growth [Str37]. Due to the different lattice constants of the semiconductor materials, strain builds up inside the sample, leading to preferential growth of nanoislands to release the strain. The quantum dots used in this thesis, based on this method, are InGaAs quantum dots embedded in GaAs, grown by molecular beam epitaxy. The sample used in paper 8 was grown by Jonathan J. Finley's group at the Technical University of Munich, while the sample in paper 9 was grown through our in-house collaboration in Paderborn by Dirk Reuter's group. The growth process is illustrated step by step

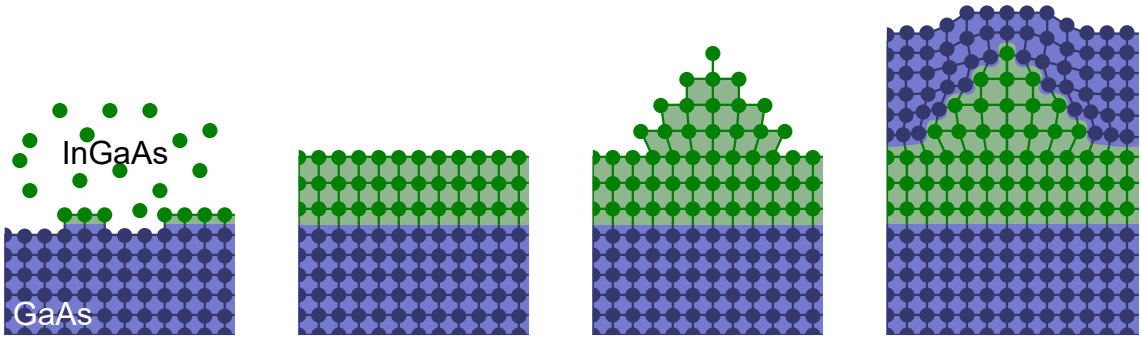

Figure 2.3 | Stranski-Krastanow grown quantum dots Deposition of few monolayers InGaAs on a GaAs substrate (panel 1,2). Island formation to relax the strain due to the lattice mismatch (panel 3). GaAs overgrowth to achieve a three-dimensional confinement (panel 4).

in Fig. 2.3. In the first step, a GaAs layer is grown on a GaAs wafer to enhance the surface quality. Next, the InGaAs deposition begins with the growth of a few monolayers (panels 1,2). Due to the significant lattice mismatch of both materials, up to 7.2 %, strain within the sample increases [Sny91]. After a few monolayers, called the wetting layer, InGaAs islands with a diameter of about 30 nm are formed to relax the strain [Guh90, Leo93] (panel 3). Finally, the islands are overgrown with GaAs (panel 4) to achieve three-dimensional confinement. Throughout the growth process, the quantum dots from both samples were embedded in a diode structure to enable charge control and emission energy tuning, as explained in Sec. 6.1.2. Additionally, the sample from paper 8 includes a bottom distributed Bragg reflector to enhance the extraction efficiency (see Sec. 6.2).
These quantum dots emit in the near-infrared spectral range around 930 nm with a

biexciton binding energy of approximately $2 - 3\,\mathrm{meV}$ and a fine structure splitting of about $10 - 100\,\mu\mathrm{eV}$ [Seg05]. The exciton lifetime is on a time scale of 300 ps to 1000 ps [Adl98, Ber07, Liu18b].

2.1.4 Al droplet etched GaAs quantum dots

Most of the studies in this thesis are conducted on Al droplet etched GaAs quantum dots grown by molecular beam epitaxy from the group of Armando Rastelli at the Johannes Kepler University Linz using the local droplet etching technique. This technique allows for the growth of strain-free lattice-matched quantum dots, in contrast to those grown using the Stranski-Krastanow mode. The local droplet etching technique was first introduced in [Wan07]. The growth of these quantum dots is illustrated in Fig. 2.4a. The process begins with the growth of an AlGaAs layer on top of a (001) GaAs substrate (not shown). By reducing the As pressure while maintaining the Al flux (panel 1), Al droplets form on the surface [Hey09] (panel 2). Subsequently, the As flux is increased again, initializing the etching of nanoholes (panel 2, 3). The As concentration gradient at the droplet-surface interface leads to the diffusion of As into the droplet, resulting in the etching (liquefaction) of the AlGaAs beneath the droplet [Hey11] (panel 3). The droplet material is then removed under As flux and crystallizes as an optically inactive AlAs ring around the droplet [Ste08a, Hey09], as well as on the planar parts between the holes [Atk12] (panel 4). The newly formed empty holes are filled with $1 - 4\,\mathrm{nm}$ GaAs deposition, followed by annealing of the sample (panel 5). Finally, the holes are covered with an AlGaAs barrier layer [Huo13] (Panel 6).

Figure 2.4b provides an artistic illustration of the whole sample structure used in papers 3, 5, and 6. To reduce the required excitation power and improve the collection efficiency, the quantum dot layer is embedded in a weak planar cavity of distributed Bragg reflectors. Additionally, a solid immersion lens is placed on top of the sample. Different methods to improve the extraction efficiency are described in Sec. 6.2.
Figure 2.4c depicts a typical spectrum under nonresonant excitation. The isolated bright line can be attributed to the neutral exciton [Huo13], as confirmed by polarization dependent photoluminescence measurements. The origin of the numerous additional lines could be determined through polarization, power, and temperature-

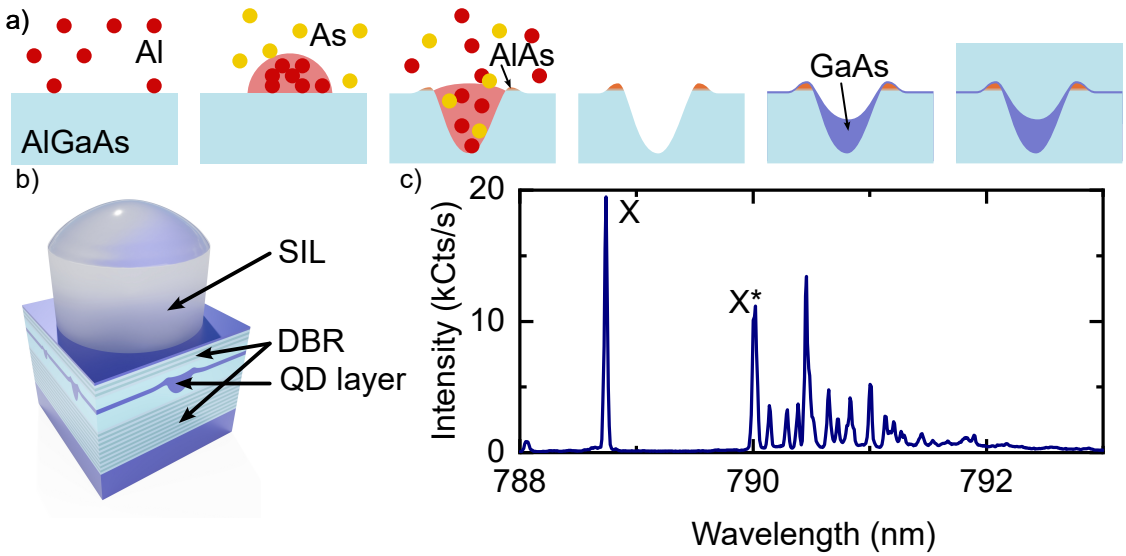

Figure 2.4 | Local droplet etching quantum dots a, Growth: Al droplets etch nanoholes into the AlGaAs substrate in an As atmosphere. The holes are filled with GaAs and are overgrown with an AlGaAs barrier layer **b**, Sample structure for papers 3, 5, and 6. The quantum dots are embedded in a planar distributed Bragg (DBR) reflector cavity and a solid immersion lens (SIL) is placed on the sample surface to improve the extraction efficiency. **c**, Typical spectrum of a GaAs quantum dot under nonresonant excitation. The neutral and charged exciton lines are indicated. b,c adapted from paper 3.

dependent photoluminescence measurements. However, these lines are most likely attributed to charged and excited (hot) excitonic states [Hub19]. Typically, the biexciton is either not visible or very faint under these excitation conditions due to competing transitions.

These quantum dots typically exhibit a much narrower wavelength distribution compared to Stranski-Krastanow quantum dots due to the homogeneous size of the nanoholes. The center wavelength is in the range of about $780 - 800\,\mathrm{nm}$, and can be controlled during growth by adjusting parameters such as the hole depth, the amount of GaAs fill, and the Al concentration in the barrier layer [Atk12]. This specific wavelength range makes this type of quantum dots particularly interesting for coupling to quantum memories based on rubidium atoms, given that both the ^{87}Rb D_1 line at $794.98\,\mathrm{nm}$ and the ^{87}Rb D_2 line at $780.24\,\mathrm{nm}$ fall within that spectral range [Ako11, Hua17]. Moreover, the highly symmetric holes in these quantum dots lead to very small average fine structure splittings of approximately $(3.9 \pm 1.8)\,\mu\mathrm{eV}$, which is on the order of the natural linewidth of the excitonic transitions [Huo13].

Their short lifetime of roughly 200 ps suggests that they are weakly confined in the potential [Hub19, Rei19]. The combination of small fine structure splitting and short lifetime makes these quantum dots promising candidates as sources of time-invariant polarization entangled photon pairs, as demonstrated in [Hub17]. Further reduction of the fine structure splitting could improve the entanglement fidelity and concurrence to near unity [Hub18]. Additionally, these quantum dots exhibit exceptional pure single-photon emission, with $g^{(2)}(0) = (7.5 \pm 1.6) \cdot 10^{-5}$ [Sch18b]. With such properties, quantum teleportation [Rei18] and entanglement swapping [BB19, Zop19] have been successfully demonstrated. Embedding the quantum dots in a diode structure [Bab21] provides a controlled charge environment with reduced noise, enabling near lifetime-limited linewidths [Zha20], near-unity indistinguishability above $V_{\mathrm{HOM}} = 95\,\%$ for photons from one quantum dot separated by 1 µs and remote indistinguishability of $V_{\mathrm{HOM}} = (90.9 \pm 0.8)\,\%$ from two quantum dots [Tom21, Zha22]. For further details regarding the local droplet etching growth and the properties of these quantum dots, refer to [Gur19] and [daS21]. These GaAs quantum dots have been used to demonstrate near-unity indistinguishability under s-shell resonant excitation of the neutral and charged exciton in paper 3, to show the intrinsic limitation of the biexciton-exciton cascade as a three-level quantum ladder system in terms of photon indistinguishability in paper 6, to investigate the origin of antibunching of a two-level system in the Rayleigh regime in paper 5, and to fabricate microparaboloids to enhance the extraction efficiency in paper 4.

2.1.5 InAsP quantum dots in InP nanowires

As-grown self-assembled quantum dots typically suffer from poor coupling efficiency to detection optics due to the high refractive index of the host material, resulting in a small critical angle for total internal reflection (see Sec. 6.2). Additionally, integration into photonic structures is challenging due to their random distribution. Quantum dots well-positioned in nanowire waveguides, however, are promising candidates as efficient sources of single photons or entangled photon pairs, as they can overcome these limitations. The fabrication of nanowire quantum dots started with top-down processes, where nanowires were etched into planar samples, that already contained self-assembled quantum dots. Due to the random distribution of the emitters, the number and position of the quantum dots inside the nanowire is either random,

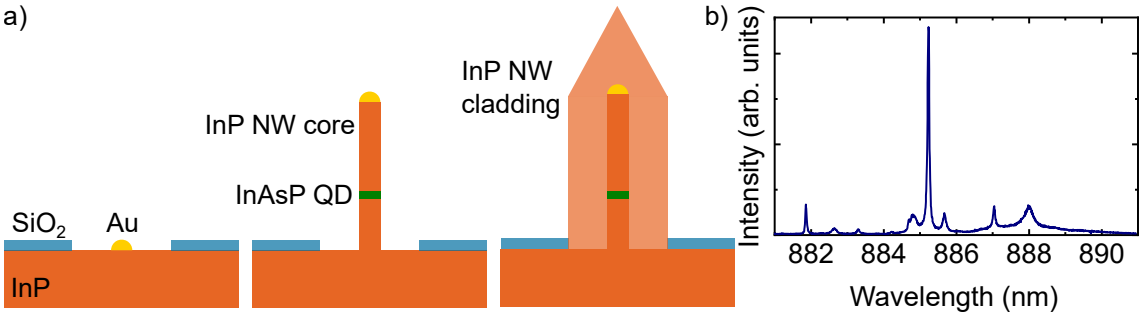

Figure 2.5 | InAsP quantum dots in InP nanowires a, growth: the InP substrate with SiO_2 is prepatterned with circular holes. Gold (Au) droplets act as catalysts for the InP nanowire (NW) core growth in vapor-liquid-solid mode. The InP cladding is grown in substrate growth mode **b**, Spectrum of the nanowire quantum dot under nonresonant excitation. b adapted from paper 2.

or the emitter has to be pre-characterized, and the position has to be determined with respect to markers. Therefore, in most cases, the emitters are off-center from the nanowire axis, which reduces the efficiency [Cla10, Ble11]. This drawback has been overcome by bottom-up processes that ensure that only one quantum dot is embedded in the center of the nanowire [Hei10, Rei12]. In these nanowires, the crystal structure alternates between wurtzite and zinc blende [Car11], leading to charge traps in the vicinity of the quantum dot, which degrades spectral properties in terms of single-photon purity, linewidth, and indistinguishability.

The nanowires used in papers 1 and 2 were grown by Philip J. Poole's group at the National Research Council of Canada in Ottawa using a new growth method that results in pure wurtzite structures [Dal12]. Depending on the growth conditions, the emitters can cover a wavelength range from 880 nm to 1550 nm. The process is illustrated in Fig. 2.5a. First, a (111)B InP substrate is coated with a layer of SiO_2. Site-controlled circular holes are written into the SiO_2 layer using electron beam lithography and HF acid wet etching (panel 1). Gold is then deposited using a self-aligned lift-off process to form approximately 20 nm diameter gold droplets inside the holes. This patterning of the substrate leads to site-controlled growth of InP nanowires [Dal09] (panel 2), which are grown by chemical beam epitaxy. First, conditions are selected to facilitate vapor-liquid-solid growth with the Au droplets as catalysts, resulting in pure wurtzite nanowires with a constant diameter determined by the size of the Au catalyst. After approximately 200 nm, the InAsP quantum

dot is created by switching one of the material sources from PH_3 to AsH_3 for a few seconds. Subsequently, the growth of the InP core is continued up to the desired length. To grow the nanowire cladding, the growth conditions are adjusted so that the vapor-liquid-solid growth is nearly stopped at the tip, and the substrate growth starts with the core as seed until a diameter of approximately 250 nm is reached (panel 3). Typically, the cladding is tapered at the tip to enhance the extraction efficiency.

In particular, quantum dots with an As content of approximately 30 %, resulting in an emission wavelength in the near-infrared spectral range, have been extensively studied and show promising results. An example spectrum under nonresonant excitation is shown in Fig. 2.5b. Due to the high symmetry [Sin09], these quantum dots exhibit very low average fine structure splittings of (3.4 ± 3.0) µeV, with more than 50 % of the nanowires below 2 µeV [Ver14], making them sources of polarization entangled photon pairs [Ver14, Hub14, Jön17]. Linewidths only a factor of two away from the lifetime limit and pure single-photon emission have been demonstrated [Rei16, Laf23]. Furthermore, these structures show great potential as integrated emitters, as they can be picked up in a controlled manner and transferred to another chip, i.e. with photonic integrated circuits, using a nanomanipulator (see Sec. 6.3) [Zad16, Els17] as we also did in paper 2. By tailoring the cladding growth, the nanowires can be optimized for various applications. Inducing a needlelike adiabatic taper at the tip results in nearly Gaussian modes [Bul14], while increasing the length enhances evanescent coupling to waveguides [Mna20]. In paper 1, the As content in the InAsP quantum dot was increased to systematically shift the emission wavelength to longer wavelengths in the telecom O- and C-band. Additionally, the effect of nanowire diameter and quantum dot size on the decay time and brightness was investigated.

2.2 Quantum emitters in transition metal dichalcogenides

Research on two-dimensional materials began with graphene in 2004 [Nov04], and the Nobel Prize in 2010. Since then, the family of two-dimensional crystals has expanded to other layered van der Waals crystals, including metals, semiconductors, and insulators. Of particular interest are materials with an optically accessible band gap, which now span over a wide spectral range from ultraviolet to telecom [Par22]. Transition metal dichalcogenides (TMDs or TMDCs) are a frequently studied group of two-dimensional materials with the stoichiometric formula MX_2, where M is a group IV, V, or VI metal and X is a chalcogen atom. Among these, MoS_2 and WSe_2 are commonly used in quantum optics, with the latter used in paper 7. Figure 2.6a,b illustrates the crystal structure of a WSe_2 monolayer from both the top and from the side (created using vesta [Mom11]) with the unit cell shown in petrol. The atoms form a two-dimensional layer consisting of three lattice planes with a hexagonal crystal structure. Within such a layer, the atoms are strongly bonded with covalent bonds, and no dangling bonds remain out of the plane. The bulk crystal is formed by stacks of such monolayers held together by van der Waals forces. This, in turn, allows the fabrication of monolayers without breaking the crystal symmetry in top-down processes from a bulk crystal. A commonly used technique is mechanical exfoliation [Nov05], which we also exploit in paper 7. A flux-grown WSe_2 bulk crystal is sandwiched between two strips of Scotch tape, which are then pulled apart, resulting in the splitting of the bulk crystal into thinner pieces. Repeating this process several times statistically yields monolayer thin flakes. The easiest way to check the flake thickness is under a light microscope, where areas of low contrast indicate fewer monolayers compared to high contrast areas. The identified monolayer flake can then be transferred to another substrate, e.g., to couple the emitter to a waveguide or cavity. In our work, we utilize an all-dry stamping process with PDMS stamps (see Sec. 6.3). While exfoliation typically yields flakes of good crystal quality, the process is time-consuming and often results in small flakes. For scalability, other fabrication methods are required, with bottom-up chemical vapor deposition growth being a commonly used approach. Various fabrication methods are discussed in [Bhi15].

From the primitive cell (Wigner-Seitz cell, green hexagon in Fig. 2.6a) it follows that

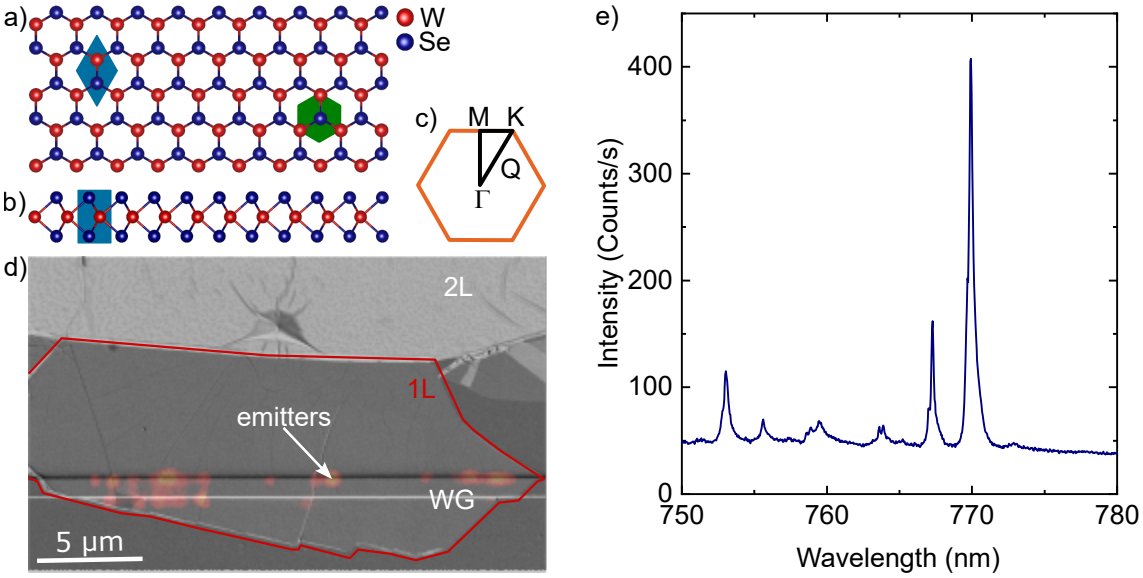

Figure 2.6 | Quantum emitters hosted in transition metal dichalcogenide monolayers a, Hexagonal crystal structure of WSe_2. The petrol parallelogram shows the unit cell with one W (red) and two Se (blue) atoms, the green hexagon is the Wigner-Seitz cell. **b**, Side view of a WSe_2 monolayer. **c**, First Brillouin zone of the crystal structure with high symmetry points Γ, Q, K, M. **d**, Scanning electron-beam microscopy picture of a WSe_2 monolayer (1L) covering a SiN waveguide (WG) overlayed with photoluminescence from single quantum emitters induced on the waveguide edges and wrinkles. The monolayer is still attached to region with bilayer (2L). **e**, Nonresonantly excited spectrum of quantum emitters hosted in a WSe_2 monolayer. d,e adapted from paper 7.

the first Brillouin zone in reciprocal space is also a hexagon, as shown in Fig. 2.6c with the high symmetry points Γ, Q, K, and M. The electronic band structure of the valence and conduction bands along the high symmetry points Γ-Q-K-M-Γ can be calculated with density functional theory for the bulk crystal and different numbers of layers [Kum12]. While the bulk WSe_2 crystal exhibits an indirect band gap from the Γ to the Q point, the material undergoes a transition to a direct band gap at the K point when thinned from a bi- to a monolayer.

Similar to quantum dots, excitonic quasiparticles can be excited in TMDs, which can recombine under the emission of a photon in the near-infrared spectral range. The first bright photoluminescence from a monolayer direct band gap material was demonstrated with MoS_2 [Mak10]. The first evidence for single-photon emission from WSe_2 followed in 2015 [Ton15, Kop15, He15]. Today, pure single-photon emission with $g^{(2)}(0) \approx 0.02$ is achieved under nonresonant excitation [Kum16]. Since the re-

combination process is very inefficient at an indirect band gap, the photoluminescence intensity increases by three orders of magnitude from a bi- to a monolayer [Mak10]. Therefore, photoluminescence signal intensity is another more reliable tool for monolayer identification.

The emitters hosted by two-dimensional materials typically appear at localized strain pockets induced by wrinkles, folds, or bubbles in the material [Ton15, Kum15, She17], or at flake interfaces [Kop15]. This phenomenon is often exploited to induce localized site-controlled emitters, such as, by transferring a monolayer onto a prepatterned substrate with small pillars [Bra17, Pal17]. Figure 2.6d shows a scanning electron-beam microscopy image of the sample used in paper 7. Here, a WSe_2 monolayer flake (highlighted in red) covers approximately 20 µm of a SiN waveguide. The sample image is superimposed with the photoluminescence signal acquired using the imaging setup described in Sec. 3.2.1. Figure 2.6e shows a typical spectrum of one of the emitters observed in Fig. 2.6d under nonresonant excitation. The emitters only appear at the edges of the waveguide, accompanied by wrinkles or ruptures in the flake at most of the emitter locations. The localization of emitters at local strain pockets suggests that the generation of single-photon emitters in two-dimensional materials is influenced by the local strain potential. However, the exact physical origin is still under debate. A theoretical model, capable of explaining many experimentally observed features, proposes the following: a strain-localized dark exciton hybridizes with the point defect state of a nearby Se vacancy, leading to the formation of an intervalley defect exciton [Lin19, Zhe19]. Another model attributes the formation of single-photon emitters to band gap modulation due to the bending of the material, e.g., in bubbles or wrinkles [Chi19]. Quantum confinement in the monolayer enhances the Coulomb interaction between the electron and the hole, resulting in a strong excitonic binding energy of a few hundred milli electronvolts [Ber13]. Consequently, excitons hosted by two-dimensional materials can be observed at room temperature, in contrast to excitons in bulk semiconductors [He14]. The strong Coulomb interaction also facilitates the formation of charged excitons and biexcitons with binding energies of a few tens of milli electronvolts, exceeding those of quantum dots in bulk materials by more than one order of magnitude [You15]. Due to the low thickness of the sample, the Coulomb interaction and hence the exciton binding energy are strongly influenced by the screening environment [Raj17]. Consequently, the substrate to which the

monolayer is transferred also affects the emission characteristics. Influences from defects, charge noise, phonons, and fluctuating electrical and strain environments additionally lead to spectral diffusion or wandering, causing a significant inhomogeneous broadening of the photoluminescence signal. A fit to the peak at 770 nm in Fig. 2.6e reveals a width of approximately 0.8 meV. Given the measured lifetime of 18 ns we expect a lifetime-limited linewidth that is more than ten times narrower. Encapsulation of TMD monolayers in hBN monolayers has been shown to reduce the linewidth, although the lifetime limit has not yet been reached [Cad17, Wie17]. This broadening mechanism has so far hindered the demonstration of indistinguishable photons from emitters hosted in TMD monolayers [Azz21]. Up to now, resonant excitation has been challenging for this type of emitter. The well-established filtering of the scattered laser signal in a cross-polarization setup for quantum dots (see Sec. 3.2.2) is not sufficient here. In paper 7 we employ side excitation (see Sec. 3.3) to utilize the waveguide for filtering a significant portion of the remaining laser. Only the scattered part entering the microscope objective used to detect the emitter signal was suppressed using polarization optics. We found that the suppression was not temporally stable, and we had to perform on-the-fly optimization. Kumar et al. [Kum16] observed a slow spectral jitter, likely due to charge noise. Consequently, the emitter was not always in resonance with the laser, and they performed temporal postselection in addition to polarization suppression. We both achieved only moderate laser suppression, resulting in $g^{(2)}(0)$ values in the order of 0.35. Although single-photon sources hosted by two-dimensional materials are relatively new and their optical properties are not yet comparable to those of self-assembled quantum dots, they possess properties that render them promising candidates for future applications [Cha19b]. Their direct access and the high resistance to strain allow for high tunability [Iff19]. Moreover, two-dimensional materials have great potential for coupling to microcavities [Duo18, Iff21] or photonic circuits [Pey19, Li21], given the relatively simple dry stamping transfer process (see Sec. 6.2.3). Furthermore, since the emitters are strain-induced, multiple emitters can be induced and coupled to the same photonic circuit, as we have also shown in paper 7 and Fig. 2.6d, which is an important building block towards scaling up quantum integrated photonic circuits.

Chapter 3

Cryogenic micro-photoluminescence spectroscopy

Contents

Single-photon emitters can be optically addressed by cryogenic micro-photoluminescence spectroscopy. The first part of this chapter starts with a brief overview of the setup used. This is followed by an in-depth discussion of the excitation methods used to obtain different conditions in the quantum system. More specific requirements for the setup will also be presented. While most of the measurements were performed in a setup with confocal geometry, measurements on photonic waveguides often require a photonic probe station, which is included at the end of this chapter.

3.1 Basic setup

Although the measurements have been carried out on different setups that have evolved over time, they all comprise three main components connected with optical fibers. The components of the system are: The excitation unit, which includes either a continuous wave or pulsed laser with a pulse shaper; the cryogenic microscope, which consists of a confocal microscope and a cryostat containing the sample; and the detection unit, which consists of filter and analyzer setups and detectors. All components can be connected in a modular fashion using polarization-maintaining single-mode fibers (Nufern PM780-HP). The fibers (DIAMOND GmbH) are fabricated using an active core alignment process that guarantees very low losses of less than 1 dB when two fibers are connected. A typical setup configuration is depicted in Fig. 3.1. Figure 3.1a illustrates the excitation unit for pulsed excitation. For the majority of experiments under pulsed excitation, we used an titanium:sapphire APE Berlin picoEmerald laser. The laser has a repetition rate of 80 MHz and a pulse duration of approximately 3 ps. It features two outputs, one for the signal (tunable from 650 to 980 nm) and another for the idler (tunable from 1080 to 2490 nm, not shown). Since our experiments require only low excitation powers, we begin by lowering the laser power to prevent nonlinear effects in the fibers. Since the polarizing beamsplitter cube transmits horizontally polarized light and reflects vertically polarized light, adjusting the laser polarization with a half-wave plate allows us to control the power entering the following setup. The horizontally polarized component is transmitted in the beamsplitter and blocked with a beam dump. To prevent back reflections that may impact the laser output stability and cause laser damage, we installed a Faraday isolator in the beam path, consisting of two linear polarizers rotated by 45° with respect to each other and a Faraday cell in between. In addition, the beam diameter is enlarged, for better spectral resolution in the following setup, by two lenses with different focal lengths mounted at a distance given by the sum of both focal lengths. A pinhole at the focal point between the lenses cuts out a Gaussian beam profile. Due to the time-bandwidth product, the short laser pulses exhibit a large spectral bandwidth. This broad laser spectrum is a disadvantage for our excitation schemes, so we spectrally shape the initial laser pulse and thus obtain longer pulses by using a pulse shaper in $4f$ geometry. The initial laser beam is depicted in gray, indicating its broad spectrum. Upon diffraction on a grating

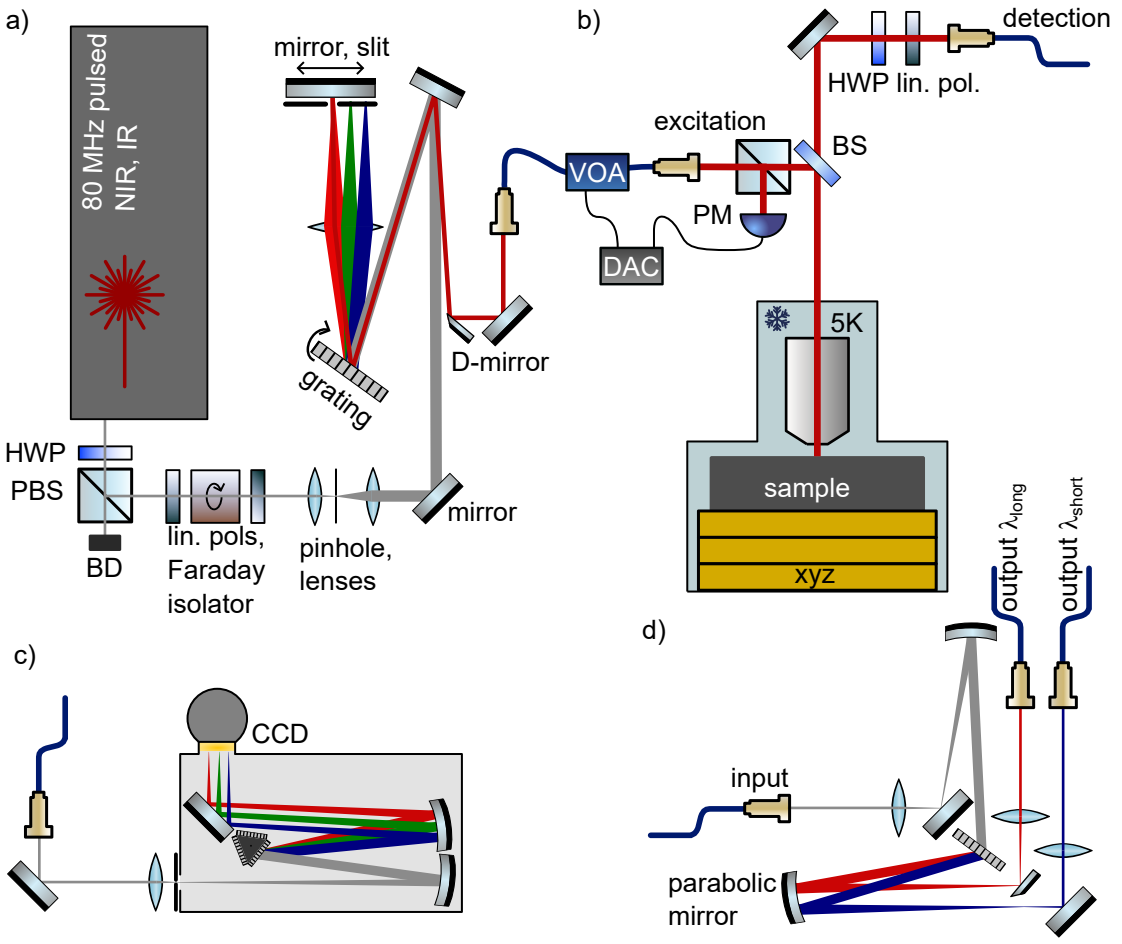

Figure 3.1 | Basic cryogenic micro-photoluminescence spectroscopy setup **a**, Excitation unit with a pulsed laser and a $4f$ pulse shaper to cut out a spectrally narrower component from the laser spectrum. **b**, Confocal cryogenic micro-photoluminescence setup. The excitation power is monitored and controlled using an optical power meter (PM), digital-to-analogue converter (DAC) and a fiber based variable optical attenuator (VOA). The laser is sent to the sample inside the cryostat with a beamsplitter (BS) and focused by a microscope objective. The emitted signal is coupled into a fiber. The half-wave plate (HWP) and lin. pol. are optional for polarization resolved measurements. **c**, Spectrometer with CCD. **d**, Transmission spectrometer to filter up to two spectral emission lines. PBS: polarizing beamsplitter, BD: beam dump, lin. pol.: linear polarizer, CCD: charge-coupled device camera

(Richardson Gratings, 1800 grooves/mm), each spectral component is diffracted at a different angle and thus spatially separated. The following lens is mounted at a distance of the focal length $f = 300\,\mathrm{mm}$ from the grating. It focuses each spectral

component onto a slit at distance f. By adjusting the slit width and horizontal position, the wavelength and spectral width of the laser can be controlled. The mirror located behind the slit folds the shaped beam (shown in red), back onto its original path. By offsetting the lens slightly, a vertical displacement is introduced in both unshaped and shaped beams. These beams can then be separated with a D-shaped mirror (shown here with a horizontal displacement). The shaped beam is coupled into a polarization-maintaining single-mode fiber using a collimator (Schäfter + Kirchhoff). It is then sent to the cryogenic confocal microscope. Continuous wave lasers exhibit a narrow linewidth and can thus directly be fiber coupled (not shown in Fig. 3.1a).

Figure 3.1b shows a simplified cryogenic setup for micro-photoluminescence spectroscopy. The sample is cooled down to approximately 5 K using a closed-cycle cryostat (AttoDry800 from attocube) to isolate the emitters from the semiconductor host matrix which disturbs the quantum system. Optical excitation of the sample from the top is possible through a window in the cryostat. Different excitation methods require modifications on the optical setup, which will be explained later in this chapter, whereas here, only the basic setup is described. The excitation laser is collimated and coupled out of the fiber using a collimator. The collimator lens in combination with the fiber results in a beam diameter of approximately 2.8 mm which matches the mode of the objective. A fiber-based variable optical attenuator based on micro-electromechanical systems (MEMS) technology is used to control and stabilize the excitation power based on an applied voltage. The laser power is monitored by tapping a part of the signal with a cube beamsplitter and detecting it with an optical power meter. A custom-built digital-to-analog converter sets the voltage for the attenuator based on the measured laser power. By applying $0 - 5\,\mathrm{V}$, the signal inside the fiber can be attenuated by up to 30 dB. To couple the laser into the cryostat, a beamsplitter is used in reflection. A microscope objective (attocube, 50×, NA= 0.81) mounted inside the cryostat focuses the laser on the sample. The sample and the objective are mounted on piezoelectric actuators (attocube) with a travel range of 5 mm, enabling positioning with sub nanometer precision of the sample under the objective and adjustment of the focus. The same objective is utilized in confocal geometry to collect the emitted signal from the sample, which is then coupled into a polarization-maintaining single-mode fiber using an identical collimator as the one

for the excitation laser. The signal can then be sent flexibly to different filtering, analysis, and detection modules. Optionally, a rotatable half-wave plate and a linear polarizer can be mounted in front of the detection fiber for polarization resolved measurements. For spectral analysis of the quantum emitter, the signal is sent to a spectrometer (Princeton Instruments HRS-750) with a focal length of 750 mm, shown in Fig. 3.1c. There are three different gratings available to choose from via a turret. Typically, a high resolution grating with 1800 lines/mm is used for the near-infrared quantum dots. This results in a diffraction window of approximately 10 nm and a resolution of around 40 µeV. The signal is detected by a liquid nitrogen cooled CCD (charge-coupled device) with 1340×400 pixels (Princeton Instruments PyLoN).
For most time-resolved correlation measurements, the detected signal has to be filtered using a self-built fiber-coupled transmission spectrometer, as illustrated in Fig. 3.1d. A lens and parabolic mirror are used to expand the beam diameter, since better resolution is achieved by illuminating a larger area of the transmission grating (Lightsmyth, 1500 lines/mm). Transmission efficiency of the grating is maximized in the Littrow configuration. Each separated spectral component of the signal is focused by a second parabolic mirror behind the transmission grating. At the focal point, a D-shaped mirror is placed on a manual translation stage to separate two spectrally distinct lines of an emitter, i.e. the exciton and biexciton lines of a quantum dot. In the separated paths, lenses collimate the signals, which are then coupled into polarization-maintaining single-mode fibers. Our transmission spectrometer has a bandwidth of 19 GHz and an end-to-end efficiency of about 60 %. The filtered signal can be routed to different correlation spectroscopy setups (see Secs. 4.3 and 5.2), where it is detected by two superconducting nanowire single-photon detectors (SNSPDs) from Single Quantum B.V. (not shown in Fig. 3.1). These detectors have efficiencies of 50 % and 60 %, respectively, low dark count rates of less than $1\,\mathrm{s}^{-1}$ and timing jitter of 20 ps and 30 ps.

3.2 Excitation methods

The excitation method for quantum emitters has a crucial influence on the properties of the emitted photons. There are two primary differentiations - pulsed or continuous wave excitation. With the latter method, the excited state can be immediately repopulated after recombination to the ground state, which often leads to higher count rates, but does not reveal any information about the emission time of the photons. Under pulsed excitation, the emission time of the photon are synchronized with the trigger of the pulsed laser, enabling the generation of single or entangled photons on-demand.

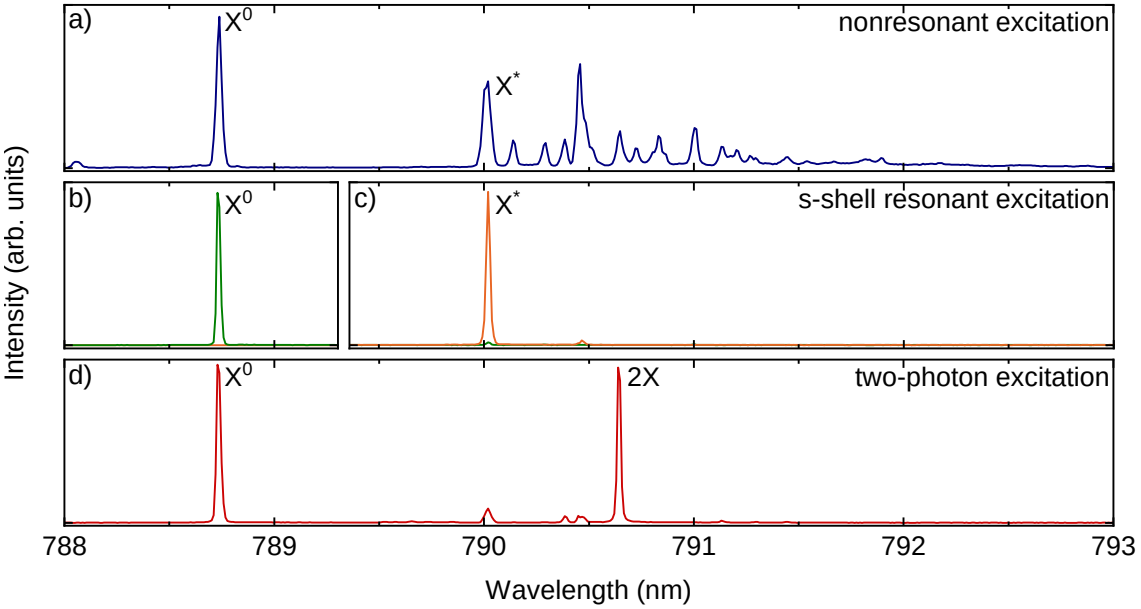

Figure 3.2 | GaAs quantum dot spectrum under different excitation conditions **a**, nonresonant **b**, s-shell resonant excitation of the neutral exciton **c**, s-shell resonant excitation of a charged exciton **d**, two-photon excitation. a-c adapted from paper 3.

Furthermore, the excitation wavelength has a significant impact on the emission properties. Figure 3.2 shows the same GaAs quantum dot under three different well-established excitation techniques. Whereas under nonresonant excitation (Fig. 3.2a), multiple states are excited simultaneously, resulting in many emission lines with slightly different wavelengths, only one state, the neutral or charged exciton can be excited under s-shell resonant excitation (Fig. 3.2b,c). Due to competing processes, a minor contribution of less than 2 % each is visible from the charged exciton when

resonantly exciting the neutral exciton, and from an unidentified higher excited state when resonantly exciting the charged exciton. Two separated lines, namely the biexciton and the exciton are visible under two-photon excitation (Fig. 3.2d). Each of these excitation methods reveals different properties of the quantum emitter and are therefore suitable for different measurements, but also have their drawbacks. Continuously, new methods are being proposed and investigated to overcome certain limitations. In this section, I provide an overview of all the excitation methods used throughout my thesis, and discuss their specific setup requirements as well as their advantages and disadvantages. Since my work focuses primarily on quantum dots as emitters, the following explanations will be based on them. For quantum emitters hosted by a two-dimensional monolayer, we only used nonresonant and s-shell resonant excitation. Examples of coherent excitation techniques not employed in this thesis include excitation with red and blue detuned pulses [He19, Koo21, Van23], as well as the swing-up scheme using two red detuned pulses [Bra21, Bra23, Kar22, Boo24]. Examples of incoherent excitation processes include excitation via the adiabatic rapid passage using chirped pulses [Wei14, Kap24] and phonon-assisted excitation of a single- or two-photon state [Ard14, Rei19]. These methods also generate single and indistinguishable photons but are more robust against fluctuations in excitation power compared to coherent excitation methods.

3.2.1 Non- and quasi-resonant excitation

Nonresonant and quasi-resonant excitation refers to techniques where the laser energy is greater than the energy of the emitted photons. This includes above-band excitation, where the energy is greater than the band gap of the surrounding semiconductor, and excitation into higher quantum dot states, such as the p- or d-shell or via longitudinal optical phonons. These excitation methods are convenient to realize experimentally, as the laser wavelength is spectrally well separated from the emission. As a result, it can be easily filtered using longpass or bandpass filters. Especially above-band and p-shell excitation is commonly employed for basic sample characterization and finding a quantum dot with certain required properties, such as a specific wavelength or low fine structure splitting. Under these excitation conditions, the electrons are excited into the conduction band or higher shells within the confined emitter leaving a hole in the valence band. Once excited, these electrons

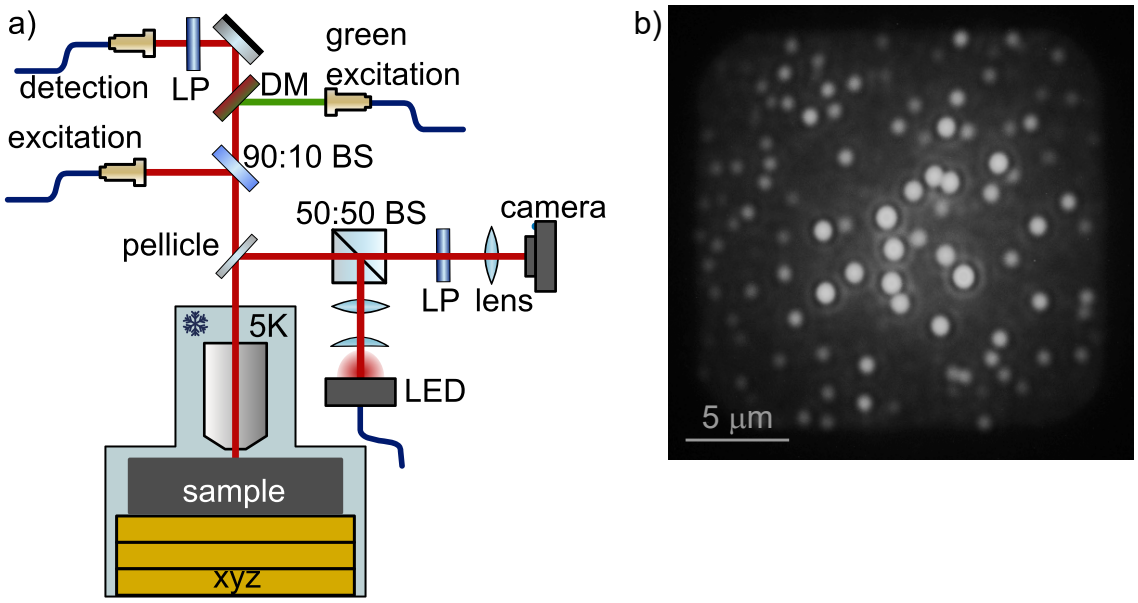

Figure 3.3 | Cryogenic microscope setup a, The excitation laser is sent via a 90:10 beamsplitter (BS) or dichroic mirror (DM) into the cryostat. A cryogenic microscope objective focuses the laser onto the sample, which can be positioned by three piezo actuators. The emitted signal is coupled into a polarization-maintaining single-mode fiber. An imaging unit can be used by inserting a flip pellicle. A fiber-coupled LED is used for flat illumination of the sample surface which is imaged using a CMOS camera. An optional longpass filter (LP), enables imaging of single emitters **b**, Imaging of a GaAs quantum dot sample. Each bright spot is the photoluminescence of a single quantum dot.

recombine with non-radiative scattering processes into the lowest confined state, from which a radiative recombination into the ground state occurs, resulting in the emission of photons. These scattering processes cause a timing jitter on the emission times. Furthermore, the lines can be inhomogeneously broadened through carrier-phonon [Leo03] or carrier-carrier [Usk01] interactions, hindering the generation of highly indistinguishable photons.

The cryogenic microscope, used for nonresonant and quasi-resonant excitation, is shown in Fig. 3.3a. When the excitation wavelength is close to the emission wavelength of the emitters, a 90:10 beamsplitter is employed to couple the laser into the cryostat. Therefore, we employ a narrow linewidth diode laser (Toptica DLPro) or the pulsed laser introduced above. Alternatively, a long-pass dichroic mirror with a cutting edge of 635 nm is used when the excitation wavelength is significantly

shorter than the emission (green diode laser (Oxxius 522-070) or red helium neon laser). Both beamsplitter and dichroic mirror are mounted on a magnetic mount for convenient removal from the beam path when not in use. The remaining setup is identical to the basic micro-photoluminescence spectroscopy configuration described earlier. Spectral filtering of the laser can be achieved through the dichroic mirror or longpass filters.
An imaging system can be inserted into the beam path by using a flip pellicle for the purpose of navigating on the sample and selecting individual emitters. A fiber-coupled LED provides flat illumination of the sample and is coupled into the beam path with a 50:50 cube beamsplitter. Imaging of the sample surface is possible with a CMOS camera (Thor labs Deluxe), which has the sensitivity to also image individual emitters. Depending on the type of emitter, either a defocused green laser or the LED serves as the excitation source. A longpass filter mounted in front of the camera blocks the excitation source. For the imaging of GaAs quantum dots, a green laser is used in combination with a longpass with a cutting edge of 750 nm. By increasing the camera gain and exposure time to approximately 2 s, individual quantum emitters can be observed, as presented in Fig. 3.3b. This technique allows for the reliable retrieval of individual emitters even after sample exchange in the cryostat or emitter localization with respect to markers for deterministic fabrication of e.g. microcavities.

3.2.2 s-shell resonant excitation

The resonant excitation of a quantum two-level system leads to the emission of resonance fluorescence (RF) photons, and only one clean dominant line is visible in the spectrum. Fig. 3.2b,c shows the resonance fluorescence of the neutral and charged exciton from paper 3. The minor other contributions account for less than 2 % and come from competing processes, e.g., phonon assisted excitation. The energy level scheme for the case of an exciton with fine structure leading to two excited states as shown in Fig. 3.4a with the resonant excitation laser (solid double arrow) and the radiative decay channels (dotted arrows). For the purposes of theoretical description, the fine structure is disregarded, and the system is modeled as a two-level system. Since the charged exciton is a true two-level system without fine structure splitting, the same theoretical description applies. Quantum mechanically, this excitation

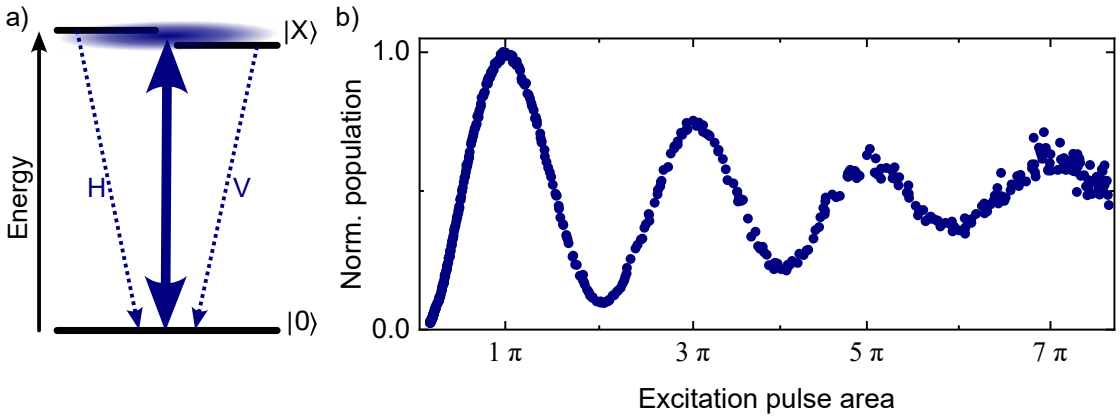

Figure 3.4 | s-shell resonant excitation a, Energy scheme of an exciton with fine structure splitting. The excitation laser (double arrow) resonantly couples to the system and excites it from the ground $|0\rangle$ to the exciton $|\mathrm{X}\rangle$ state. Linearly cross-polarized resonance fluorescence photons (dotted arrows) are emitted upon recombination. **b**, Rabi oscillations of an exciton in a GaAs quantum dot, adapted from paper 6.

method can be described by a laser field of frequency ω_0 resonantly coupled to the ground $|\mathrm{g}\rangle$ and excited $|\mathrm{e}\rangle$ state of a quantum two-level system [Fox06]. The system is in a superposition of the two states, $|\Psi\rangle = c_\mathrm{g}(t)\,|\mathrm{g}\rangle + c_\mathrm{e}(t)\,|\mathrm{e}\rangle$, with probabilities $|c_{\mathrm{g,e}}(t)|^2$ of finding the system in the respective states. Moreover, $|c_\mathrm{g}(t)|^2 + |c_\mathrm{e}(t)|^2 = 1$. By solving the Schrödinger equation, we obtain $|c_\mathrm{e}(t)|^2 = \sin^2\left(\frac{\Omega_0 t}{2}\right)$, which means that under strong driving of the two-level system, the system's probability to be in a particular state oscillates with the Rabi frequency $\Omega_0 = \left|\frac{\mu_\mathrm{eg} E_0}{\hbar}\right|$. Here, μ_eg denotes the dipole moment and E_0 is the amplitude of the driving electromagnetic field. The Rabi frequency is proportional to both the electric field and the square root of the excitation power, i.e. $\Omega_0 \propto E_0 \propto \sqrt{P}$. For pulsed excitation, the electric field amplitude becomes time-dependent and thus the Rabi frequency as well. Therefore, a pulse area $\Theta = \left|\frac{\mu_\mathrm{eg}}{\hbar}\int_{-\infty}^{+\infty} E_0(t)dt\right|$ is defined, and the excited state population can be expressed as $|c_\mathrm{e}(t)|^2 = \sin^2\left(\frac{\Theta}{2}\right)$. In reality, these oscillations are dampened by various mechanisms, which can be classified into two types: damping mechanisms that reduce the population of the excited state as described by the time constant T_1 and decoherence effects as described by T_2. The former is caused by the spontaneous emission itself. A system in its excited state tends to decay back to its ground state under the emission of a photon caused by vacuum fluctuations. Other non-radiative decay channels may also affect T_1, but are usually insignificant during resonant

excitation of the two-level system. T_1 can therefore be regarded as the excited state lifetime. The damping resulting from decoherence is described by the total dephasing rate $\frac{1}{T_2} = \frac{1}{2T_1} + \frac{1}{T_2^*}$. The first term accounts for loss of phase coherence in the wave function as a result of recombination. Population-conserving dephasing mechanisms, also known as pure dephasing, are characterized by the time constant T_2^*, and are caused by the interaction of the two-level system with the environment. The quantum dots are embedded in a semiconductor host matrix, where longitudinal acoustic phonons are the main source of dephasing [Ram10, För03]. Cooling the sample to cryogenic temperatures partially decouples the system from the semiconductor environment and reduces the number of phonons, thus reducing the pure dephasing.

The damped Rabi oscillations can be observed by analyzing the intensity of the excited transition for increasing excitation pulse area as shown in Fig. 3.4b for an exciton in a GaAs quantum dot. As the laser suppression is non-trivial with this excitation method (see next paragraph), even moderate powers lead to a laser background in the signal. However, in order to show the oscillations more clearly, I have subtracted the laser contribution determined here with a fit. The most efficient way to excite the system is through a π-pulse, where near-unity population inversion from the ground to the excited state is accomplished. This excitation condition is chosen for all resonant pulsed measurements included in this thesis.

Gibbs demonstrated the first observation of Rabi oscillations with rubidium atoms [Gib72, Gib73]. Whereas it was first shown for a quantum dot under resonant optical excitation and detection in the photocurrent by Zrenner et al. [Zre02]. Muller et al. [Mul07] first showed resonance fluorescence with quantum dots in a microcavity in 2007. Optical selection rules limit this excitation method to excitons and charged excitons. In order to resonantly excite the biexciton, two-photon excitation is required, which is introduced in Sec. 3.2.3. With this excitation scheme, near-unity indistinguishability and pure single-photon emission has been presented [He13, Tom21]. We used this excitation scheme in paper 3 to show near-unity indistinguishability (see Ch. 5) on neutral and charged excitons in GaAs quantum dots without the need of Purcell enhancement. Furthermore, the limitations and advantages of quantum two- and three-level systems were investigated by comparing the same quantum dots under this and two-photon excitation (paper 6). In paper 5 we used this excitation method

in continuous wave operation to investigate a two-level system in the Rayleigh regime. For paper 7 also s-shell resonant continuous wave excitation was explored to show resonance fluorescence from a quantum emitter in a WSe_2 monolayer.

Polarization suppression

Under s-shell resonant excitation, the excitation laser can no longer be spectrally filtered, but only via polarization. We use a setup design similar to the one presented by Kuhlmann et al. [Kuh13], which is depicted in Fig. 3.5a. The resonant excitation laser is linearly vertically polarized using a nanoparticle linear film polarizer in a motorized rotation stage. The laser is directed to the sample using a polarizing beamsplitter cube in reflection and passes through a quarter-wave plate also mounted in a motorized rotation stage. The same objective described in Sec. 3.2.1 is used. Since both the laser and the emitter have the same wavelength, the laser beam can be well focused to a spot size of about 1 µm. The emitted signal from the sample is collected in a confocal geometry through the same objective, and only horizontally polarized components of the signal pass through the polarizing beamsplitter in transmission and a fixed nanoparticle linear film polarizer that is well aligned with the horizontal polarization. The detection signal is coupled into a polarization-maintaining single-mode fiber. The reflection of a highly focused polarized signal always exhibits a perpendicular polarization component (here horizontally polarized) with a cloverleaf distribution in the far field [Nov01]. This component is transmitted through the polarization optics, while the majority of the backscattered laser remains vertically polarized and is strongly suppressed by reflection in the polarizing beamsplitter cube and absorption in the linear polarizer. Figure 3.5b shows this characteristic horizontally polarized intensity distribution of the remaining laser, recorded with a beam profiler in front of the detection fiber. Since the backscattered laser shows an intensity minimum in the center, where the emission of the quantum emitter is located, the laser can be further suppressed by using the detection fiber with a core diameter of 5 µm as a spatial filter. By carefully and iteratively aligning the input linear polarizer and the quarter-wave plate angles, which compensates for small birefringence effects from optical components in the beam path or from the sample itself, laser suppression of almost eight orders of magnitude can be achieved (see Fig. 3.5c). The suppression is highly sensitive on the quarter-wave plate angle, and

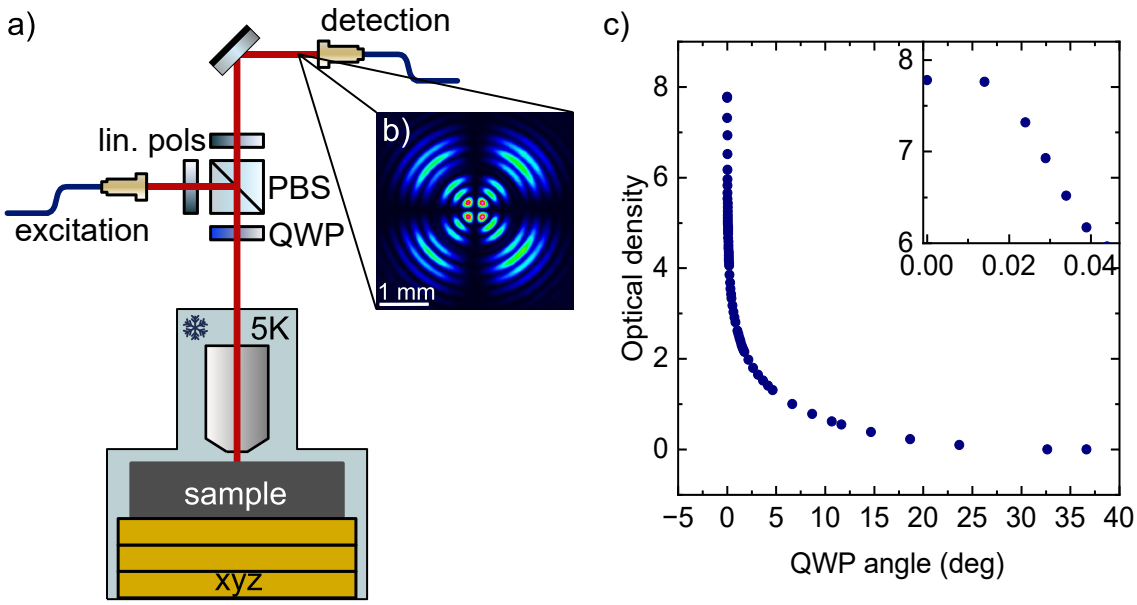

Figure 3.5 | Cryogenic microscope setup with polarization suppression a, For resonant excitation, the linearly polarized laser is sent onto the sample via a polarizing beamsplitter cube (PBS). The backscattered laser signal is polarization filtered by the PBS and a linear polarizer (lin. pol). The quarter wave plate (QWP) compensates for small imperfections in the polarization. **b**, Far-field beam profile of the back reflection of the strongly focused excitation laser. **c**, Optical density of the laser suppression as a function of the QWP angle.

a change of 40 mdeg reduces the suppression already by two orders of magnitude, as shown in the inset Fig. 3.5c. Although the degree of suppression depends on the sample (e.g. material, surface quality, etc.), and achieving the same degree of suppression is not always feasible, the power needed to achieve π-pulse excitation can be effectively suppressed. Additionally, the quarter-wave plate angle required to achieve optimal suppression is highly sensitive to the wavelength. Consequently, a pulsed laser with a spectral width much broader than the quantum dot emission cannot be uniformly suppressed. Therefore, the signal is always filtered with our transmission spectrometer before any correlation measurement is conducted.

At this point it is worth returning to the energy level scheme in Fig. 3.4a. Charged excitons, as true two-level systems, emit circularly polarized light. However, due to polarization suppression, only horizontally polarized light can be detected. Since circular polarization can be expressed as $|\mathrm{R,L}\rangle = \frac{1}{\sqrt{2}}(|\mathrm{H}\rangle \pm i\,|\mathrm{V}\rangle)$ it indicates that

only the horizontal component can be detected. Consequently, this results in a single exponential decay when measuring the lifetime (see paper 3 and Sec. 4.3). The exciton typically exhibits fine structure splitting (see Sec. 2.1.2), resulting in two excited states with perpendicular linear polarizations H and V. The polarization of the excitation laser determines the polarization of the initial exciton spin. If none of the quantum dot axes align with the excitation polarization, as determined by the polarizing beamsplitter cube, the spin starts precessing on the Poincaré sphere until the state recombines [Ste08b]. When the quantum dot axis is aligned at an 45° angle with respect to the setup polarization, the spin precesses around the equator of the Poincaré sphere, and the wave function becomes

$$|\Psi_{\mathrm{X}}(t)\rangle = \frac{1}{\sqrt{2}}\left(|\mathrm{V}\rangle\, e^{-i\frac{E_{\mathrm{V}}t}{\hbar}} + |\mathrm{H}\rangle\, e^{-i\frac{E_{\mathrm{H}}t}{\hbar}}\right) = \frac{1}{\sqrt{2}} e^{-i\frac{E_{\mathrm{V}}t}{\hbar}}\left(|\mathrm{V}\rangle + |\mathrm{H}\rangle\, e^{-i\frac{E_{\mathrm{FSS}}t}{\hbar}}\right) \quad (3.1)$$

with the energies of the two fine structure states $E_{\mathrm{H,V}}$ and the fine structure splitting $E_{\mathrm{FSS}} = E_{\mathrm{H}} - E_{\mathrm{V}}$. The frequency of the spin precession is thus given by $\frac{E_{\mathrm{FSS}}}{\hbar}$. If the angle between the excitation polarization and the quantum dot axis differs from 45°, the spin precesses on other latitudes of the Poincaré sphere. Given that only one polarization component is detected in our setup, the lifetime measurement is modulated with an oscillation, known as quantum beats [Fli01, Dad16].

3.2.3 Two-photon excitation

For resonant excitation of the biexciton state, a two-photon excitation process must be used. The energy level scheme is shown in Fig. 3.6a. The ground and exciton states remain the same as for the s-shell resonant excitation, but now the biexciton level is also included. Due to the Coulomb interaction between the charge carriers, the biexciton energy is not precisely twice the exciton energy. Here we only use samples with a positive biexciton binding energy, where the biexciton-exciton transition has a lower energy than the exciton-ground state transition, since two-photon excitation competes with phonon-assisted excitation of the exciton in samples with negative biexciton binding energy [Jus20]. To resonantly excite the biexciton, a laser with half the energy of the biexciton state (solid double arrows in Fig. 3.6a) is employed, exciting the state through a two-photon process via a virtual state. Since the exciton state has higher energy than the laser photons, it is not directly populated

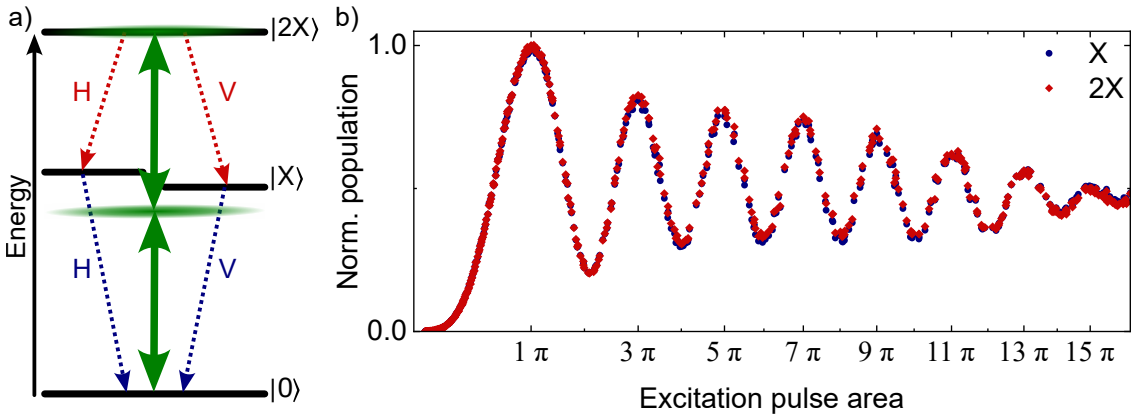

Figure 3.6 | Two-photon excitation a, Energy level scheme. The biexciton state $|2X\rangle$ is resonantly excited in a two-photon process (green double arrows). The system recombines back to the ground state $|0\rangle$ in a cascaded emission (dotted arrows) via the intermediate exciton state $|X\rangle$. **b**, Rabi oscillations of the exciton (X) and biexciton (2X) of a GaAs quantum dot, adapted from paper 6.

resonantly or via phonons. This excitation method was initially demonstrated by Brunner et al. in 1994 [Bru94] on quantum dots. To recombine the biexciton back to the ground state, the first electron-hole pair recombines into one of the two fine structure states of the exciton by emitting a biexciton photon (red dashed arrows). Subsequently, the remaining exciton recombines to the ground state by emitting the exciton photon (blue dashed arrows). This decay process is called radiative cascade or biexciton-exciton cascade. Two emission lines of equal intensity from the biexciton and the exciton are characteristic features of the spectrum of a quantum dot under two-photon excitation. Figure 3.2d shows a typical spectrum of a GaAs quantum dot used in paper 3. For these quantum dots, the separation between the exciton and biexciton lines is approximately 1.9 nm (3.9 meV). Thus, the excitation laser is well separated from both emission lines, allowing for either polarization suppression or spectral filtering (e.g., narrow volume Bragg grating filters). In Fig. 3.2d the laser is polarization suppressed. The remaining other small contributions arise from a charge carrier captured after biexciton excitation or weak phonon-assisted excitation of the charged exciton and other states [Ard14, Qui15, Bou15], as the charged exciton transition in this type of quantum dots usually aligns closely with the required laser wavelength. This excitation method coherently controls the biexciton state, observable through Rabi oscillations. Since the laser is spectrally separated, much

higher excitation powers can be applied than in s-shell resonant excitation, and more oscillations can be distinguished experimentally, as shown in Fig. 3.6b.
The radiative cascade inherently provides polarization entangled photon pairs. This, along with the coherent nature of the excitation process, renders two-photon excitation the preferred method for on-demand generation of polarization entangled photon pairs [Mül14], facilitating the realization of more complex quantum optical experiments, such as entanglement teleportation [Rei18] and entanglement swapping [BB19, Zop19]. Cascaded emission also protects the system from so-called re-excitation [Han18] and ensures the purest single-photon emission [Sch18b]. In contrast to direct s-shell resonant excitation, two-photon excitation suffers from limited Hong-Ou-Mandel indistinguishability (see Ch. 5) of consecutively emitted photons, as we have demonstrated in paper 6. It can be explained in a simplified picture not encompassing the entire theory the following: the exciton lifetime leads to a finite linewidth of the exciton state due to the time-bandwidth product. This is the final state of biexciton decay, and thus introduces an energy jitter on consecutively emitted biexciton photons. On the other hand, the biexciton lifetime introduces a timing jitter in the exciton state population and thus in the decay. We demonstrated that the indistinguishability is limited by the ratio of the two lifetimes $V_{\mathrm{HOM}} = \frac{T_{\mathrm{X}}}{T_{\mathrm{X}}+T_{2\mathrm{X}}}$ [Sim05]. The theoretical lifetime ratio is $\frac{T_{2\mathrm{X}}}{T_{\mathrm{X}}} = 0.5$, as the biexciton has two potential decay channels while the subsequent exciton has only one. This restricts the degree of indistinguishability to 67 %. To restore near-unity indistinguishability of the exciton, modifications to the two-photon excitation scheme introduced in paper 8 and Sec. 3.2.4 are necessary. Certain applications, such as entanglement-based quantum repeaters (e.g., the scheme of Lloyd et al. [Llo01]), require the simultaneous generation of near-unity indistinguishable and highly entangled photon pairs. Engineering the state lifetimes with microcavities could mitigate this limitation. Asymmetric Purcell enhancement can shorten the biexciton lifetime, thereby reducing the lifetime ratio and restoring good indistinguishability (see paper 6 Supplementary).
A related excitation method, more robust to laser power and wavelength fluctuations, is phonon-assisted two-photon excitation with a slightly blue-detuned laser [Glä13]. While it does not provide coherent control of the system, it also achieves near-unity population inversion [Ard14] and shows no further decrease in indistinguishability [Rei17].

3.2.4 Stimulated two-photon excitation

To overcome the intrinsic limitation of Hong-Ou-Mandel indistinguishability under two-photon excitation, we developed an extension of this excitation method presented in paper 8. The energy level scheme is illustrated in Fig. 3.7a. After resonant excitation of the biexciton state, the system can spontaneously decay via the radiative cascade (dotted arrows), resulting in the population evolution of the biexciton and exciton states, as depicted in Fig. 3.7b (dashed lines). The biexciton decays to the exciton state in a mono-exponential decay. This gradually increases the exciton population, which then decays exponentially to the ground state. The slow rise of the population causes the timing jitter in the exciton decay, thus reducing the indistinguishability. In the here presented stimulated two-photon excitation scheme, a second laser pulse with a short delay to the two-photon excitation pulse τ_{Stim}, resonantly couples to the biexciton-exciton transition (orange arrow in Fig. 3.7a), to selectively depopulate the biexciton and prepare the exciton state. To confirm the coherent driving of the biexciton-exciton transition by the stimulation pulse, Rabi oscillations between the biexciton and exciton transition are recorded in Fig. 3.7c. Initially, the two-photon excitation pulse is set to a constant pulse area π to ensure optimal population of the biexciton state. To measure the biexciton intensity, the horizontally polarized stimulation laser must be polarization suppressed, and only the photons in the vertical decay path are detected. Increasing the power of the stimulation pulse reveals clear Rabi oscillations. At the power corresponding to a π-pulse, a minimum in biexciton intensity is observed, indicating that the spontaneous biexciton emission is almost completely suppressed and the population is successfully transferred to the exciton state. The following measurements are performed with pulse areas of π for both pulses. By varying the delay between the two pulses τ_{Stim} in comparison to the exciton lifetime T_{X}, we identified the following four regimes:

- $\tau_{\mathrm{Stim}} \leq 0$: The biexciton state is not yet populated, and the stimulation pulse cannot stimulate this transition, resulting in the normal radiative cascade and thus the same indistinguishability as for two-photon excitation.

- $\tau_{\mathrm{Stim}} \approx 0.03 \cdot T_{\mathrm{X}} = 9\,\mathrm{ps}$: The biexciton is populated by the two-photon excitation pulse. The population is then transferred to the exciton state by the stimulation pulse, from where it spontaneously decays. This leads to a reduced timing

jitter in the exciton decay, as shown in Fig. 3.7b with solid lines. Consequently, this process leads to improved indistinguishability, comparable to that achieved under s-shell resonant excitation.

- $\tau_{\mathrm{Stim}} \approx T_{\mathrm{X}}$: The biexciton decays spontaneously, and is re-excited by the stimulation laser followed by the normal radiative cascade, leading to an even larger timing jitter and thus to a reduced indistinguishability compared to two-photon excitation.

- $\tau_{\mathrm{Stim}} \gg T_{\mathrm{X}}$: The system decays spontaneously via the radiative cascade before the stimulation pulse arrives, and the indistinguishability is again the same as for two-photon excitation.

By measuring the indistinguishability of the exciton under stimulated two-photon excitation with different delays τ_{Stim} and comparing it with two-photon excitation, we verified the four scenarios above. Furthermore, by comparing the same quantum dot under s-shell resonant excitation, we could demonstrate that the same degree of indistinguishability of $V_{\mathrm{HOM}} = 86.4^{+0.9}_{-1.2}\%$ could be achieved with stimulated two-photon excitation. This is most likely the intrinsic limit of this quantum dot due to dephasing mechanisms. In contrast to s-shell resonant excitation, stimulated two-photon excitation requires only spectral filtering, which is experimentally more robust than polarization suppression. Moreover, the polarization of the stimulating laser selects the decay channel so that nearly all exciton photons have the same polarization (here horizontal). As a result, this excitation method shows nearly doubled count rates while preserving the same level of single-photon purity as under two-photon excitation, and exhibits a degree of indistinguishability comparable to that achieved through direct population of the exciton under s-shell resonant excitation.

The experimental setup for this scheme is depicted in Figure 3.7d. As the required laser energies are similar, a single laser with approximately 120 fs long pulses is utilized. The output is split into two paths, each directed into a separate pulse shaper (see Sec. 3.1) to cut out the necessary wavelength and spectral width from the original laser pulse. The stimulation pulse is delayed by τ_{Stim} with respect to the two-photon excitation pulse using a variable delay line. Half-wave plates are employed to set the polarization of both pulses. The polarization of the two-photon

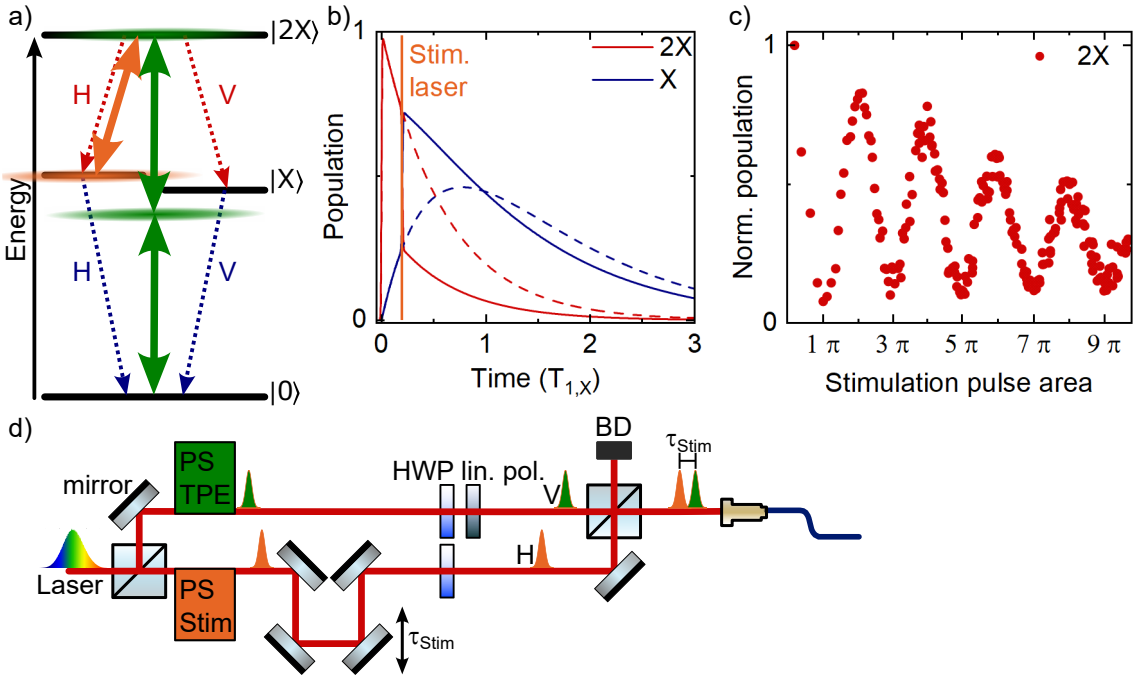

Figure 3.7 | Stimulated two-photon excitation **a**, Energy level scheme. The system is excited to the biexciton state with a two-photon excitation process (TPE, green). The radiative cascade is shown in red (2X) and blue (X). An additional laser (orange) stimulates the 2X transition. **b**, Populations of the 2X and X states under TPE (dashed) and stimulated TPE (solid). After a short time delay, the stimulation laser (orange line) stimulates the 2X transition and thus inverts the 2X and X population. Therefore, the timing jitter on the X population is reduced. **c**, Rabi oscillations of the V polarized 2X photons. **d**, Setup to prepare the excitation pulses. The femtosecond laser pulse is split up and two individual spectral components for TPE (green) and the stimulation process (Stim, orange) are cut out in pulse shapers (PS). A variable delay τ_{Stim} is introduced on the latter pulse. a-c adapted from paper 8.

excitation pulse is set to vertical with respect to the quantum dot fine structure axis and is further cleaned by a linear polarizer. The polarization of the stimulation pulse is set to be horizontal. The two pulses are then combined using a beamsplitter cube. In Hong-Ou-Mandel experiments (see Sec. 5.2), this beamsplitter is employed as the first splitter in the delay line to create double pulse pairs with a delay of τ_{HOM}, which is not shown in Fig. 3.7d. The pulses are transmitted through an optical fiber to the cryogenic microscope. The stimulation laser polarization (horizontally polarized in this case) sets the decay channel, which is stimulated. Consequently, polarization suppression cannot be applied to the stimulation pulse. Therefore, the two-photon

excitation pulse is partially suppressed by polarization suppression (see Sec. 3.2.2). However, the main filtering is achieved through a filtering setup similar to the pulse shaper introduced in Sec. 3.1. For more information, refer to paper 8.

3.2.5 Stimulated down-conversion

This excitation method represents an extension of the two-photon excitation that allows for optical control of photons emitted by a quantum dot. It is introduced and investigated in more detail in [Hei15] and paper 9. The scheme is illustrated in Fig. 3.8a. The system is populated in the biexciton state using two-photon excitation (green). A nonresonant control laser (orange), which is energetically close to the biexciton-exciton transition (here, blue detuned), creates a virtual state. Consequently, the system can decay not only via the known radiative cascade but also via the virtual state, emitting a photon in a stimulated down-conversion (SDC) process (petrol) satisfying

$$E_{2X} = E_{Ctrl} + E_{SDC}, \tag{3.2}$$

with the energies of the biexciton E_{2X}, the control laser E_{Ctrl} and the stimulated down-conversion photon E_{SDC}. Figure 3.8b shows the schematic setup. A picosecond pulsed laser (Coherent Mira900) in continuous wave mode is used for two-photon excitation. The control laser (Ctrl) is a tunable continuous wave diode laser (Toptica CTL900). Both lasers are coupled out of a single-mode fiber using a collimator. To define the polarization of the control laser, it is first cleaned by a linear polarizer and then manipulated by either a half-wave plate for linear polarization or a quarter-wave plate for circular polarization. Both lasers are combined with a 70 : 30 beamsplitter cube and then coupled into the cryostat via another beamsplitter. The collected emission is passed through the beamsplitter into the detection path. To analyze the polarization of the signal, an identical wave plate as in the control laser path and a linear polarizer are used. Both lasers are spectrally filtered by several tunable volume Bragg grating filters (Optigrate) before the detection fiber (not shown).
The spectrum in Fig. 3.8c shows the exciton and biexciton emission from the radiative cascade, both lasers which are not fully suppressed, and the stimulated down-conversion emission on the longer wavelength side of the exciton. Due to the high excitation power, the positively charged exciton is also visible here. The same colors

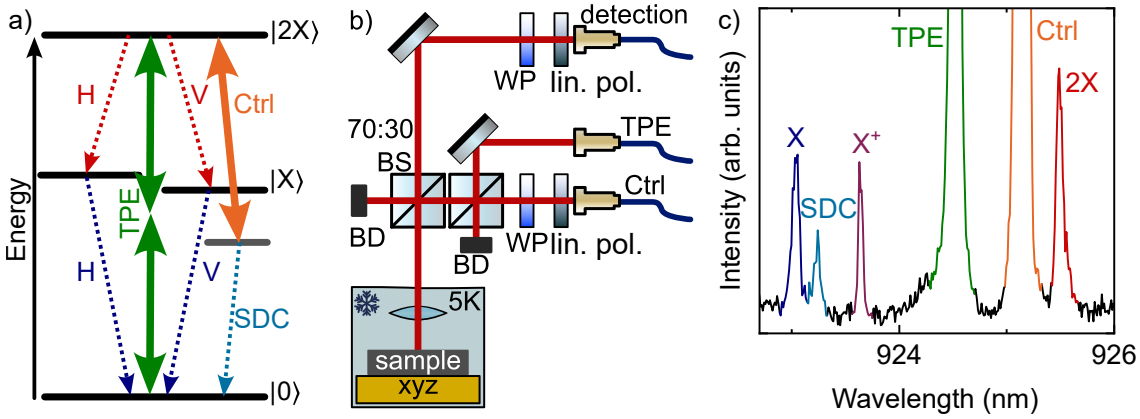

Figure 3.8 | Stimulated down-conversion a, Energy level scheme. The system is excited to the biexciton (2X) state with a two-photon excitation process (TPE, green). The radiative cascade is shown in red (2X) and blue (exciton, X). A control laser (Ctrl, orange), here blue detuned to the 2X transition defines a virtual state which enables the stimulated down-conversion (SDC, petrol). **b**, Setup. The TPE and Ctrl lasers are combined using a 70:30 beamsplitter (BS). Both lasers are coupled to the sample using another 70:30 BS. The signal is detected in a confocal geometry and coupled into a single-mode fiber. To investigate the polarization dependence of the SDC emission on the Ctrl laser polarization, a set of linear polarizer (lin. Pol.) and half- or quarter-wave plate (WP) can be mounted in the Ctrl laser and detection path each. **c**, Spectrum of the cascade and SDC emission in the configuration shown in a. The positively charged exciton (X^+, purple) is visible due to phonon assisted excitation by the TPE laser.

as in Fig. 3.8a are used. The stimulated down-conversion process also works with the control laser near the exciton transition and with red or blue detuning to the respective transition, always satisfying Eq. (3.2). This allows tuning of the stimulated down-conversion emission by approximately 0.5 meV around each transition. Here, the quantum dot is tuned by changing the gate voltage of the diode, i.e., by exploiting the quantum confined Stark effect (see Sec. 6.1.2), instead of tuning the laser. Thus, there was no need to readjust the spectral filtering of the laser. The high excitation powers of the two-photon excitation laser allow for robust population of the biexciton state via phonon-assisted two-photon excitation over the entire tuning range.
Furthermore, the polarization of the stimulated down-conversion photon can be controlled by manipulating the polarization of the control laser. Given the optical selection rules for a two-photon process with a total angular momentum of zero, the photon spins of the control laser and the stimulated down-conversion process must

sum up to zero. Thus, for a linearly polarized laser, the stimulated down-conversion emission has the same linear polarization, whereas for circular polarization, the polarizations are opposite. In general, for any polarization, the stimulated down-conversion process can be represented as a reflection of the control laser polarization on the equatorial plane of the Poincaré sphere.
The radiative cascade and the decay via the stimulated down-conversion process compete, with the latter having a much lower probability, resulting in the diminished intensity of the stimulated down-conversion photon. To address this issue in the future, the quantum dot could be embedded inside a cavity with high Purcell enhancement. To maintain polarization control, a polarization-degenerate cavity such as a micropillar or bullseye cavity could be used. The biexciton state can be prepared on demand by using a pulsed two-photon excitation laser. By employing a pulsed control laser with variable delay to the two-photon excitation laser pulse and variable pulse length, the timing and spectral shape of the stimulated down-conversion photon could be controlled. This can be realized as in Sec. 3.2.4, where two pulse shapers are used to cut single pulses from the same femtosecond laser. This method has the potential for all-optical control of emission energy, spectral shape, and polarization of single photons, as proposed theoretically [Hei15, Bre16, Bre18].

3.3 Photonic probe station

A photonic probe station serves the purpose to characterize photonic integrated circuits or facilitates the coupling of light to and from a waveguide to excite integrated quantum emitters and/or detect their emitted signals coupled to the waveguide. This setup has been used in papers 2 and 7. The cryostat contains a photonic probe station, depicted in Fig. 3.9. A lensed fiber (OZ Optics) [Son18] is clamped to a stack of three piezoelectric actuators, enabling movement in all three directions. This stack is mounted adjacent to the sample on the piezoelectric actuators used to position the sample in the previously described setups. The laser is sent through the fiber and scatters at its tip, a feature visible in the imaging unit introduced in Sec. 3.2.1 (not shown), helping in identify the fiber position. Once the fiber is positioned near the cleaved waveguide edge, the waveguide output is monitored by the imaging system, and the fiber position is adjusted to maximize the scattered signal at the waveguide

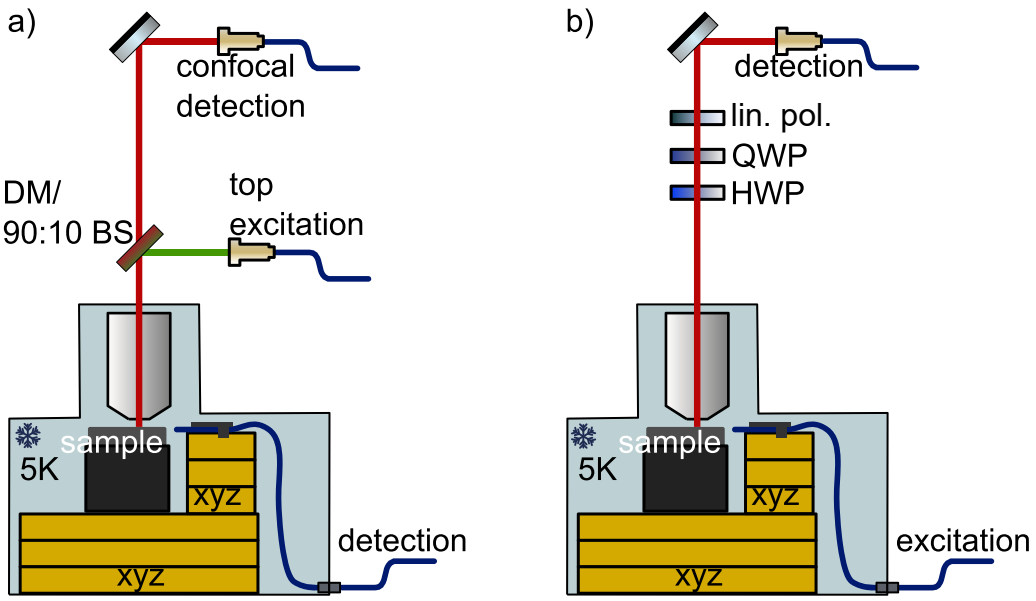

Figure 3.9 | Photonic probe station a, for nonresonant excitation. The laser is coupled to the cryostat with a dichroic mirror (DM) or 90:10 beamsplitter (BS) and excites the sample from top through the microscope objective. The emission can be detected confocally from top or through the waveguide and the lensed fiber mounted on a set of piezoelectric actuators. **b**, for resonant excitation. The sample is excited in-plane by coupling the resonant excitation laser via the lensed fiber to the waveguide. The detection is out-of-plane from top through the objective. To filter the scattered laser, the laser polarization is suppressed using a half- and quarter-wave plate (HWP, QWP) and a linear polarizer (lin. pol.).

output. Figure 3.9a illustrates the geometry for top excitation and detection through the waveguide and lensed fiber. The quantum emitters hosted in the WSe_2 monolayer (paper 7) were nonresonantly excited with either a green continuous wave diode laser or a pulsed red laser diode at 638 nm with a variable repetition rate, while the InAsP nanowire quantum dots (paper 2) were nonresonantly excited with a picosecond pulsed laser at 795 nm. The laser is coupled to the sample from the top via either a dichroic mirror or a 90 : 10 beamsplitter and the same microscope objective as in the other setups. The emitted photons can be detected in two geometries. A portion of the signal is coupled to the waveguide, which can be detected via the lensed fiber in the photonic probe station. Another portion of the signal is emitted to the top and can be collected in a confocal geometry.

For resonant excitation of the quantum emitters hosted by the WSe_2 monolayer in

paper 7, the excitation and detection have been swapped, as depicted in Fig. 3.9b. The linearly polarized excitation laser is coupled to the waveguide via the lensed fiber and then used to excite the emitter. The waveguide geometry aids in confining most of the laser signal in the horizontal plane, while only a small portion is scattered out of the waveguide and collected by the objective. To suppress this scattered portion, we use a set of half-wave and quarter-wave plates along with a linear polarizer to suppress the polarization of the laser. Unfortunately, achieving well-defined laser polarization is challenging in this setup, as the lensed fiber is not polarization-maintaining, the waveguide has a rough surfaces, and the scattering process slightly scrambles the polarization. Consequently, a lower laser suppression is attained compared to the confocal geometry described in Sec. 3.2.2. Nonetheless, this suppression is sufficient to observe single-photon emission.

Chapter 4

Single photons

Contents

Quantum light sources that emit pure single photons are essential for various quantum technology applications, particularly in the field of quantum communication, for example for quantum key distribution based on the BB84 protocol [Ben14]. To grasp the fundamental differences to classical light sources, it is crucial to identify their distinct characteristics. Hence, this chapter introduces three different types of light: coherent light, thermal light, and non-classical Fock states. These types of light feature different probability distributions of photon numbers in a mode, resulting in different photon number variations. Moreover, the second-order intensity correlation function is introduced as a tool to determine the photon statistics of a light source. Experimental realization is demonstrated using a Hanbury-Brown and Twiss type interferometer. Typically, this experiment is used by us to demonstrate the non-classical behavior of a light source and determine the single-photon purity.

4.1 Types of light

The emission of light from single quantum systems fundamentally differs from that of thermal or coherent light sources, which consist of many or clusters of emitters. In order to describe these differences, it is necessary to introduce the concept of non-classical light, i.e. the possibility of creating states of light that are occupied by a defined and fixed number of quanta, i.e. photons. Consequently, light can no longer be fully described classically as an electromagnetic wave; instead quantization of the field is necessary [Fox06]. In a simplified picture, the emission of a light source can be viewed as a flux of photons. Depending on the type of source, the photons adhere to different photon statistics. In the following discussion, three types of light are introduced and classified based on their probability distribution $\mathcal{P}(n)$ to detect n photons in a mode and the photon number fluctuation characterized by the standard deviation Δn. A detailed description can be found in standard books on quantum optics [Fox06, Lou00].

Coherent light A coherent state of light, also known as Glauber state, is described by an electromagnetic wave with constant phase, frequency, and amplitude. Glauber [Gla63] provided a complete quantum mechanical description of these states. The probability of finding n photons in a mode follows a Poisson distribution:

$$\mathcal{P}(n) = \frac{\overline{n}^n}{n!}\mathrm{e}^{-\overline{n}}, \qquad \Delta n = \sqrt{\overline{n}}, \tag{4.1}$$

with the mean photon number $\overline{n}$. The photon number distribution peaks at $\overline{n}$, as depicted in Fig. 4.1a for $\overline{n} = 10$. At high intensities, the relative photon number fluctuation vanishes: $\frac{(\Delta n)^2}{\overline{n}^2} = \frac{1}{\overline{n}} \xrightarrow[\overline{n}\to\infty]{} 0$. As the Glauber state describes a monochromatic wave with constant phase and amplitude, $\Delta n = \sqrt{\overline{n}}$ represents the lower limit for the intensity fluctuations of classical light. A good approximation for coherent light is the emission of a single-mode continuous wave laser.

Thermal light Light sources composed of many emitters are subject to classical intensity fluctuations. For instance, an incandescent light bulb, which is a blackbody radiator, has a broad spectrum of modes that can be described by harmonic oscillators coupled to a thermal bath and a radiation field. The number of photons in a single

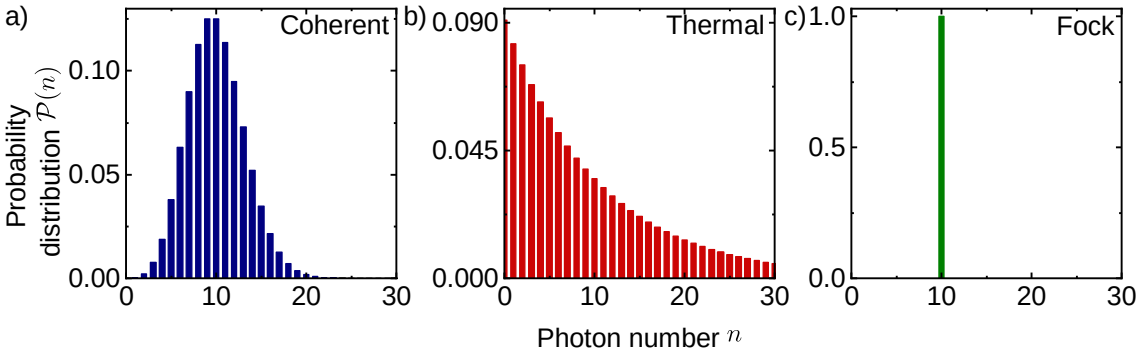

Figure 4.1 | Types of light Photon number distribution for **a**, coherent light states, showing a Poisson distribution, **b**, thermal light states with a Bose-Einstein distribution and **c**, Fock states with a sub-Poissonian distribution. For all types, the mean photon number is $\overline{n} = 10$.

mode follows the Bose-Einstein distribution:

$$\mathcal{P}(n) = \frac{1}{\overline{n}+1}\left(\frac{\overline{n}}{\overline{n}+1}\right)^n, \qquad \Delta n = \sqrt{\overline{n}+\overline{n}^2}. \tag{4.2}$$

The additional classical intensity fluctuations result in a larger standard deviation and a broader probability distribution compared to coherent light, leading to super-Poissonian statistics. Moreover, the probability of finding an empty mode is consistently the highest, as shown in Fig. 4.1b for $\overline{n} = 10$.

Fock state Light with a probability distribution narrower than coherent light, $\Delta n < \sqrt{\overline{n}}$, is considered non-classical and follows a sub-Poissonian distribution. The purest states of light are Fock states, which are the basis states of the quantized field Hamiltonian for a single mode ω.

$$\hat{\mathcal{H}} = \frac{\hbar\omega}{2}\left(\hat{a}\hat{a}^\dagger + \hat{a}^\dagger\hat{a}\right) = \hbar\omega\left(\hat{n} + \frac{1}{2}\right). \tag{4.3}$$

Here, $\hat{a}$ and $\hat{a}^\dagger$ represent the lowering (annihilation) and raising (creation) operators, respectively, and $\hat{n} = \hat{a}^\dagger\hat{a}$ is the photon number operator. The Fock state is the eigenstate of the photon number operator $\hat{n}\,|n\rangle = n\,|n\rangle$ and is thus a direct consequence of the second quantization. The exact photon number in a given mode implies a

delta-like probability distribution with vanishing standard deviation:

$$\mathcal{P}(n) = \delta_{n\overline{n}}, \qquad \Delta n = 0, \tag{4.4}$$

which is shown in Fig. 4.1c for $\overline{n} = 10$. A Fock state with $n = 1$ can be generated by a single quantum emitter, such as single atoms or ions [Hig16], color centers in diamond [Kur00, Sch11b], or silicon, semiconductor quantum dots [Mic00, Sch18b], or emitters in two-dimensional materials [Ton15, Kop15, He15]. In the course of this thesis, the focus was primarily on the latter two, which are discussed in more detail in Ch. 2. It is interesting to note the distinction between Fock states and photon number states: a Fock state contains a certain number of photons in a single and well-defined mode [Man66], while a photon number state is an operational term for the state detected by a photon number resolving detector, which usually cannot distinguish between modes. Therefore, all Fock states are photon number states, but not vice versa [Bie23].

4.2 Second-order correlation function

Classifying a light source by its photon number distribution is experimentally challenging. Realistic setups suffer from losses due to imperfect optical transmission and non-uniform detection efficiency. As a consequence, a source with a Fock state character will have a Poissonian character with an increased standard deviation $\Delta n > 0$ [Fox06]. One solution is to characterize light fields by field correlation functions. The first-order intensity correlation function $g^{(1)}(\tau)$ quantifies the electric field fluctuations in time and is a measure of the coherence time T_2 of a light source. It can be measured with a Michelson interferometer [Mic87], but is not considered further here. The second-order intensity correlation function $g^{(2)}(\tau)$, hereafter referred to as the second-order correlation function, quantifies the intensity fluctuations, and is a measure of the probability of detecting a photon after a certain time delay from a first photon. When both photons come from the same source, it is called the second-order autocorrelation function, as opposed to the crosscorrelation function where the photons come from two sources or two transitions in the same source. It

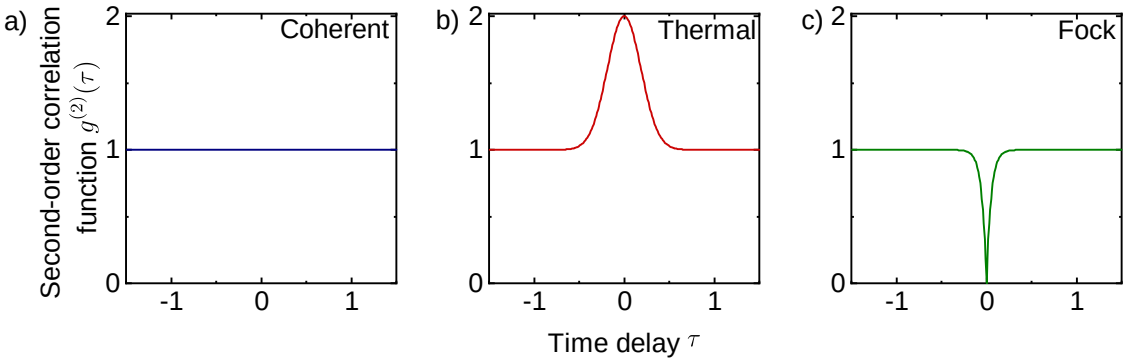

Figure 4.2 | Second-order correlation function $g^{(2)}(\tau)$ **a**, Coherent light shows no correlation on any time scale. **b**, Thermal light shows bunching on the time scale of the coherence time. Here a thermal light source with Gaussian broadening is shown. **c**, Fock state with $n = 1$ shows antibunching behavior with the width of the dip given by the emitter lifetime.

is classically defined as

$$g^{(2)}(\tau) = \frac{\langle I(t)I(t+\tau)\rangle}{\langle I(t)\rangle \langle I(t+\tau)\rangle}, \tag{4.5}$$

where $I(t)$ is the intensity of the light at time t and $\langle \dots \rangle$ is an average over a long integration time. In the case of a single-mode radiation field only, the second-order correlation function can be expressed quantum mechanically as

$$g^{(2)}(\tau) = \frac{\left\langle \hat{a}^\dagger \hat{a}^\dagger \hat{a} \hat{a} \right\rangle}{\langle \hat{a}^\dagger \hat{a} \rangle^2}. \tag{4.6}$$

Since signals are not correlated on long time delays, the second-order correlation function is always one for large τ. The value at zero time delay $g^{(2)}(\tau = 0)$ determines the probability of detecting two photons simultaneously. It can be shown that [Lou00]:

$$g^{(2)}(0) = 1 + \frac{\Delta n^2 - \overline{n}}{\overline{n}^2}. \tag{4.7}$$

To distinguish between the different types of light introduced in Sec. 4.1, the respective standard deviations from Eq. (4.1, 4.2 and 4.4) can be inserted and we obtain the following probabilities of detecting two photons simultaneously:

Coherent light $g^{(2)}(0) = 1$. This type of light has no intensity fluctuations and therefore has the same probability of detecting a second photon for all time delays with $g^{(2)}(\tau) = 1$. The second-order correlation function is shown in Fig. 4.2a.

Thermal light $g^{(2)}(0) = 2$. The probability of multiple photons being emitted at the same time is increased, and the photons bunch. This intensity correlation occurs only on the time scale of the coherence time T_2, and the value of the second-order correlation function drops to one for longer delays. The shape is determined by a Gaussian for a thermal light source such as a light bulb (shown in Fig. 4.2b) or a Lorentzian for a homogeneously broadened source [Fox06].

Fock state $g^{(2)}(0) = 1 - \frac{1}{n} \leq 1$. For Fock states and photon number states, the probability of detecting multiple photons at the same time is reduced, which is called antibunching. The time scale for this intensity correlation is determined by the lifetime of the emitter. For a single photon source ($n = 1$), $g^{(2)}(0) = 0$, as shown in Fig. 4.2c. Note that photon antibunching and a sub-Poissonian photon statistic both show non-classical behavior of light, but conditions can be constructed where one of the two effects does not imply the other [Sin83, Zou90].
Since $g^{(2)}(0) = 0.5$ for a two-photon source, 0.5 is the threshold to demonstrate single-photon emission [Grü19].

4.3 Time correlated single-photon counting

Due to the lack of detectors without timing jitter and dead time, the second-order correlation function cannot be measured directly. An experimental realization is a so-called Hanbury-Brown and Twiss (HBT) interferometer. It was originally developed by Hanbury-Brown and Twiss to measure the diameter of stars [Han56].
A schematic of the setup is shown in Fig. 4.3a. The signal is split on a non-polarizing 50 : 50 beamsplitter with detectors coupled to the two output ports. Since the intensity is proportional to the detected photon number $n_{1,2}(t)$ at each detector, Eq. (4.5) can be rewritten as

$$g^{(2)}(\tau) = \frac{\langle n_1(t) n_2(t+\tau) \rangle}{\langle n_1(t) \rangle \langle n_2(t+\tau) \rangle}. \tag{4.8}$$

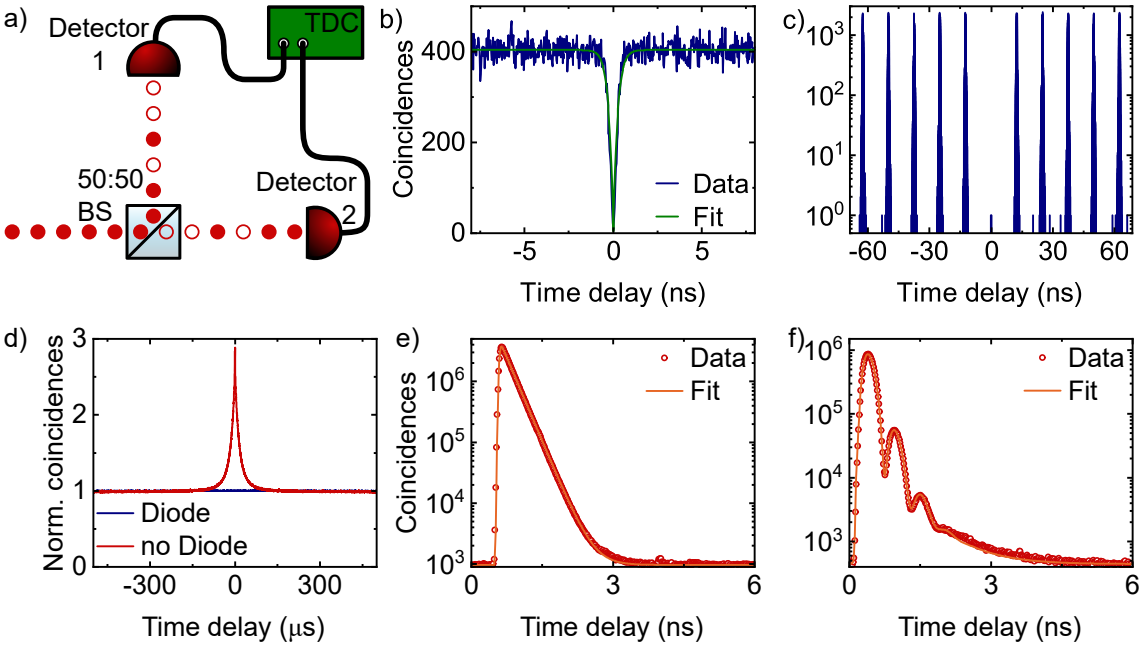

Figure 4.3 | Time correlated single-photon counting a, Schematic Hanbury-Brown and Twiss experiment setup consisting of a non-polarizing $50:50$ beamsplitter (BS) and two single-photon detectors at the outputs. The arrival times are recorded with a time-to-digital (TDC) converter. The red filled circles denote photons, whereas the empty circles show the positions of photons, which took the other path on the BS. **b**, Second-order autocorrelation histogram with fit of an exciton in a GaAs quantum dot under resonant continuous wave excitation with $g^{(2)}(0) = 0.0 + 0.027$. **c**, Second-order autocorrelation histogram of an biexciton in an GaAs quantum dot under pulsed two-photon excitation with $g^{(2)}(0) = (4.5 \pm 3.2) \cdot 10^{-5}$. **d**, Normalized second-order autocorrelation histogram for long time scales revealing strong blinking for an uncontacted sample. The blinking is suppressed in quantum dots embedded in a diode structure. **e**, Lifetime measurement of a charged exciton in a GaAs QD. The fit reveals a lifetime of (236 ± 2) ps **f**, Lifetime measurement of the neutral exciton. The fit yields a lifetime of (196 ± 2) ps and a fine structure splitting of (7.44 ± 0.05) µeV. e,f adapted from paper 3.

Correlating the detection events on both detectors results in a histogram that resembles the unnormalized second-order correlation function $G^{(2)}(\tau)$. Typically, we filter the emission line in a transmission spectrometer (see Sec. 3.1) before sending it into a fiber-coupled evanescent beamsplitter connected to SNSPDs (Single Quantum B.V.), which have a timing jitter of 20 and 30 ps. Only for paper 8, we used single-photon avalanche photo diodes with substantially longer timing jitters of approximately 300 ps. The electrical output of the detectors is sent to

a time-to-digital converter (PicoQuant HydraHarp 400 or qutools quTAG), which records the time stamps of the detection events. The time-tagged data are analyzed using ETA [Lin21], a self written software by my colleagues, or the Python script readPTU [Bal19] from our collaborators in Brian Gerardo's group at Heriot-Watt University in Edinburgh, which provides histograms of coincidences versus time delay. The autocorrelation histogram of an exciton in a GaAs quantum dot (see Sec. 2.1.4) under resonant continuous wave excitation is shown in Fig. 4.3b. The data was fitted by using [Mic03]

$$G^{(2)}(\tau) = C\left[1 - \left(1 - g^{(2)}(0)\right) \mathrm{e}^{-\frac{|\tau-\tau_0|}{T_1}}\right] \tag{4.9}$$

with the Poisson level C, which is the number of coincidences for long time delays where the photons are not correlated, the excited state lifetime T_1, and a time offset τ_0. The fit yields a single-photon purity of $g^{(2)}(0) = 0.0 + 0.027$ and a lifetime of $T_1 = (242 \pm 9)\,\mathrm{ps}$.

Pulsed excitation is often used to generate triggered or on-demand single photons, which are often required in experiments or future quantum technology applications. Figure 4.3c shows the resulting autocorrelation histogram of a biexciton in a GaAs quantum dot under two-photon excitation in a semi-logarithmic plot. It features peaks with exponential decays corresponding to the excited state lifetime as the flanks superimposed with a histogram for continuous wave excitation, leading to the missing peak at zero time delay. The peaks occur approximately every 12.5 ns, which corresponds to the repetition rate of our 80 MHz laser. For pulsed measurements, all photons emitted within an excitation pulse are considered, and thus the re-excitation emission (especially in the case of s-shell resonant excitation) is included, even though the photons are not emitted simultaneously, but with a short delay. Due to the timing jitter of the detectors and electronics, they cannot be separated. Despite filtering or suppressing the excitation laser, avoiding ambient stray light to coupling into the setup by darkening the laboratory, and using SNSPDs with extremely low dark count rates far below $1\,\mathrm{s}^{-1}$, the count rates on the detectors still contain a small contribution from the just mentioned sources, which also leads to false coincidences in the histogram. Since it is difficult to obtain the exact count rates of the individual contributions, and since future applications can also only suppress them to a certain degree, we only obtained the raw value for $g^{(2)}(0)$ as followed: Since the peaks in the histogram are well separated, we define a window 3.2 ns wide around each peak,

more than 10× longer than the excited state lifetime, where we sum the number of coincidences to obtain the peak area. The ratio of the center peak area A_0 to the average side peak area $\overline{A_i}$ gives the single photon purity. In the shown measurement it results in a single-photon purity of $g^{(2)}(0) = (4.5 \pm 3.2) \cdot 10^{-5}$, which is the highest purity measured for quantum light sources up to now, thanks to the suppressed re-excitation in the radiative cascade [Han18, Sch18b] (see Sec. 3.2.3), good laser suppression, and low detector dark counts.

The first demonstration of a single-photon source with a Hanbury-Brown and Twiss type experiment was with a stream of sodium atoms in 1977 [Kim77]. The proof for quantum dots was in 2000 [Mic00] and for quantum emitters hosted by two-dimensional materials in 2015 [Ton15, Kop15, He15]. The highest single-photon purity among all solid state emitters was shown with a GaAs quantum dot under two-photon excitation, where re-excitation is strongly suppressed [Sch18b].

Analyzing the autocorrelation measurement on long time scales reveals the so-called blinking of a light source, as shown in Fig. 4.3d. The blinking leads to an additional correlation in the form of a bunching with exponential decay. This can be attributed to slowly varying charge states inside or in the vicinity of the quantum dot [Hou12, Tho16], leading to a shift of the transition into and out of resonance with the excitation laser [Jah15]. The GaAs quantum dots from paper 3, 5, and 6 all show blinking with an on/off ratio of about 3 and a timescale in the microsecond range. This phenomenon can be observed under both continuous wave and pulsed excitation. Embedding the quantum dots in a diode structure (see Sec. 6.1.2) can stabilize the charge state and the environment and thus suppress the blinking as shown in Fig. 4.3d.

Hanbury-Brown and Twiss-type measurements were performed in all papers of this thesis to prove the single-photon character of the investigated quantum light sources and determine the purity. In paper 6 we show the limit of s-shell resonant excitation in terms of single-photon purity, which we attribute to re-excitation, and also show that this is almost completely suppressed under two-photon excitation [Han18]. In paper 5 we investigate the origin of antibunching under weak continuous wave excitation conditions, the so-called Rayleigh regime. By narrow filtering, the antibunching dip disappears in the autocorrelation measurement. As proposed by López Carreño et al. [Car18], homodyne detection restores the antibunching, but would require a

blinking free source, which we did not have at that time.
Instead of splitting the signal and performing an autocorrelation measurement, it can be correlated with different signals to reveal other properties of the source. Recording the electrical clock of the pulsed excitation laser and correlating it with the signal of the studied transition, often referred to time-correlated single-photon counting, reveals the lifetime of the excited state. The corresponding histograms of a charged and neutral exciton in a GaAs quantum dot under pulsed resonant excitation are shown in Fig. 4.3e and f in a semi-logarithmic plot. The histogram for the charged exciton shows a steep rising edge due to the finite laser pulse duration and setup time resolution and a slow exponential decay due to the excited state lifetime of the studied transition. Fitting the data with an exponential decay convolved with a Gaussian yields a lifetime of $(236 \pm 2)\,\mathrm{ps}$. The decay histogram of the neutral exciton in Fig. 4.3f is additionally modulated with a sinusoidal square wave. These so-called quantum beats [Fli01, Dad16] with the frequency $\frac{E_{\mathrm{FSS}}}{\hbar}$ determined by the fine structure splitting are a consequence of the polarization suppression setup (see Secs. 2.1.2 and 3.2.2). The fit yields a lifetime of $(196 \pm 2)\,\mathrm{ps}$ and a fine structure splitting of $(7.44 \pm 0.05)\,\mu\mathrm{eV}$. The lifetimes of GaAs quantum dots of around 200 ps observed here are in agreement with the reported lifetimes of these quantum dots [Rei17, Rei19] and are remarkably shorter than for InGaAs quantum dots with an exciton decay on a time scale of $300 - 1000\,\mathrm{ps}$ [Adl98, Ber07, Liu18b] and InP nanowire quantum dots with $1000 - 2600\,\mathrm{ps}$ [Laf23] and paper 1.
A crosscorrelation measurement between two transitions of a quantum emitter can reveal if they both originate from a cascaded emission, i.e. if they are a biexciton-exciton pair. In contrast to an antibunching in an autocorrelation measurement, a strong bunching can be observed since an exciton photon is expected after the emission of a biexciton photon [Mor01].

Chapter 5

Indistinguishable photons

Contents

An ideal quantum light source emits not only single photons with high purity, as introduced in the previous chapter, but also indistinguishable photons. This means that two photons have the same properties such as energy, polarization, coherence, spectral and temporal shape, and the spatio-temporal mode. When two indistinguishable photons impinge on a beamsplitter, they interfere, which is a pure quantum mechanical effect with no classical analog. This so-called two-photon interference is used to determine the degree of indistinguishability in a Hong-Ou-Mandel (HOM) type experiment. The interference effect is also a prerequisite for more advanced quantum optics experiments such as entanglement teleportation [Bou97] and entanglement swapping [Pan98]. It will also find applications in future quantum technologies such as linear optical quantum computing [Kni01], boson sampling [Aar13], quantum repeaters based on the scheme proposed by Lloyd et al. [Llo01], long-distance quantum communication networks [Kim77, Eke91], quantum metrology with N00N

states [Lee02, Mül17], and others [Bou20].
In this chapter, I explain two-photon interference, also known as the Hong-Ou-Mandel effect. Additionally, I present the experiment to determine the indistinguishability of photons emitted subsequently from a single quantum emitter.

5.1 Two-photon interference

Two single photons impinging simultaneously on a beamsplitter through two input ports interfere if they are indistinguishable. In the following, we assume an ideal non-polarizing beamsplitter with no losses and a perfect 50 : 50 splitting ratio ($|\mathcal{R}|^2 = |\mathcal{T}|^2 = 0.5$, with complex reflection and transmission coefficients $\mathcal{R}$ and $\mathcal{T}$), and perfect overlap of both single-photon wave packets ($V = |\int E_{\mathrm{a}}^*(t) E_{\mathrm{b}}(t) dt|^2 = 1$, with complex wave packet amplitudes $E_{\mathrm{a,b}}(t)$). Figure 5.1a shows the beamsplitter with the corresponding input ports a, b and output ports c, d.
To describe a single photon Fock state entering a beamsplitter at port a, the corresponding creation operator $\hat{a}^\dagger$ must be applied to the vacuum state $|0\rangle_{\mathrm{a}}$. The input state is therefore $|\Psi\rangle_{\mathrm{in}} = \hat{a}^\dagger |0\rangle_{\mathrm{a}} = |1\rangle_{\mathrm{a}}$ [Ger04]. Due to the beamsplitter interface, the creation operators of the two output ports c and d become $\hat{a}^\dagger \overset{\text{beamsplitter}}{\longrightarrow} \frac{1}{\sqrt{2}} \left(\hat{c}^\dagger + i\hat{d}^\dagger\right)$, where the complex phase i occurs on reflection at the beamsplitter interface, while the phase is unaffected on transmission. The output state of a photon entering a beamsplitter at port a is thus given by

$$|\Psi\rangle_{\mathrm{out}} = \frac{1}{\sqrt{2}} \left(\hat{c}^\dagger + i\hat{d}^\dagger\right) |0\rangle_{\mathrm{c}} |0\rangle_{\mathrm{d}} = \frac{1}{\sqrt{2}} \left(|1\rangle_{\mathrm{c}} |0\rangle_{\mathrm{d}} + i\, |0\rangle_{\mathrm{c}} |1\rangle_{\mathrm{d}}\right), \tag{5.1}$$

which means that the photon can be found in each output port with equal probability of 50 %. Adding a second photon in port b gives the input state
$|\Psi\rangle_{\mathrm{in}} = \hat{a}^\dagger \hat{b}^\dagger |0\rangle_{\mathrm{a}} |0\rangle_{\mathrm{b}} = |1\rangle_{\mathrm{a}} |1\rangle_{\mathrm{b}}$. For the output state, it is then [Ger04]

$$\begin{aligned} |\Psi\rangle_{\mathrm{out}} &= \frac{1}{2} \left(\hat{c}^\dagger + i\hat{d}^\dagger\right) \left(i\hat{c}^\dagger + \hat{d}^\dagger\right) |0\rangle_{\mathrm{c}} |0\rangle_{\mathrm{d}} \\ &= \frac{1}{2} \left(i\hat{c}^{\dagger 2} + \hat{c}^\dagger \hat{d}^\dagger - \hat{d}^\dagger \hat{c}^\dagger + i\hat{d}^{\dagger 2}\right) |0\rangle_{\mathrm{c}} |0\rangle_{\mathrm{d}} \\ &= \frac{i}{2} \left(|2\rangle_{\mathrm{c}} |0\rangle_{\mathrm{d}} + |0\rangle_{\mathrm{c}} |2\rangle_{\mathrm{d}}\right). \end{aligned} \tag{5.2}$$

In the last step, the bosonic nature of the photons was taken into account, since

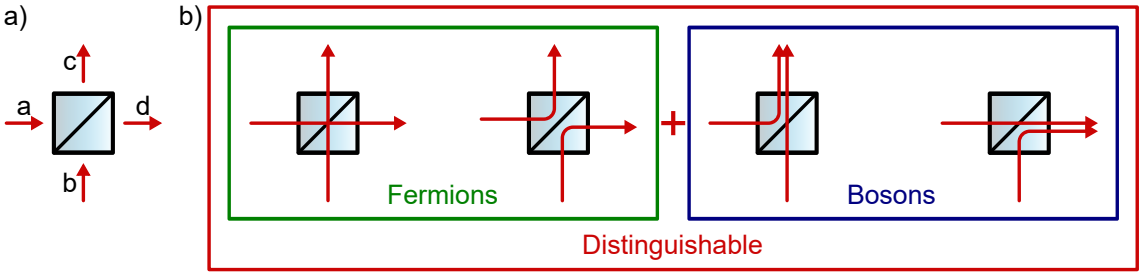

Figure 5.1 | Two-photon interference a, Ideal beamsplitter with entry ports a, b, and output ports c, d. **b**, All configurations for two photons entering a beamsplitter through a and b. For distinguishable or classical particles, all four configurations have the same probability, photons (i.e. bosons) always leave the beamsplitter together through the same port, whereas fermions always use different ports.

bosons commute and thus satisfy $[\hat{c}^\dagger,\hat{d}^\dagger] = \hat{c}^\dagger\hat{d}^\dagger - \hat{d}^\dagger\hat{c}^\dagger = 0$. From Eq. (5.2) it follows that two indistinguishable photons entering an ideal non-polarizing beamsplitter simultaneously through different entry ports a and b will always exit through the same port either c or d, as shown in Fig. 5.1b. This phenomenon is purely quantum mechanical with no classical analog and is also called the Hong-Ou-Mandel effect [Hon87]. It was first described theoretically in 1986 [Gho86] and demonstrated experimentally shortly thereafter with photons from parametric down-conversion, but without the use of a beamsplitter yet [Gho87]. Due to the antisymmetric nature of fermions, obeying the anticommutator, fermions always leave the beamsplitter through different ports. Distinguishable particles do not interfere in the beamsplitter, and thus all four combinations occur with the same probability of 25 %.

5.2 Hong-Ou-Mandel experiment

The experimental realization to measure the indistinguishability of two consecutive photons from the same source is usually done in a Hong-Ou-Mandel type setup, named after the authors of the first demonstration [Hon87], who used this setup to measure the length of a photon wavepackage generated by a parametric down-conversion process. Later, the setup was used for measuring the degree of indistinguishability of photons or for demonstrating more advanced quantum optical experiments.
In the following, I present the setup as it was used in our experiments to measure the indistinguishability of photons generated by one source with a short delay, smaller

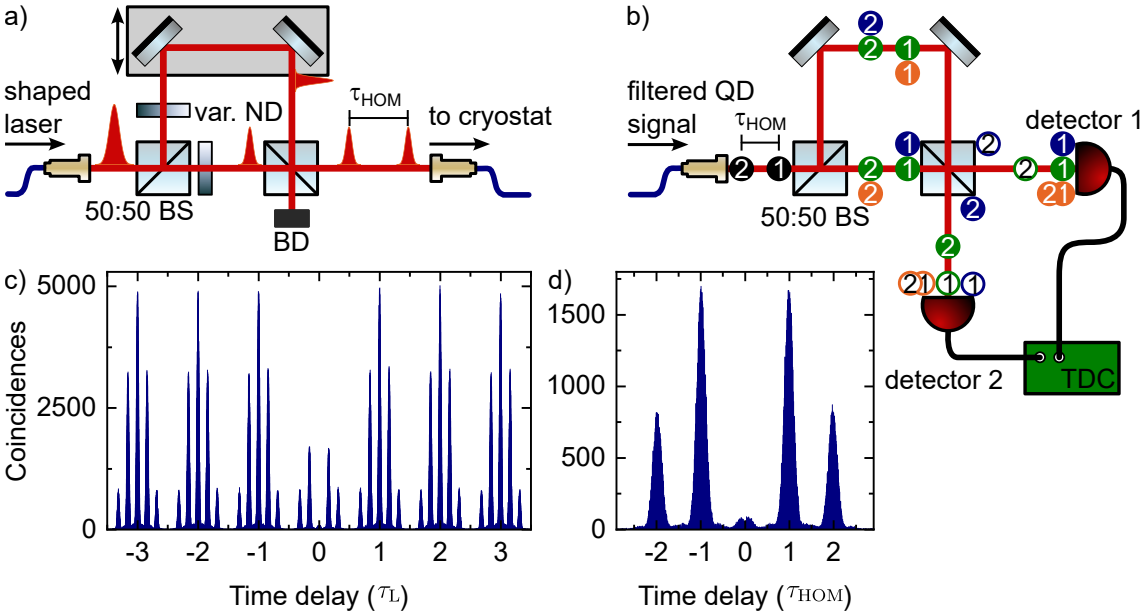

Figure 5.2 | Hong-Ou-Mandel experiment a, Variable delay line to generate double excitation pulses. **b**, Unbalanced Mach-Zehnder interferometer to overlap two consecutive photons (black circles) with delay τ_{HOM} on the second BS to perform two-photon interference. Both outputs are coupled to single-photon detectors and time tags are recorded with a time-to-digital converter (TDC). Colored circles illustrate photons to explain build up of the histogram. Solid (empty) circles after the second BS refer to positive (negative) delays. Only in the case of the orange circles, the photons interfere. (var. ND: variable neutral density filter, BD: beam dump) **c**, Two-photon interference histogram of an exciton under resonant excitation **d**, Center quintuplet from c) at zero time delay revealing $V_{\mathrm{HOM}} = (92.3 \pm 1.6)\,\%$, adapted from supplementary of paper 3.

than the repetition rate of the pulsed excitation laser.

To generate photons with such a delay, double pulses are generated with a delay line set up like an unbalanced Mach-Zehnder interferometer, as shown in Fig. 5.2a. The shaped excitation laser is sent to a non-polarizing $50:50$ beamsplitter, which splits the pulse equally into two paths of different lengths. The length of the long path can be adjusted by two mirrors mounted on a linear translation stage. Both paths are recombined by an identical beamsplitter. Each input laser pulse is now split into double pulses with a variable delay τ_{HOM}. The power of both pulses can be adjusted and equalized with continuously variable neutral density filters in each arm. One output of the beamsplitter is blocked by a beam dump, while the other is coupled into a fiber and sent to the micro-photoluminescence setup, where it is used

to twice excite a transition in a quantum dot. The filtered signal is then sent to the Hong-Ou-Mandel type setup shown in Fig. 5.2b. It consists of a similar unbalanced Mach-Zehnder interferometer, but with a fixed delay. In the papers 3 and 6 we used a fiber-coupled interferometer with a delay of 2 ns, while in paper 8 we used a free-space interferometer with a delay of 3.3 ns. The delay τ_{HOM} set by the stage position in Fig. 5.2a must match the fixed delay in the interferometer in Fig. 5.2b in order for the successive photons (black circles with numbers 1 and 2 for first and second photon) to overlap at the second beamsplitter where the two-photon interference takes place. Both outputs of the second beamsplitter are connected to the same fiber-coupled single-photon detectors as in Sec. 4.3. The following acquisition of the time-tagged detection events and the analysis to create a histogram is also identical as described in the previous chapter.

The histogram of a Hong-Ou-Mandel measurement of a s-shell resonantly excited exciton in a GaAs quantum dot is shown in Fig. 5.2c, which shows quintuplets with a delay $\tau_{\mathrm{L}} \approx 12.5\,\mathrm{ns}$ given by the repetition rate of the laser and a delay $\tau_{\mathrm{HOM}} = 2\,\mathrm{ns}$ between the individual peaks. Figure 5.2d shows a zoom in of the quintuplet centered around zero time delay resulting from photons coming from the same laser repetition cycle. As in the autocorrelation measurements in the previous chapter, the peaks resemble exponential decays given by the excited state lifetime together with quantum beats [Fli01, Dad16]. Furthermore, the center peak shows a volcano shape with a dip at zero time delay, which can only be resolved due to our high setup time resolution. This feature comes from interference of photons from a homogeneously broadened emission line and the width of the dip is determined by the coherence time [Leg03, Leg04].

The peaks with different ratios come from the following combinations of the two photons in the unbalanced Mach-Zehnder interferometer. The first photon takes the short path and the second the long path (blue circles in Fig. 5.2b). This results in a doubled time delay and the photons do not enter the beamsplitter simultaneously and therefore cannot interfere. Coincidence with a delay of $2\tau_{\mathrm{HOM}}$ can be detected. Negative delays occur when the two detectors are swapped. Positive and negative delays are differentiated by solid and empty circles respectively. In addition, both photons can take the same path (green circles) in the interferometer and thus maintain the initial delay of τ_{HOM}, leading to peaks in the histogram at $\pm\tau_{\mathrm{HOM}}$. Since this

happens in both interferometer arms, the peaks in the resulting histogram have twice the area compared to those at $\pm 2\tau_{\mathrm{HOM}}$. Finally, the most interesting combination: if the first photon takes the long arm and the second the short one, the photons impinge on the beamsplitter simultaneously. If they are indistinguishable, they will interfere and thus leave the beamsplitter through the same output port, leading to no coincidences at zero time delay and thus to a vanishing peak. For distinguishable photons, there is a peak with the same area as the one at $\pm\tau_{\mathrm{HOM}}$. This leads to a quintuplet with the peak area ratios $1:2:0(2):2:1$ for completely indistinguishable (distinguishable) photons. The other quintuplets come from photons from different laser cycles. Here, the different combinations of photons inside the unbalanced Mach-Zehnder interferometer lead to peak ratios of $1:4:6:4:1$.
The Hong-Ou-Mandel visibility is given by [San02]

$$V_{\mathrm{HOM}} = 1 - \frac{2A_3}{A_2 + A_4} \tag{5.3}$$

with the peak area at zero time delay A_3 and the areas of the two adjacent peaks at $\pm\tau_{\mathrm{HOM}}$ $A_{2,4}$. For a beamsplitter with a splitting ratio close to 50 % and a source of high purity $g^{(2)}(0) \approx 0$, the visibility is a direct measure of the degree of indistinguishability [Fis18], which is a justified assumption in our case. To determine the peak areas, we sum the number of coincidences in each peak, similar to the analysis of autocorrelation measurements. Due to the short delay and lifetimes of approximately 200 ps, neighboring peaks overlap slightly and the integration windows have to be determined carefully as explained in the supplementary of paper 3. In addition, it is worth mentioning that fitting rather than summing up to determine the peak areas will overestimate the visibility, especially if the time resolution is too low to resolve quantum beats and the volcano shape of the center peak. For the example measurement shown in Fig. 5.2d, we obtain a raw Hong-Ou-Mandel visibility of $V_{\mathrm{HOM}} = (92.3 \pm 1.6)\,\%$ without corrections for a non-perfect setup or non-ideal single-photon emission.
The first demonstration of the indistinguishability of consecutively emitted photons from a quantum dot was shown by Santori et al. in 2002 [San02]. Here, the quantum dot was nonresonantly excited, causing a timing jitter in the emission due to non-radiative decay processes [San04] and a homogeneous linewidth broadening due to scattering processes with phonons and charge carriers, which limits the indistin-

guishability [Ben05, Fla10]. This dephasing process can be strongly suppressed by s-shell resonant excitation of the transition, which significantly increases the degree of indistinguishability [He13, Som16]. However, slowly varying charge states inside and in the vicinity of the quantum dot lead to spectral fluctuations [Hou12, Tho16], which still prevent good indistinguishability when increasing the time delay between the interfering photons. Adding some nonresonant laser or white light can stabilize the charge environment and thus increase the indistinguishability [Gaz13, Rei17]. This can also be achieved in a more controlled manner by embedding the quantum dot in a diode structure, and highly indistinguishable photons with visibilities above 95 % can be maintained for long time delays of 1 µs [Tom21, Zha22]. Two-photon interference has been used to demonstrate entanglement teleportation [Rei18], entanglement swapping [BB19, Zop19], and boson sampling [He17] with quantum dots.
For the development of scalable quantum communication networks, remote sources of indistinguishable photons are inevitable. The first two-photon interference of photons from separate sources was shown with parametric down-conversion sources in 2003 [DR03], followed by atoms and ions [Beu06, Mau07]. The advantages of these sources is that the photons intrinsically emit at the same wavelength, unlike quantum dots, which require a tuning mechanism to bring both emitters into resonance (see Sec. 6.1). Early experiments demonstrating two-photon interference of remote quantum dot sources [Pat10, Fla10, Gol14] showed relatively low Hong-Ou-Mandel visibilities of up to approximately 50 %, limited by dephasing due to nonresonant excitation and an unstabilized charge environment. Again, resonant excitation [You21] and charge stabilization significantly increased the performance to up to $V_{\mathrm{HOM}} = (90.9 \pm 0.8)\,\%$ [Zha22].
We have performed Hong-Ou-Mandel experiments in papers 3, 6 and 8. In paper 3 we showed high visibilities for GaAs quantum dots without the need for Purcell enhancement under s-shell resonant excitation. In paper 6 we showed intrinsic limitations of the three-level quantum ladder system in terms of indistinguishability by exciting a quantum dot under two-photon excitation. The finite linewidth of the exciton transition leads to an energy broadening of the biexciton transition. On the other hand, the finite biexciton lifetime introduces a timing jitter on the exciton transition. Both effects reduce the degree of indistinguishability to approximately 67 %, which is determined by the lifetimes of both states. Engineering the

lifetime ratio by asymmetric Purcell enhancement can increase the intrinsic limit of indistinguishability. A way to restore the indistinguishability of the exciton to the same values as under s-shell resonant excitation can be achieved by stimulating the biexciton transition and thus reducing the timing jitter, as we have shown in paper 8.

Chapter 6

Tailoring quantum emitter properties

Contents

The semiconductor quantum dots studied here undergo a statistical growth process, resulting in a distribution of emission wavelengths, fine structure splitting, dipole orientation, and electrical environment. Moreover, the majority of emitted light is trapped within the bulk sample due total internal reflection, significantly reducing the source brightness. Despite their promising characteristics, these limitations hinders their utility as building blocks in quantum technology applications. In this chapter, I explore various methods for tailoring the properties of quantum emitters. I categorize these methods into tuning methods, influencing the wavelength and the fine structure splitting, structures to improve the extraction efficiency and thus the source brightness, and on-chip guiding of the light for quantum photonic integrated circuits. Additionally, I provide a brief overview of enhancement methods for quantum emitters in two-dimensional materials.

6.1 Tuning mechanisms

Various techniques have been used to tune the emission wavelength of emitters or to minimize the fine structure splitting. Different growth methods have been developed and modified e.g. to produce quantum dots with intrinsically low fine structure splitting or narrow wavelength distribution (see Sec. 2.1.4 and 2.1.5), or to cover new wavelength ranges [Pau17] (see Sec. 2.1.5 and paper 1). Post-growth thermal annealing has been demonstrated to reduce fine structure splitting [Lan04, Tar04] and to shift the emission wavelength [Mal97]. However, all of these techniques affect all of the emitters on the sample in a semi-controllable, statistical, and non-reversible manner. For many measurements, a controlled and reversible tuning mechanism is necessary.

Temperature tuning is the simplest to implement on any sample, as it does not require any special steps during growth or sophisticated setups. It relies on the thermal expansion of the solid, resulting in a reduction of the band gap. Experiments with solid state emitters are typically conducted at the lowest possible temperature in a cryostat, limiting this technique to red tuning only. Another drawback is the generation of more phonons at higher temperatures, leading to dephasing, hence to increased linewidth and reduced indistinguishability [Tho16]. Gold et al. [Gol14] used

temperature tuning to tune two quantum dots into resonance and perform remote two-photon interference. Temperature tuning has also been used to tune the emitter into resonance with cavity modes. The optical ac Stark shift, applied by adding a far detuned continuous wave laser, has been used to tune the fine structure splitting to zero and demonstrate polarization entanglement [Mul09a]. Application of an external magnetic field to the sample induces a diamagnetic shift and Zeeman splitting of the emission lines, providing another method to tune the emission energy [Rin96]. An in-plane magnetic field has been used to tune the fine structure splitting to zero [Ste06b]. In the following, I will focus on strain and electric field tuning.

6.1.1 Strain tuning

Strain tuning relies on mechanical straining of the sample via the piezoelectric (piezo) effect, inducing deformation of the band structure and thereby tuning of the emission energy. Additionally, the applied strain influences the crystal symmetry and therefore the coupling constants in different axis, hence also tuning the fine structure splitting [Plu13] (see Sec. 2.1.2). The piezoelectric effect, discovered in 1880 [Cur80], describes the creation of dipoles in crystal unit cells and hence the occurrence of an electric field under elastic deformation. The inverse effect conversely mean, applying a voltage to a piezoelectric material leads to deformation. Seidl et al. [Sei06] were the first to transfer the deformation as stress to a quantum dot sample. They used a uniaxial piezoelectric stack and glued the sample with the [110] crystal axis parallel to the stack on one side. By straining the sample along one of the main crystal axes, they enhanced the symmetry of the quantum dot, thereby reducing fine structure splitting and tuning of the emission wavelength. Since then, many experiments have confirmed the controllability of various emission properties of quantum dots, including the emission wavelength, the biexciton binding energy, and the fine structure splitting, by applying uniaxial strain [Din10, Plu11, Jön11, Che16]. Strain tuning has also facilitated demonstration of remote quantum dot indistinguishability [Fla10, Rei17], and tuning the emission wavelength in resonance with an atomic transition for later quantum memory experiments [Kum11, Tro16]. However, unless the strain is applied along a symmetry axis of the quantum dot, the exciton states undergo anticrossing with the applied strain, preventing the fine structure splitting from being tuned to zero [Sin10]. To address this limitation, biaxial strain can be applied, and polarization

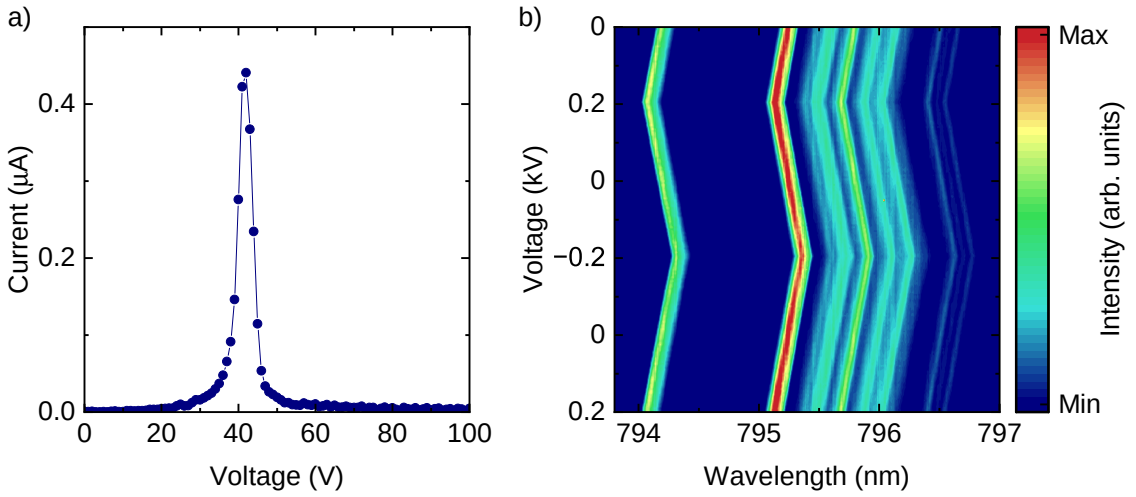

Figure 6.1 | Strain tuning of quantum dots a, Piezoelectric poling current as a function of the applied voltage at room temperature. **b**, Reversible strain tuning of a GaAs quantum dot.

entanglement has been demonstrated [Tro14, Che16]. Applying uni- or biaxial strain to tune the fine structure splitting inevitably affects the wavelength as well. To achieve full control over both the fine structure splitting and the emission wavelength, strain along a third axis was applied using a six-legged device [Wan12a, Tro15, Let21]. Strain tuning of the emission wavelength of emitters in a WSe_2 monolayer has also been demonstrated [Iff19]. Iff et al. present an impressive reversible tuning range of 18 meV. This can be attributed to the high resistance of two-dimensional materials to stress and the proximity of the emitters to the piezoelectric crystal, allowing optimal strain transfer. A review on strain tuning of different semiconductor emitters is available in [Mar17].

In papers 2 and 4, we use PMN-PT, known for its large piezoelectric response at low temperatures. To optimize strain transfer to the sample, the PMN-PT crystal is polished, as the electric field at a given external voltage is higher in thinner substrates. Subsequently, the crystal is metallized on both sides to allow application of a voltage later. In the case of paper 4, the fabricated paraboloids are bonded to the piezoelectric actuator using SU8 photoresist due to its high strain transfer attributed to its low viscosity [Zis17]. In paper 2, the photonic circuit is directly fabricated on the PMN-PT substrate to avoid wafer bonding (see Sec. 6.3).

A PMN-PT crystal exhibits randomly oriented ferroelectric domains (Weiss domains)

and hence a net zero electric field. By gradually applying an external voltage, the domains align along the electric field, resulting in a characteristic curve shown in Fig. 6.1a. As the voltage increases, more domains flip, resulting in a measurable increase in current, until most domains align along the field, after which the current decreases. This process is called poling. The piezoelectric material maintains polarization at low temperatures, but to prevent spontaneous domain flipping during the cooling process of the sample, we keep the external voltage applied. Typically, in our strain tuning experiments, voltages from $-600\,\mathrm{V}$ to $+600 - 800\,\mathrm{V}$ are applied. Figure 6.1b illustrates the reversible tuning of the emission energy of a GaAs quantum dot under nonresonant excitation. In paper 4 we achieve a tuning rate of $0.5\,\mathrm{pm/V}$. In paper 2, the nanowire quantum dot is placed on a photonic circuit and is bound only by van der Waals forces. We have demonstrated that encapsulation of the nanowire enhances strain transfer, leading to a fourfold increase in the tuning rate from $0.325\,\mathrm{pm/V}$ to $1.33\,\mathrm{pm/V}$, corresponding to a total tuning range of $1.6\,\mathrm{nm}$. An advantage of strain tuning is that the emission intensity is not affected. However, it is important to consider piezo creeping, which causes continued shifting in the same direction after reaching the target voltage. To mitigate this, the target value must be approached in small steps and readjusted after settling. Subsequently, the emission wavelength remains stable for hours, well below the resolution limit of the spectrometer [Zeu18].

6.1.2 Electric field tuning

Applying an electric field to a quantum dot also allows for tuning the emission properties. The emission energy can be described by [Fry00b]

$$E = E_0 + \mu F + \alpha F^2, \tag{6.1}$$

where the electric field is denoted F to avoid confusion, E_0 is the emission energy at zero electric field, μ represents the permanent dipole moment of the quantum dot, and α stands for the polarizability of the excitonic quasiparticle (e.g., a neutral or charged exciton) in the field direction. The permanent dipole arises from a slight shift of the electron and hole wave functions with respect to each other [Bar00, Fry00b]. The polarizability characterizes the dipole moment induced by the applied electric

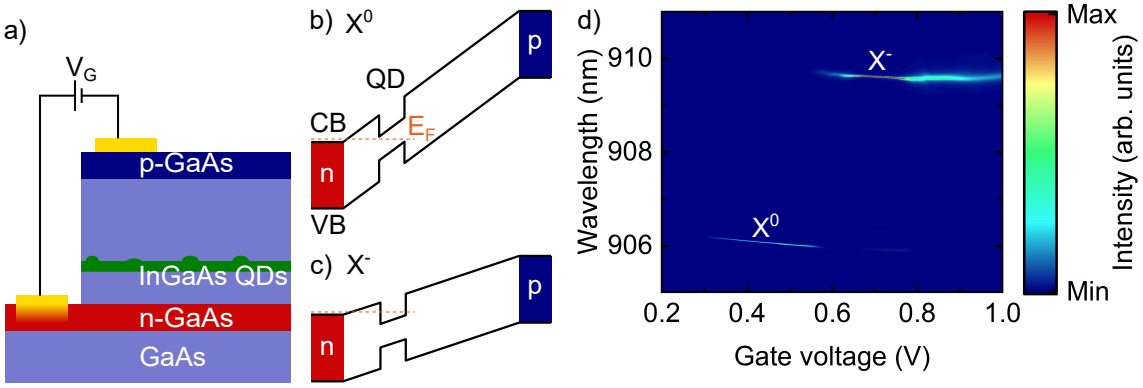

Figure 6.2 | Stark tuning of quantum dots a, p-i-n diode structure. Doped GaAs layers define the n- and p-region of the diode where an external gate voltage V_G can be applied. The quantum dots are located in the intrinsic region. **b**, Band diagram of the neutral exciton. The Fermi-level E_F is below the electron band of the quantum dot resulting in the emission of excitons (X^0). (CB: conduction band, VB: valance band) **c**, For higher positive voltages, the bands are less bent and the lowest electron state is below E_F, resulting in negatively charged exciton (X^-). **d**, Gate voltage dependent photoluminescence measurements showing well separated charge plateaus for the X^0 and X^-.

field and typically varies for each emitter and its different states. This phenomenon is known as the quantum confined Stark effect [Mil84] and was first used in quantum well structures in 1982 [Men82] followed by quantum dots in 1998 [Ray98]. To achieve sufficiently high electric fields at the emitter, an external vertical (growth direction) or lateral (in-plane) gate voltage is applied via electrodes on the sample.

In papers 8 and 9 we apply a vertical electric field, which is the more common geometry. The electric field is usually applied by embedding the quantum dots in a p-i-n diode structure, as illustrated in Fig. 6.2a. During the epitaxial growth process, a silicon-doped layer is deposited during GaAs growth to form the n-region of the diode. The InGaAs quantum dots are then embedded in the intrinsic layer. Finally, a carbon-doped GaAs layer is deposited to form the p-region. Depending on the doping concentration, the thickness of the GaAs layer (intrinsic layer), and the band gap energy, the quantum dots already experience a built-in field. After growth, the samples are fabricated to contact the doped layers and apply an external voltage. Since defects in the sample can create ohmic contacts between the layers, fabrication of several small diodes on a sample is beneficial to increase the likelihood of functional diodes. By bonding the sample, it can be connected to coaxial lines in

the cryostat, allowing external voltage to be applied using a low-noise voltage source (Stanford Research Systems DC205 or mech0nics ag NOVA5). The electric field causes bending of the conduction band and valence band as shown in Figure 6.2b,c, resulting in deterministic charging of the quantum dot and tuning of the emission energy. Figure 6.2d shows the gate voltage dependent photoluminescence of an InGaAs quantum dot in a diode structure. For voltages around $0.35 - 0.55\,\mathrm{V}$, the electron Fermi level E_F lies below the electron band of the quantum dot (Fig. 6.2b), resulting in the emission of a neutral exciton. For higher voltages, the bands are less bent, and the lowest electron states are below the Fermi level (see Fig. 6.2c), leading to a negatively charged quantum dot and hence the emission of negatively charged exciton. For voltages below approximately $0.35\,\mathrm{V}$ the bands are so strongly bent that carriers tunnel out of the potential faster than the exciton lifetime, resulting in a measurable current instead of photoluminescence. This regime is also known as the photocurrent regime. Particularly before sufficient laser filtering was possible, this technique was utilized to measure under resonant excitation [Zre02, Est06].
The primary purpose of the diode structure in paper 8 was to provide a charge-stabilized environment for the quantum dots and enable photoluminescence over a wide voltage range. An additional n-doped layer on top of the quantum dot layer was induced in the sample structure to reduce the built-in field and thus expand the photoluminescence regime. Furthermore, the proximity of the quantum dot layer to an n-doped layer allows quick tunneling of charge carriers, resulting in well-separated charging plateaus, similar to the exemplary voltage-dependent photoluminescence measurement in Fig. 6.2d. This configuration is called charge-stabilized. In paper 9, wavelength tuning was required to tune transitions relative to laser energies (see Sec. 3.2.5). However, the relatively small confinement of approximately $0.2\,\mathrm{eV}$ limits the electric field to a few tens of kV/cm before the carriers tunnel out [Fry00a], restricting the tuning range to approximately $2\,\mathrm{meV}$.
Tailoring the diode structure, such as exploiting heterostructures with larger band gaps [Ben10a], Schottky diodes [Mar10, Gha12], and lateral fields, enables larger tuning ranges of up to $25\,\mathrm{meV}$ [Pat10], as well as the manipulation of the fine structure splitting and biexciton binding energy. Electric field tuning has been used in various experiments, including tuning the emission of separate quantum dots into resonance to demonstrate indistinguishability of remote quantum dots [Pat10,

Zha22], and to tune the emitter into resonance with an atomic transition [Ako10] or cavity mode [Rak08, Lau09, Now14, Som16, Liu18a]. Since all states within a quantum dot shift differently, the biexciton binding energy can also be manipulated with lateral electric fields, allowing the biexciton and exciton transitions to be tuned into resonance [Kan11, Rei11]. Similarly, fine structure splitting can be tuned with both vertical [Mar10, Ben10b] and lateral fields [Kow05, Ger07, Kow07, Vog07], however, the latter often yielded unreproducible results and is thus no longer used. Reducing the fine structure splitting below the linewidth of the transition enables the generation of polarization entangled photon pairs from the quantum dot [Ben10b, Gha12]. Engineering low-capacitance diodes enables ultrafast tuning on timescales of 20 ps [Wid21], which is below the decoherence or lifetime of the quantum dots. So far this has been used to achieve a robust state population via rapid adiabatic passage [Muk20], sensing of ultrafast electric signals [Wid21] and phase control of an exciton [Wid18]. In the future, ultrafast tuning of excitonic transitions in and out of resonance with the excitation laser could make polarization filtering under resonant excitation (see Sec. 3.2.2) obsolete. Electric field tuning has also found application in tuning the emission energy [Cha17] and fine structure splitting [Cha19a] of quantum emitters hosted by transition metal dichalcogenide monolayers, for controlled generation of charged excitons [Cha18] and to perform gate switching [Höt21].

6.2 Extraction efficiency

A quantum dot in a bulk semiconductor radiates isotropically, as shown in Fig. 6.4a. Furthermore, the semiconductor materials used for growth are high refractive index materials, i.e. $n_{GaAs} = 3.7$ and $n_{AlGaAs} = 3.4$ at 800 nm, leading to total internal reflection for angles larger than approximately 17°. The numerical aperture (NA) of the collecting optics results in an even smaller detectable cone. In the setup for the majority of our measurements, we use a microscope objective with NA= 0.81 for collection, resulting in the red shaded detection cone in Fig. 6.4a. This combined yields a collection efficiency in the first lens of approximately 1 % [Bar02]. Different approaches are used in the quantum optics community to increase the extraction efficiency [Lod15], which can be divided into two groups: (i) the emitter is placed

inside a waveguiding structure, which has a steering effect towards the collection optics, (ii) the emitter is placed inside a cavity, which additionally requires resonance effects. Fermi's golden rule states that the spontaneous emission rate is proportional to the density of the final state of a radiative transition [Dir27]. According to cavity quantum electrodynamics, the density of states increases for an emitter in resonance with a cavity mode [Har89]. Therefore, spontaneous emission into the cavity mode can be enhanced, known as the Purcell effect. This enhancement is characterized by the ratio of the emission rates of an emitter without and with cavity, called the Purcell factor, given by

$$F_P = \frac{3}{4\pi^2}\frac{Q}{V}\left(\frac{\lambda}{n}\right)^3 \tag{6.2}$$

with the refractive index n, the wavelength in vacuum λ, the mode volume V and the quality factor Q, which is a measure for both the damping in the cavity and the spectral bandwidth.

6.2.1 Lightguiding structures and microcavities

I will provide a brief overview of different strategies to increase the extraction efficiency, while delving into more detail on the methods we used in our experiments. The simplest approach to increase the source brightness is to place a metallic mirror or distributed Bragg reflector (DBR) below the quantum dot layer to direct downward emitted photons towards the collection optics. Such a back mirror can be combined with many of the structures presented below. A DBR consists of several alternating layers of materials with different refractive indices. The layer interfaces cause partial reflection and refraction of light. When the layer thickness is one-fourth of the wavelength, the reflected light interferes constructively. The wavelength range that satisfies this condition experiences high reflectivity and is called the stopband. The reflectivity of the DBR depends on the refractive indices of the materials and the number of layer pairs [She95]. The sample in paper 8 has a lower DBR consisting of 17 pairs of alternating AlAs and GaAs layers.

The addition of a second DBR with lower reflectivity on top of the quantum dot layer forms a planar Fabry-Pérot cavity with a relatively large mode volume and low quality factor. Such a cavity was used to demonstrate the first resonance fluorescence of a quantum dot [Mul07] as well as the first two-photon interference measurement

in a Hong-Ou-Mandel experiment under resonant excitation [He13].
In the papers 3, 5, and 6 we used the same sample where the quantum dots are embedded in a λ cavity with nine pairs of bottom and two pairs of top DBRs composed of $Al_{0.95}Ga_{0.05}As$ and $Al_{0.2}Ga_{0.8}As$. This cavity structure is directly included in the growth process (see Sec. 2.1.4). Another planar approach has been demonstrated by Huang et al. [Hua21]. By embedding a quantum dot membrane in a broadband optical antenna consisting of a metallic back reflector and a semi-transparent metallic top mirror, they achieved a maximum collection efficiency of 19 % into a NA of 0.85, an average intensity enhancement factor of 17, a wide bandwidth of 30 nm and a low Purcell factor of 0.7 to 1.4 depending on the wavelength. The advantage of such large planar cavities is that multiple emitters can be enhanced simultaneously, and a flat sample surface allows the additional use of a solid immersion lens (see below). With a curved instead of a planar back mirror, the directionality of the emission can be improved, as with optical horn antennas [Tak07, Gro13] and cone structures [Sue13].

Microparaboloids are micrometer-sized parabolic mirrors with a single quantum dot at the focal point that collimates the emission. They have a similar working principle as the horn antennas mentioned above, but have an increased focusing power [Mor18]. The concept and fabrication process were developed by Thomas Lettner at KTH in Stockholm and are presented in paper 4. A schematic sketch is depicted in Fig. 6.3a. The parabolic back mirror, combined with the planar sample-air interface, forms a weak microcavity, as part of the emission is reflected back into the structure, which can result in a weak Purcell enhancement. But also emission wavelengths that are not in resonance with a cavity mode experience a broadband increase in extraction efficiency. Finite difference time domain (FDTD) simulations enable optimization of the structure design regarding collection efficiency, Purcell factor, or far-field emission profile. The simulations predict collection efficiencies of up to 63 % for a NA of 0.8. Experimentally, we observed a collection efficiency into the first lens of 12 %, an average enhancement factor of 6.2, and a record enhancement of 21.6 compared to as-grown quantum dots on the sample. To validate the effect of the parabolic shape, we compared quantum dots inside a paraboloid with those on a planar gold back mirror, as shown in Fig. 6.3b. The quantum dot inside the paraboloid is enhanced by more than one order of magnitude, whereas we observed an average enhancement of approximately 4 compared to the planar

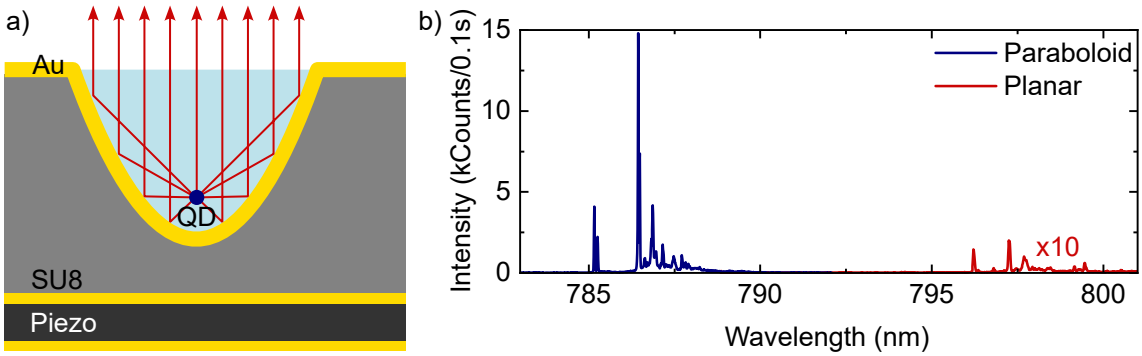

Figure 6.3 | Microparaboloid a, Sample structure. The emission of a quantum dot at the focal point of the parabolic gold mirror leaves the sample collimated **b**, Spectra of two quantum dots on a planar gold mirror reference (red) and inside a paraboloid (blue).

back mirror. The simulated far-field emission patterns exhibit a large overlap with a Gaussian beam profile. Furthermore, the paraboloid diameter is comparable to the core diameter of a single-mode fiber and possesses a planar top surface, potentially enabling direct coupling of the source to a lensed fiber [Mus20]. While our structure is based on a GaAs quantum dot sample (see Sec. 2.1.4), it can be adapted for other types of quantum dots. The basic fabrication steps involve writing circles in photoresist on the sample, follows by reflow of the photoresist [Nus97], and subsequent reactive ion etching with inductively coupled plasma. The reflow process converts the cylindrical photoresist shapes into paraboloids, which are then transferred into the underlying AlGaAs during etching. The etching selectivity of the sample material and the photoresist determine the height and diameter of the resulting paraboloids. Subsequent metallization with 100 nm gold provides the back mirror. Next, the sample is flipped and bonded to a piezoelectric substrate using epoxy (SU8) [Zis17] for strain tuning of the emission wavelengths. The piezoelectric substrate preparation is described in Sec. 6.1.1. Finally, the remaining GaAs bulk material is removed by wet chemical etching. The process is based on a regular array of paraboloids, with our dependence on the statistical distribution of quantum dots ensuring that some paraboloids contain a well-positioned single quantum dot at the focal point. Although the structure provides some robustness against lateral displacement (see supplementary of paper 4), deterministic integration of pre-characterized emitters would greatly improve the yield of these structures.

Nanowires are structures that do not rely on a cavity effect but on dielectric screening [Ble11], which leads to preferred emission in the fundamental HE_{11} waveguide mode and suppresses emission in radiation modes. Needlelike conical tapering of the nanowire [Cla10] supports adiabatic coupling of the mode to free space, suppresses back reflection from the gold catalyst, and nearly Gaussian mode profiles have been shown [Bul14]. A reverse conical taper, forming so-called photonic trumpets, maintains a good mode profile [Mun13, Ste15], but additionally provides the possibility to attach them directly to single-mode fibers [Cad16]. Nanowires have shown a collection efficiency of up to 75 % in the first lens. In papers 1 and 2 we use bottom-up grown InAsP nanowire quantum dots. A more detailed introduction is given in Sec. 2.1.5.

Solid immersion lenses (SILs) address the challenge of only a small amount of light leaving the sample-air interface due to total internal reflection by reducing the refractive index step between these two surfaces. A solid immersion lens is a small plano-convex lens with a very short focal length. They were first used in microscopy to increase spatial resolution [Man90]. Later, their potential to collect light from a point source more efficiently was discovered [Wu99, Koy99]. In 2000, they were first used to image and excite a single quantum dot [Wu00]. By reducing the refractive index step between the sample and air, the critical angle for total internal reflection is increased, allowing more light to leave the sample. A cubic zirconia solid immersion lens with refractive index $n_{\mathrm{SIL}} = 2.1$ was used in paper 9, leading to a critical angle for total internal reflection of $\theta_c = 37°$ instead of approximately 17°. In papers 3, 5, and 6, a lanthanum dense flint (N-LASF9) glass solid immersion lens with $n_{\mathrm{SIL}} = 1.83$ was used, resulting in a critical angle for total internal reflection of $\theta_c = 31°$. The solid immersion lens geometry additionally ensures that all light leaving the sample reaches the lens surface at a small angle, thereby avoiding total internal reflection. There exist two typical geometries with the first being a hemisphere (See Fig. 6.4b). Given that the quantum dots are only a few hundred nanometers below the sample surface and a solid immersion lens is few hundred micrometers large, it can be approximated that the quantum dot is located in the center of the solid immersion lens. Consequently, all light reaches the lens surface under normal incidence, resulting in no diffraction. In the case of a glass solid immersion lens, the collection efficiency into the microscope objective (NA= 0.81)

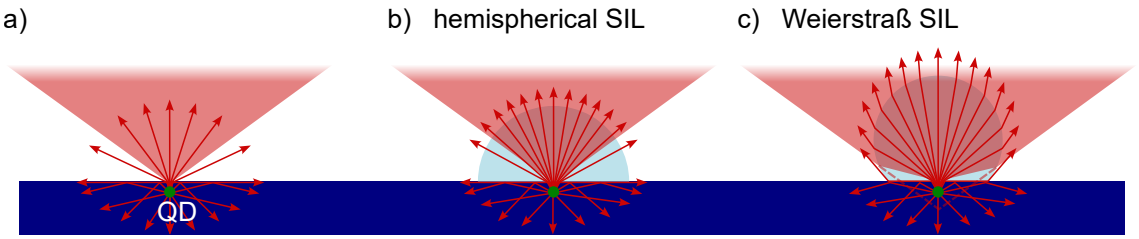

Figure 6.4 | Solid immersion lens (SIL) a, Planar sample without SIL. The red cone symbolizes the NA of the collection optics. **b**, Hemispherical SIL. The smaller refractive index change increases the critical angle for total internal reflection and more photons can leave the semiconductor. The hemispherical shape prevents diffraction at the SIL-air interface **c**, Weierstraß SIL. The super-hemispherical shape leads to an additional diffracting towards the collection optics. Furthermore, the excitation spot is further focused, leading to increased power density.

would increase to approximately 8 % [Zwi02]. The cubic zirconia solid immersion lens has a Weierstraß geometry, namely a truncated sphere with height $h = r\,(1 + 1/n_{\mathrm{SIL}})$, where r is the radius of the sphere [Bar02] (See. Fig. 6.4c). As a result, the quantum dot is not at the center of the sphere, and the light no longer impinges on the lens-air interface under normal incidence. The Weierstraß solid immersion lens therefore additionally refracts the light leaving the sample into a smaller numerical aperture, leading to a faster increase in collection efficiency with increasing numerical aperture compared to the hemispherical lens. The maximum numerical aperture for this lens is $\mathrm{NA}_{\mathrm{max}} = \frac{1}{n_{\mathrm{SIL}}} = 0.48$, which means that our collection optics with NA= 0.68 in this setup does not limit the collection efficiency of about 8 %. Additionally, the excitation laser is more strongly focused, as illustrated by the red shaded area in Fig. 6.4c. This results in a smaller spot size and thus higher power density, which can be beneficial for experiments where laser power or filtering magnitude is limited. Due to the short working distance of the objective in our mostly used setup, a Weierstraß solid immersion lens could not be used. Instead, in the papers 3, 5, and 6, we opted for a glass solid immersion lens with a height falling between the geometries of the hemispherical and the Weierstraß solid immersion lens. For easier handling with a pair of tweezers, the sides were polished off, giving it a more cylindrical shape. A sketch of the entire sample structure is shown in Fig. 2.4b.

For the collection efficiency estimations, usually an unrealistically perfect contact between the sample surface and the solid immersion lens is assumed. However, small

dust particles and scratches on either the sample or lens surface can introduce a small air or glue gap, resulting in additional reflections that diminish the achievable collection efficiency [Moe03]. To mitigate this, we applied a thin layer of vacuum grease as an adhesive and carefully positioned the solid immersion lens under a microscope. High refractive index solid immersion lenses, back mirrors, and optimized distance between the sample and lens can significantly enhance the collection efficiency. Chen et al. [Che18] demonstrated an extraction efficiency of 65 % with a numerical aperture of 0.4 using a GaP solid immersion lens ($n_{\mathrm{GaP}} = 3.5$).
An alternative approach to placing macroscopic solid immersion lenses on a planar sample after growth are nanofabricated microscopic lenses on pre-selected emitters. Various lens geometries and microobjectives have been printed using three-dimensional direct laser writing [Sar17, Bre20, Sar21]. Furthermore, fabricating lenses in quantum dot host materials using in-situ low-temperature electron beam lithography followed by reactive ion etching has shown collection efficiencies exceeding 20 % (NA= 0.4) [Gsc15]. Additionally, Ma et al. [Ma15] propose an extraction efficiency of 90 % through deterministic fabrication of a microlens on top of a quantum dot combined with a metallic back mirror.

Microcavities Although some of the structures described above are cavities, they exhibit a low Purcell factor, so that the most improvement in brightness is due to the guiding effects of the mirrors. Equation (6.2) shows that the highest enhancement arises from cavities with small mode volumes and a high quality factors, resulting in narrower cavity resonance. Such cavities can be achieved with different designs.
Microdisk resonators rely on total internal reflection at the disk edges, with the formation of whispering gallery modes [McC92]. The first demonstration of single-photon emission from a solid state source was in 2000, using a quantum dot inside such a cavity [Mic00].
Another cavity design, the photonic crystal cavity is based on Bragg scattering rather than total internal reflection. A photonic crystal is a dielectric material with a periodically modulated refractive index. The modes in such a structure undergo strong dispersion, resulting in phenomena like slow light and a photonic band gap [Yab87] if the Bragg scattering is strong enough [Lod15]. In a two-dimensional photonic crystal, this refractive index modulation can be realized by etching holes in

a semiconductor material. Here, in-plane light propagation is suppressed due to the photonic band gap, permitting light to only exit the structure out-of-plane within a small cone given by the critical angle for total internal reflection. Introducing defects into the photonic crystal, such as omitting a few holes, generates a cavity with quality factors reaching up to 10^6 [Lai14]. These cavities have demonstrated extraction efficiencies exceeding 40 % (NA= 0.6) [Mad14], and high indistinguishability on quantum dots has been demonstrated [Lau05, Liu18a].

Micropillar cavities are obtained by etching pillars into a planar DBR cavity sample. Besides confinement in the z direction, the sidewalls of the pillars provide in-plane confinement similar to nanowires, yielding small mode volumes and large quality factors. Indistinguishability of photons emitted from a quantum dot was first measured in 2002 by Santori et al. using a micropillar cavity [San02]. Since then, the performance of quantum dots coupled to micropillar cavities could be improved, including combining them with a diode structure and performing s-shell resonant excitation, yielding bright, single, and indistinguishable photon sources [Som16]. Furthermore, Gaussian boson sampling was demonstrated with a quantum dot inside a micropillar [He17]. By modifying the micropillar shape, the emission properties can be tailored. Tapering the pillar similar to a photonic trumpet, can shape the far-field emission profile, predicting 80 % outcoupling efficiency with a Gaussian beam profile [Gre16]. A more sophisticated hourglass geometry suggests an even higher collection efficiency of 95 % [Ost19, Gaá22]. An elliptical pillar cross-section instead of a circular one results in the emission of highly polarized photons [Gay98, Gür21] and eliminates the need for polarization suppression under s-shell resonant excitation, which otherwise limits the collection efficiency to a maximum of 50 %. Wang et al. demonstrated a collection efficiency of 60 % under resonant excitation while preserving pure single-photon emission and indistinguishability by using an elliptical micropillar [Wan19a]. Most micropillar cavities have a high quality factor and thus narrow modes, excluding the support of both biexciton and exciton from the radiative cascade, hindering the extraction of entangled photon pairs. To date, only a design featuring two coupled pillars has succeeded in generating polarization entangled photon pairs [Dou10]. Recently, a broadband micropillar design with high extraction efficiencies of nearly 70 % [Gin22] has been presented, potentially overcoming this limitation. This remarkably high collection efficiency for a cavity with low quality

factor can be attributed to a destructive interference effect occurring for certain ratios of emitter wavelength to pillar size [Wan21].
Rather recently, circular Bragg grating or bullseye cavities have garnered attention for their broadband operation and Gaussian far-field emission profile [Dav11]. This cavity design was initially introduced for vertically emitting lasers [Gre04] and later adopted to enhance the extraction efficiency of quantum dots [Dav11]. Concentric rings are etched into a suspended semiconductor wafer with the emitter positioned in the center. Similar to the photonic crystal cavity, in-plane confinement is achieved via a photonic band gap arising from the periodic changes in the refractive index. To achieve out-of-plane confinement through total internal reflection, the structure is suspended by under-etching [Dav11, Kol19]. The collection efficiency can be further increased by transferring the cavity to a metallic back mirror with a SiO_2 spacer as insulator [Liu19]. Both Liu et al. [Liu19] and Wang et al. [Wan19b] demonstrated a quantum light source based on a quantum dot inside a bullseye cavity with a photon pair collection efficiency surpassing 60 % (NA= 0.65), high indistinguishability, and single-photon purity, and entanglement fidelity of 0.88 and 0.9, respectively. Recently, Rota et al. [Rot22] combined a similar sample with a six-legged piezoelectric actuator to nearly eliminate the fine structure splitting through strain tuning, thereby increasing the fidelity to 0.96. Similar to the elliptical micropillar cavity, an elliptical bullseye can eliminate the need for polarization suppression of a resonant laser [Wan19a, Bar24].

6.2.2 Deterministic fabrication

Most of the enhancement strategies discussed here rely on the precise spatial positioning of the quantum dot within the microstructure. Additionally, microcavities also require spectral matching. However exceptions are, bottom-up grown nanowire quantum dots, as they do not rely on post-growth fabrication, planar cavities, and macroscopic solid immersion lenses, as they enhance all emitters uniformly. Achieving a well-positioned quantum dot inside of a photonic structure can be attained through the fabrication of numerous such structures. Given the random distribution of quantum dots, some structures statistically align well spatially and spectrally with an emitter. Alternatively, deterministic fabrication around pre-characterized emitters is pursued. This involves characterizing the quantum dot in terms of optical properties

and localizing it with respect to markers [Sap15, Liu17] at cryogenic temperatures. The desired structures can then be written in non-cryogenic conditions using electron beam lithography or through in-situ electron beam [Gsc13] or photo [Dou08] lithography. To achieve reproducible and reliable results, high precision in fabrication must be met. Unfortunately, the optical properties of the quantum dot may change after nanofabrication, for instance due to changed strain potentials and charge environment. Consequently, tuning the emitter into resonance with the cavity mode is necessary. This can be achieved for example via temperature [Rei04], electric field [Lau09, Now14, Som16, Liu18a] or strain tuning [Moc19, Moc20, Rot22].
An open Fabry-Pérot cavity [Cui06, Hun10] offers a fully tunable system to address these challenges. It consists of a planar bottom DBR in the sample below the quantum dot layer, and an external curved mirror. The external mirror can be incorporated into the tip of an optical fiber through focused ion beam milling and applying a dielectric coating [Ste06a, Her18]. Alternatively it can be a SiO_2 plate with a dielectric curved DBR composed of SiO_2 and tantalum [Naj19]. By adjusting the cavity length using a piezo actuator, tuning of the cavity mode in resonance with a quantum dot has been demonstrated [Mul09b, Bar11]. Especially with the design by Najer et al. [Naj19], high quality factors of 10^6 and an outstanding end-to-end efficiency up to 71 % [Tom21, Din23] are achieved while maintaining near-unity photon indistinguishability.

6.2.3 Enhancement methods for emitters in two-dimensional materials

Additionally to quantum dots, some enhancement techniques are also applicable to quantum emitters hosted by transition metal dichalcogenide monolayers. As introduced in Sec. 2.2, these emitters can be induced by strain [Kum15], allowing regular arrays of emitters [Bra17, Pal17].
Bullseye cavities are particularly interesting for those emitters due to their broad operating bandwidth, with high Purcell enhancement, and relatively easy design modification to target different wavelength ranges. Seven times higher photoluminescence intensity and Purcell factors of about five have been demonstrated with WSe_2 monolayers on bullseye cavities [Duo18, Iff21], and even better performance has been proposed theoretically [Hek23].

Moreover, an open cavity based on Bragg mirrors demonstrated a collection efficiency of 42 % and a Purcell factor above seven [Fla18, Dra23]. While this cavity design allows for wavelength tuning, it does not take advantage of the easy scalability of quantum emitters hosted by two-dimensional materials on a photonic chip.

6.3 Quantum photonic integrated circuits

In most quantum optics experiments, the quantum light source, manipulation unit such as interferometers and filters, and the detection unit are separated and connected by free-space optics or optical fibers, requiring considerable laboratory space and careful alignment procedures. However, on-chip integration is inevitable to scale up quantum technology and advancing towards practical applications [O'B09, Sil16]. Quantum photonic integrated circuits [Pol09] are constructed by combining various elements from different building blocks, including quantum light sources, nonlinear processes, circuit manipulation elements, memories, and detectors, with waveguides serving as routing elements for an individual use case. These waveguides consist of a core with a high refractive index compared to the cladding, enabling in-plane light propagation through total internal reflection, similar to glass fibers. Recent review and roadmap papers [Wan20b, Pel22] on quantum photonic integrated circuits summarize an overview of possible use cases, integration possibilities, and building blocks.

6.3.1 Material platform

Throughout the evolution of photonic circuits, various material platforms have been utilized based on specific application requirements. Silicon, being the most mature material platform in industrial fabrication, owing to its compatibility with CMOS processes in electronics, is widely used [Sie21, Kim20]. It offers low losses at long wavelengths and tunable circuits, but lacks direct light sources. Other promising platforms include InP and GaAs, which provide monolithically integrated high-quality quantum dots, or $LiNbO_3$ on insulator [Qi20, Zhu21], which offers large second and third order nonlinearity, facilitating a wide range of on-chip signal generation and manipulation. In recent years SiN on insulator [Blu18] has gained attention due to its complementary properties to silicon photonic circuits and CMOS compatible

fabrication. It offers broadband operation as the transparency window spans from the visible to the mid-infrared spectral range, and exhibiting very low losses [Sac17]. Especially the near-infrared spectral range around $700 - 950\,\mathrm{nm}$ is of interest, as most of our quantum light sources emit in this range. Additionally, its refractive index is high enough to combine it with SiO_2 as bottom cladding. However, due to the relatively small refractive index contrast, photonic circuits based on SiN on SiO_2 suffer from larger bending radii for waveguides compared to the silicon-on-insulator platform. In the course of this thesis, SiN on insulator was used in papers 2 and 7.

6.3.2 Quantum emitter integration

The core of a quantum integrated photonic circuit lies in the quantum light source, with quantum dots being one of the most promising candidates as integrated emitter. To combine them with the mature silicon and SiN photonic platforms, a heterogeneous or hybrid integration approach is necessary [Kim20]. In heterogeneous integration, multiple material platforms, such as a SiN substrate and a III-V semiconductor material containing quantum dots, are brought into contact, typically through wafer bonding. Several processing steps create waveguides and emitter-containing structures enabling evanescent coupling of up to 90 % [Dav17].
In hybrid integration, the emitter is transferred from a separate growth chip after waveguide fabrication. This is typically accomplished using a pick-and-place device that allows both deterministic picking and positioning of emitters with sub 100 nm and sub 1° accuracy [Els17, Kat18].
Nanowire quantum dots are well-suited for this transfer technology due to their geometry, facilitating easy transferability, and their Gaussian emission profile [Cha23]. However, successful transfer of other emitter types, such as quantum dots [Kat19], and color centers in diamond [Mou15, Wan20a] has also been demonstrated, albeit requiring the fabrication of an underetched transfer structure to facilitate pick-up. The individual placement of each pre-selected emitter limits scalability of quantum photonic integrated circuits. This can be addressed by using emitters embedded in two-dimensional materials [Cas14]. In this approach, strain-induced emitters are generated, by transferring a single two-dimensional monolayer flake, resulting in multiple emitters at the waveguide edges that are multiplexed into the circuit, as we did in paper 7.

Transfer can be facilitated using a nanomanipulator based on a fine needle (typically made of tungsten [Zad16] or glass [Cad16]) or an atomic force microscope tip [Sch11a] mounted on a multi-axis stage. The needle adheres to a selected transferable structure through van der Waals forces. During transfer, the connection to the growth chip breaks, and the structure is aligned with respect to markers at the desired location on the photonic circuit using a microscope. Upon contact with the secondary chip, the transferable structure remains there, due to greater contact area and hence greater van der Waals forces. Due to the growth mode, nanowire quantum dots are typically transferred using such a nanomanipulator as shown by Zadeh et al. in 2016 [Zad16]. In paper 2, we used the same setup to transfer a nanowire quantum dot in front of a tapered waveguide facet with sub 500 nm and sub 2° accuracy. An alternative method involves using a stamp with a viscoelastic polymer, typically PDMS, enabling adhesion based on kinetic control [Mei06]. Under fast movements, the adhesion is stronger, which is exploited when picking up the transferable structure. In the printing step, the stamp with the attached structure is brought into contact with the photonic structure by pressing down. By very slowly peeling off the stamp, the adhesion is lower, so that the structure remains on the new substrate and the PDMS detaches from it. This method is particularly suitable for transfer of fragile two-dimensional monolayers. The first integration of single-photon emitters in two-dimensional materials into a photonic waveguide was demonstrated by Tonndorf et al. [Ton17]. Since then, several groups, e.g. [Pey19, Li21], have demonstrated integration of emitters in various two-dimensional materials into different types of waveguides. We transferred a WSe_2 monolayer covering about 20 µm of a SiN waveguide in paper 7. Other emitters embedded in a transfer structure have been transferred using both methods.

To improve the coupling from quantum dots to waveguides, several approaches have been demonstrated. Butt coupling to the end facet of a waveguide can be enhanced with an adiabatic taper for better mode matching. Evanescent coupling benefits from long tapered devices, with coupling efficiencies up to 70 % achieved from a nanowire quantum dot to a waveguide [Mna20]. Structures facilitating transfer of quantum dots in bulk material often also inherit an adiabatic taper [Dav17] or a nanobeam cavity [Kat19], which show single-photon source efficiencies above 70 % and theoretically achievable efficiencies above 90 %. However, the aforementioned

advantage of easy generation of multiple emitters in two-dimensional monolayers at the waveguide edges is a disadvantage in terms of coupling efficiency at the same time. Our 3D FDTD simulations yield a coupling efficiency well below 1 % for a dipole at the edge of a waveguide, as the field maximum of the fundamental TE00 and TM00 modes of a waveguide is at the center (see Supplementary of paper 7). Inducing the emitter centered at the top of the waveguide or even encapsulating it would significantly enhance the coupling. Structured waveguides with pillars [Bra17, Pal17] or gaps, the use of cavities [Par22] or different types of two-dimensional emitters could potentially overcome this challenge.

6.3.3 Building blocks

To conduct on-chip experiments in quantum photonic integrated circuits, various building blocks must be integrated to manipulate the signal. One of the most important effects to achieve quantum interaction with photons is two-photon interference [Hon87] (see Chaper 5). Directional couplers therefore serve as one of the most basic but versatile building blocks for quantum photonic integrated circuits. They are based on evanescent coupling between two closely spaced waveguides. The splitting ratio can be tuned by adjusting the distance and the length of the waveguides in the coupler region [Pol09]. Another critical aspect is spectral filtering and wavelength-dependent routing of the light, which is essential for cleaning the signal from background, scattered laser or other emission lines. Structures such as one-dimensional nanobeam cavities [Che10], Bragg gratings [Wan12b], and ring resonators [Gra15, Par22], act as notch filters by transmitting the majority of the signal while filtering out a narrow portion that is on resonance with the resonator or lies within the stopband of the Bragg grating. These structures can be used to filter an excitation laser that is spectrally close to the emission lines, for instance in the case of two-photon or quasi-resonant excitation. Add-drop filters, consisting of a resonator placed between two waveguides, routes the spectral component of a signal in resonance with the resonator to the other waveguide, while the rest of the signal remains in the first waveguide. This way, the filtering of a narrow emission line and the omission of the rest is also possible. Add-drop filters based on nanobeam cavities [Yu21], microdisk resonators [Agh19] and ring resonators [Els17] have been realized.

Incorporating single-photon detectors is essential to combine all basic building blocks on a photonic chip. Superconducting nanowire single-photon detectors are particularly promising due to the superior performance and compatibility with nanofabrication. The first on-chip single photon detectors achieved a detection efficiency exceeding 90 % and a timing jitter as low as 18 ps [Per12]. While Reithmaier et al. [Rei13] were the first to show on-chip generation and detection of quantum light, Schwartz et al. [Sch18a] proved the single-photon emission. These groups both fabricated the chip heterogeneously. Najafi et al. [Naj15] were the first to integrate multiple detectors into a photonic circuit using a transfer printing process. This method allows for the deterministic transfer of pre-characterized, well-performing detectors, resulting in a higher yield compared to heterogeneous integration methods. Today, wavelength sensitive detection has also been demonstrated with an on-chip spectrometer [Che19].
For advanced applications, reconfigurable circuits are essential. This includes, for example, changing the splitting ratio in directional couplers [Gyg21], adjusting the phase in phase shifters [Woo00], and tuning the resonant frequency in filters [Els17], or the emitter wavelength [Far07, Kat20]. Various techniques exist to manipulate these properties. The tuning methods introduced above to tune emitter properties or resonances of microcavities such as temperature [Far07, Har14, Els17], strain and electric field [Ell18] can also be applied in photonic circuits. In particular, temperature tuning by local heating of a structure, e.g. by current flowing near the structure, can suffer from crosstalk with nearby structures. However, impressive pump beam suppression of 95 dB has been demonstrated [Har14, Els17]. In paper 2, we first demonstrated strain tuning of the emission energy of a waveguide coupled nanowire quantum dot by 1.6 nm. In a second step, we showed the tuning of a ring resonator resonance by 0.12 nm. Another tuning method is based on MEMS [Err20], where mechanical tuning changes the physical position of an element. Actuation can be achieved via piezoelectric or electrostatic effects, or thermal expansion. The former two methods hold an advantage over temperature tuning due to their lower power consumption and thus reduced heat dissipation. Yet another tuning approach is based on electro-optic effects. Materials such as $LiNbO_3$ change their refractive index upon application of an electrical field (Pockels effect). This property is often used to create e.g. phase shifters or adjustable beamsplitters [Sha17].
Coupling to and from the chip is unavoidable, especially for photonic circuits that do

not contain all the components. In-plane coupling to the cleaved facet of a waveguide can be achieved using a freespace objective or a lensed fiber. We used the latter with a photonic probe station (see Sec. 3.3) in paper 2 and 7. To achieve a better mode match and improve the coupling efficiency, an adiabatic taper was added at the end of the waveguide in paper 2 [Son18]. A photonic wire bond can provide a non-freespace connection between two chips [Lin12] or a chip and an optical fiber [Lin15]. For out-of-plane coupling, periodic structures such as grating couplers [Dak70, Roe07] are commonly used, theoretically predicting near unity coupling efficiency with inverse design [Mic18], although they allow only narrow-band coupling. Broadband coupling has been demonstrated using three-dimensional laser-written waveguide structures that form an out-of-plane bend [Geh19a, Geh19b].

6.3.4 Fabrication

The sample fabrication process for paper 7 started with deposition of a 3.3 µm SiO_2 layer as bottom cladding on a silicon substrate. Subsequently, a 250 nm thick stoichiometric SiN film is deposited on the substrate to form the waveguide core. The fabrication of the waveguied with a cross-section of 250×800 nm is achieved through electron beam lithography, reactive ion etching and resist stripping. By cleaving the sample perpendicular to the waveguides, we obtain facets that we use to couple the signal to and from the waveguide. For paper 2 a new method is presented to fabricate the photonic circuit directly on a piezoelectric crystal. This method avoids wafer bonding and hence provides better strain transfer. The process starts with polishing a 300 µm thick PMN-PT crystal. Subsequently, the top and bottom surfaces of the piezo crystal are metallized by chromium and gold deposition to form the electrical contacts. For the photonic circuit, a 2 µm SiO_2 layer followed by a 230 nm SiN film are deposited by plasma-enhanced chemical vapor deposition. The waveguides are also fabricated using electron beam lithography, reactive ion etching, and resist stripping.

Chapter 7

Summary and Outlook

The efforts in bringing quantum optics experiments from the lab to real world applications, especially in quantum networks depends on the development of ideal quantum light sources. Despite notable advancements, such as entanglement distribution and quantum key distribution via deployed fibers or satellite communication [Yin20, Neu22], these demonstrations are constrained by the quality of the quantum light sources.

In this thesis we primarily investigated semiconductor quantum dots emitting in the near-infrared spectral range under various excitation conditions. Our research has yielded a fundamentally deeper understanding of quantum two- to four-level systems, laying the groundwork for future improvements in quantum light sources. To address a quantum two-level system, we performed s-shell resonant excitation of neutral and charged excitons in a GaAs quantum dot in paper 3. We achieved near-unity photon indistinguishabilities with raw Hong-Ou-Mandel visibilities of up to $V_{\mathrm{HOM}} = 95.0^{+5.0}_{-6.1}$ %. However, the single-photon purity is limited due to re-excitation processes. To mitigate the re-excitation, we used the radiative cascade of a three-level quantum ladder system [Han18], which can be addressed by resonantly exciting the biexciton under two-photon excitation leading to the highest purity of single-photons among all quantum light sources today [Sch18b]. But this cascade also leads to a reduced indistinguishability intrinsically limited by the lifetime ratio

of the two transitions, as we have shown in paper 6. This limitation is inherent for all quantum ladder schemes and not only subject to quantum dots, which we used to prove the theoretical model and quantum optical simulations. The limitation for the first transition, in our case the biexciton transition, can be understood by an energy jitter added by the finite linewidth of the intermediate state, here the exciton. For the second transition, a timing jitter is added to that transition, in our case the exciton, due to the finite lifetime of the biexciton state, reducing the indistinguishability of this transition. The lifetimes of the respective transitions in the quantum dots lead to Hong-Ou-Mandel visibilities limited to approximately 67 %. The reduced indistinguishability of the exciton photons can be addressed by reducing the timing jitter. Therefore we proposed a novel excitation method based on two-photon excitation and subsequent stimulation of the biexciton transition (Paper 8). By comparing the same quantum dot (in this case an InGaAs quantum dot) under this and the above mentioned excitation methods we showed, that we reach the near-unity Hong-Ou-Mandel visibility of the two-level systems while maintaining good single-photon purity of a three-level system. Furthermore, the polarization of the stimulation laser allows control of the exciton polarization leading to almost twice the brightness compared to the exciton in a two-level system, where the excitation laser is filtered by polarization suppression. Another excitation variation was introduced, where a control laser was tuned close to either the biexciton or exciton transitions, offering a virtual state facilitating a stimulated down-conversion process (paper 9). This allows for laser-controlled manipulation of single-photon energy and polarization. Additionally, our studies extended to the two-level system in the Rayleigh regime, where most of the signal arises from coherently scattered laser photons. We addressed this regime by exciting a GaAs quantum dot under low-power continuous-wave s-shell resonant excitation (paper 5). While we observed single-photon emission and a spectral component with sub-natural linewidth, these properties could not coexist simultaneously. Since the antibunching in this regime comes from interference of coherently scattered and incoherent photons, the antibunching dip disappeared upon narrow filtering of the signal.

The other key focus of this thesis was the improvement of single-photon sources to make them more practical for future real-world applications beyond the laboratory. One crucial aspect targeted for improvement was the brightness of the single-photon

sources. In paper 4, we introduced a novel photonic microparaboloid structure, which shows a nearly Gaussian emission profile and an average six-fold increase in count rates compared to as grown quantum dots. Moreover, this structure was integrated onto a piezoelectric substrate enabling stable and reversible wavelength tuning. Such tunability is essential for applications like coupling quantum dots to atomic quantum memories or enabling two-photon interference from separate sources. For efficient long-distance transmission of qubits through optical glass fibers, photons in the telecom O- or C-band offer advantages due to lower losses. Hence, efforts have been made to shift the emission wavelength of established InAsP nanowire quantum dots from the near-infrared to the telecom C-band at 1550 nm (paper 1). In order to facilitate experiments and applications with more complex architectures, there is a necessity for miniaturization of setups, making the integration of quantum light sources into quantum photonic circuits necessary. Nanowire quantum dots emerge as promising candidates for this purpose, given their capability for deterministic transfer and positioning. As shown in paper 2, we coupled an InAsP nanowire quantum dot into a photonic circuit directly fabricated on a piezoelectric substrate, allowing for tuning of both emitter wavelength and an on-chip optical resonator. Another type of quantum emitter suitable for integration into photonic circuits are emitters hosted by two-dimensional materials. We demonstrated this by coupling an emitter in a WSe_2 monolayer to a waveguide and demonstrated propagation of single-photons and resonance fluorescence in paper 7.

While our studies have already provided insights into quantum-level schemes, it is crucial to note that experiments conducted on quantum dots hosted in solid state materials are susceptible to noise originating from phonons and charge carriers in the vicinity. Embedding quantum dots into a diode structure not only facilitates energy tuning via the quantum confined Stark effect but also stabilizes the charge environment. Towards the end of this thesis, preliminary measurements were undertaken, with GaAs quantum dots embedded in a p-i-n diode structure. These measurements indicate narrow linewidths, with only a factor less than 1.1 above the Fourier-transform limit, and show no signs of blinking over hundreds of microseconds, consistent with the results of Zhai et al. [Zha20]. These developments of samples lead to cleaner quantum-level schemes, thereby paving the way for more fundamental studies. It enabled us to extensively investigate the coupling of a two-level system

with phonons in the solid state, and preliminary data were obtained demonstrating the theoretically proposed reappearance of Rabi oscillations [Vag07]. Moreover, it should enable homodyne detection, which can restore the antibunching lost upon narrow filtering, as discussed in paper 5, potentially leading to subnatural linewidth single photons [Car18]. Additionally, this advancement facilitates the study of other fundamental processes, such as dark states or light hole-heavy hole mixing. A comprehensive understanding of the level structures in quantum light sources and different interaction mechanisms with the environment hopefully yield to better optimized sources and excitation conditions. The clean level structure also allows the measurement of two-photon interference with near-unity visibility of photons with long temporal delays or between separate quantum dots, as demonstrated in recent works [Tom21, Zha22]. Two-photon interference of remote sources [Zha22] will enable the demonstration of quantum teleportation or entanglement swapping of remote sources, which is a prerequisite for quantum repeaters, for example based on the scheme from Lloyd et al. [Llo01]. Another crucial property of quantum light sources is the generation of highly entangled photon pairs. Quantum dots are capable of intrinsically generating polarization entangled photon pairs under two-photon excitation. However, the excitation scheme introduced in paper 8 overcomes the reduced Hong-Ou-Mandel visibility for the exciton photon but also sacrifices the biexciton photon, thus preventing the emission of entangled photon pairs. To combine all properties simultaneously, it is essential to manipulate the lifetime ratio of both transitions. This can be achieved by selectively shortening the biexciton lifetime through an asymmetric Purcell enhancement. Therefore, the quantum dot must be positioned inside a photonic structure providing strong Purcell enhancement for the biexciton but not for the exciton, ideally maintaining a high extraction efficiency for both photons. While the microparaboloid structures from paper 4 feature high broadband extraction efficiency with a mode profile close to an ideal Gaussian, they do not exhibit this desired feature. However, deterministic positioning of the paraboloids and direct fiber coupling hold the potential for a bright fiber-coupled source.

A platform offering eavesdropping-free quantum communication channels will protect critical infrastructure such as financial transactions, healthcare data transmission, and diplomatic communication from cyber attacks. The award of the Nobel Prize in

Physics in 2022 "for experiments with entangled photons, establishing the violation of Bell inequalities and pioneering quantum information science", along with significant funding from various countries, will hopefully push the field further. Despite the numerous challenges that remain, I am confident that the research on quantum dots will help in the eventual realization of a quantum internet.

Acknowledgments

This thesis was a team effort, and I couldn't have done it without the help of many amazing people!
First of all, a huge thank you to my supervisor, Prof. Dr. Klaus D. Jöns. Klaus, you've supported me every step of the way throughout my thesis, but also your trust in me while building the new group in Paderborn meant a lot to me. Thank you for sharing your knowledge and all the ice cream breaks! A big thank you also to Prof. Dr. Christine Silberhorn for being my second reviewer. Christine, your feedback was invaluable and I really appreciate your advice for my future career. I am also very thankful for my third reviewer Prof. Dr. Rinaldo Trotta. Rinaldo, but beyond that, I am even more grateful for my visits to your group in Rome and the time we spent on workshops together! I also want to thank Prof. Dr. Stefan Schumacher and Dr. Viktoryia Zolatanosha for completing the committee for my defense.
Thanks to Val Zwiller for welcoming me into his group at KTH in Stockholm and for his continued support throughout my time there. A big thank you to the entire quantum nano photonics group: Ali, Art, Carlos, Lily, Marijn, Mikael, Stephan and Ulrika. It's been a pleasure working with all of you, and I appreciated the fruitful discussions and the helpful assistance when challenges arose. The friendly and inclusive atmosphere within the group, both inside and outside the lab, has made my time here truly enjoyable. Special thanks to my fellow PhD students: Katha, Lukas, Thomas, Samuel, and Julien. I am beyond grateful for everything I learned from each of you, as well as for the fun times we spent together, whether it was eating together, hiking, running too fast, bouldering too hard, swimming on summer nights, and much more. Your friendship has made my time at KTH unforgettable.
Many thanks to Artur Zrenner and his team, especially Björn and Alex, for welcoming

us when the Hybrid Quantum Photonic Devices group was still very new and small at Paderborn University. Your support made our start much easier.
And now a huge thank you to the whole hqpd team: Atzin, Christopher, Eva, Francesco, Gerhard, Hermann, Ioannis, Jan-Gabriel, Klaus, Liang, Lukas, Maran, Marc, Nico, Oscar, Patricia, Rebecca, and Santiago. We've built more than a lab. Together we've built a team with a great atmosphere. I want to thank you for all the time we've spent together - whether it was constructing, aligning, measuring, trying things out, redoing things, or discussing at the university or at conferences. But it's not all work; I've also enjoyed our chats over coffee and ice cream breaks. I'm also thankful for the memories we've made outside the lab, cooking together, picking blueberries, water skiing, and more. It's been more than just colleagues working together. We've become friends, and you've really made my time in Paderborn more enjoyable. Thank you very much! And of course, our research wouldn't be possible without everyone else around us - the janitors, the building services, the post office, the procurement office, etc., and especially Reiner and Heike. They all help to keep things running smoothly, and I'm grateful for your help.
I would also like to thank our collaborators. Without the interaction with colleagues from other groups, my research time would not have been half as successful and enjoyable. Whether you provided us with samples or theory for our measurements, engaged in discussions to overcome challenges and exchange ideas, or visited each other for research purposes, your contributions were indispensable. Thanks to Armando Rastelli and his team in Linz for the exceptional quality of the quantum dots and the always valuable and fruitful scientific exchange. Thanks also to Dan Dalacu and Philip J. Poole and their groups for the high quality nanowires, and to Dirk Reuter and Jon J. Finley and their groups for the high grade InGaAs quantum dots in diodes. Special thanks to Kai Müller, Lukas, and Friedrich for the opportunity to visit Munich and for the exciting results we obtained. Many thanks to the minions Michele, Francesco, Julia, Giuseppe, Mattia and Alessandro. I had an amazing time during my visits in Rome and learned a lot from you! I would also like to express my gratitude to all the other collaborators from Heriot-Watt University Edinburgh, TU Munich, JKU Linz, La Sapienza University Rome, Stanford University, University of Wolverhampton, University of Madrid, NRC Canada, and Delft University whom I haven't mentioned by name. I have always appreciated our collaboration, your

valuable feedback, and the time we spent together at conferences.
Besides the fascinating world of quantum optics, there is another world, the world of family and friendship. I'm grateful for the friends I've made around the world - from Germany to Norway, Lesotho, South Africa, Tanzania, Sweden and beyond. You provide balance, stand by me during hectic times, and remain patient when things get tough. Thank you for always being there for me and for the great times we spend together. A big thank you to my parents, Tina and Achim, and my brother Simon. Without you I would not be standing here. You have supported me in every possible way throughout my entire life, and you also sparked my passion for physics at an early age by introducing me to the wonders of science.
Finally, I would like to thank Lukas. Working with you in the lab is a pleasure and I really appreciate your help. But more than that, I'm beyond grateful for the moments we share outside of the lab. The way you support me and believe in me, and knowing that you are always there for me, means the world to me. You make the good times more fun and the hard times easier. You're simply the best.

Bibliography

[Aar13] S. Aaronson, A. Arkhipov, *The Computational Complexity of Linear Optics*, Theory of Computing **9**, 143–252 (2013) (Cited on page 67.)

[Adl98] F. Adler, M. Geiger, A. Bauknecht, D. Haase, P. Ernst, A. Dörnen, F. Scholz, H. Schweizer, *Self-Assembled InAs/GaAs Quantum Dots under Resonant Excitation*, Journal of Applied Physics **83**, 1631–1636 (1998) (Cited on pages 24 and 66.)

[Agh19] S. Aghaeimeibodi, J.-H. Kim, C.-M. Lee, M. A. Buyukkaya, C. Richardson, E. Waks, *Silicon Photonic Add-Drop Filter for Quantum Emitters*, Optics Express **27**, 16 882–16 889 (2019) (Cited on page 95.)

[Aha16] I. Aharonovich, D. Englund, M. Toth, *Solid-State Single-Photon Emitters*, Nature Photonics **10** (2016) (Cited on page 15.)

[Ako10] N. Akopian, U. Perinetti, L. Wang, A. Rastelli, O. G. Schmidt, V. Zwiller, *Tuning Single GaAs Quantum Dots in Resonance with a Rubidium Vapor*, Applied Physics Letters **97**, 082 103 (2010) (Cited on page 82.)

[Ako11] N. Akopian, L. Wang, A. Rastelli, O. G. Schmidt, V. Zwiller, *Hybrid Semiconductor-Atomic Interface: Slowing down Single Photons from a Quantum Dot*, Nature Photonics **5**, 230–233 (2011) (Cited on pages 9 and 25.)

[Ara82] Y. Arakawa, H. Sakaki, *Multidimensional Quantum Well Laser and Temperature Dependence of Its Threshold Current*, Applied Physics Letters **40**, 939–941 (1982) (Cited on page 16.)

[Ard14] P.-L. Ardelt, L. Hanschke, K. A. Fischer, K. Müller, A. Kleinkauf, M. Koller, A. Bechtold, T. Simmet, J. Wierzbowski, H. Riedl, G. Abstreiter, J. J. Finley, *Dissipative Preparation of the Exciton and Biexciton in Self-Assembled Quantum Dots on Picosecond Time Scales*, Physical Review B **90**, 241 404 (2014) (Cited on pages 39, 47, and 48.)

[Aru19] F. Arute, K. Arya, R. Babbush, D. Bacon, J. C. Bardin, R. Barends, R. Biswas, S. Boixo, F. G. S. L. Brandao, D. A. Buell, B. Burkett, Y. Chen,

Z. Chen, B. Chiaro, R. Collins, W. Courtney, A. Dunsworth, E. Farhi, B. Foxen, A. Fowler, C. Gidney, M. Giustina, R. Graff, K. Guerin, S. Habegger, M. P. Harrigan, M. J. Hartmann, A. Ho, M. Hoffmann, T. Huang, T. S. Humble, S. V. Isakov, E. Jeffrey, Z. Jiang, D. Kafri, K. Kechedzhi, J. Kelly, P. V. Klimov, S. Knysh, A. Korotkov, F. Kostritsa, D. Landhuis, M. Lindmark, E. Lucero, D. Lyakh, S. Mandrà, J. R. McClean, M. McEwen, A. Megrant, X. Mi, K. Michielsen, M. Mohseni, J. Mutus, O. Naaman, M. Neeley, C. Neill, M. Y. Niu, E. Ostby, A. Petukhov, J. C. Platt, C. Quintana, E. G. Rieffel, P. Roushan, N. C. Rubin, D. Sank, K. J. Satzinger, V. Smelyanskiy, K. J. Sung, M. D. Trevithick, A. Vainsencher, B. Villalonga, T. White, Z. J. Yao, P. Yeh, A. Zalcman, H. Neven, J. M. Martinis, *Quantum Supremacy Using a Programmable Superconducting Processor*, Nature **574**, 505–510 (2019) (Cited on page 7.)

[Atk12] P. Atkinson, E. Zallo, O. G. Schmidt, *Independent Wavelength and Density Control of Uniform GaAs/AlGaAs Quantum Dots Grown by Infilling Self-Assembled Nanoholes*, Journal of Applied Physics **112**, 054 303 (2012) (Cited on pages 24 and 25.)

[Azz21] S. I. Azzam, K. Parto, G. Moody, *Prospects and Challenges of Quantum Emitters in 2D Materials*, Applied Physics Letters **118**, 240 502 (2021) (Cited on page 32.)

[Bab21] H. G. Babin, J. Ritzmann, N. Bart, M. Schmidt, T. Kruck, L. Zhai, M. C. Löbl, G. N. Nguyen, C. Spinnler, L. Ranasinghe, R. J. Warburton, C. Heyn, A. D. Wieck, A. Ludwig, *Charge Tunable GaAs Quantum Dots in a Photonic n-i-p Diode*, Nanomaterials **11**, 1–19 (2021) (Cited on page 26.)

[Bal19] G. Ballesteros, R. Proux, C. Bonato, B. Gerardot, *readPTU: A Python Library to Analyse Time Tagged Time Resolved Data*, Journal of Instrumentation **14**, T06 011–T06 011 (2019) (Cited on page 64.)

[Bar00] J. A. Barker, E. P. O'Reilly, *Theoretical Analysis of Electron-Hole Alignment in InAs-GaAs Quantum Dots*, Physical Review B **61**, 13 840–13 851 (2000) (Cited on page 79.)

[Bar02] W. Barnes, G. Björk, J. Gérard, P. Jonsson, J. Wasey, P. Worthing, V. Zwiller, *Solid-State Single Photon Sources: Light Collection Strategies*, The European Physical Journal D - Atomic, Molecular, Optical and Plasma Physics **18**, 197–210 (2002) (Cited on pages 82 and 87.)

[Bar11] R. J. Barbour, P. A. Dalgarno, A. Curran, K. M. Nowak, H. J. Baker, D. R. Hall, N. G. Stoltz, P. M. Petroff, R. J. Warburton, *A Tunable Microcavity*, Journal of Applied Physics **110**, 053 107 (2011) (Cited on page 91.)

[Bar13] N. Bar-Gill, L. M. Pham, A. Jarmola, D. Budker, R. L. Walsworth, *Solid-State Electronic Spin Coherence Time Approaching One Second*, Nature Communications **4**, 1743 (2013) (Cited on page 15.)

[Bar24] A. Barbiero, G. Shooter, T. Müller, J. Skiba-Szymanska, R. M. Stevenson, L. E. Goff, D. A. Ritchie, A. J. Shields, *Polarization-Selective Enhancement of Telecom Wavelength Quantum Dot Transitions in an Elliptical Bullseye Resonator*, Nano Letters **24**, 2839–2845 (2024) (Cited on page 90.)

[Bay02] M. Bayer, G. Ortner, O. Stern, A. Kuther, A. A. Gorbunov, A. Forchel, P. Hawrylak, S. Fafard, K. Hinzer, T. L. Reinecke, S. N. Walck, J. P. Reithmaier, F. Klopf, F. Schäfer, *Fine Structure of Neutral and Charged Excitons in Self-Assembled In(Ga)As/(Al)GaAs Quantum Dots*, Physical Review B **65**, 195 315 (2002) (Cited on pages 21 and 22.)

[BB19] F. Basso Basset, M. B. Rota, C. Schimpf, D. Tedeschi, K. D. Zeuner, S. F. Covre da Silva, M. Reindl, V. Zwiller, K. D. Jöns, A. Rastelli, R. Trotta, *Entanglement Swapping with Photons Generated on Demand by a Quantum Dot*, Physical Review Letters **123**, 160 501 (2019) (Cited on pages 26, 48, and 73.)

[Bec20] J. N. Becker, E. Neu, *Chapter Seven - The Silicon Vacancy Center in Diamond*, in C. E. Nebel, I. Aharonovich, N. Mizuochi, M. Hatano (Editors) *Semiconductors and Semimetals*, volume 103 of *Diamond for Quantum Applications Part 1*, pages 201–235 (Elsevier, 2020) (Cited on pages 9 and 15.)

[Ben00] O. Benson, C. Santori, M. Pelton, Y. Yamamoto, *Regulated and Entangled Photons from a Single Quantum Dot*, Physical Review Letters **84**, 2513–2516 (2000) (Cited on page 21.)

[Ben05] A. J. Bennett, D. C. Unitt, A. J. Shields, P. Atkinson, D. A. Ritchie, *Influence of Exciton Dynamics on the Interference of Two Photons from a Microcavity Single-Photon Source*, Optics Express **13**, 7772–7778 (2005) (Cited on page 73.)

[Ben10a] A. J. Bennett, R. B. Patel, J. Skiba-Szymanska, C. A. Nicoll, I. Farrer, D. A. Ritchie, A. J. Shields, *Giant Stark Effect in the Emission of Single Semiconductor Quantum Dots*, Applied Physics Letters **97**, 031 104 (2010) (Cited on page 81.)

[Ben10b] A. J. Bennett, M. A. Pooley, R. M. Stevenson, M. B. Ward, R. B. Patel, A. B. de la Giroday, N. Sköld, I. Farrer, C. A. Nicoll, D. A. Ritchie, A. J. Shields, *Electric-Field-Induced Coherent Coupling of the Exciton States in a Single Quantum Dot*, Nature Physics **6**, 947–950 (2010) (Cited on page 82.)

[Ben14] C. H. Bennett, G. Brassard, *Quantum Cryptography: Public Key Distribution and Coin Tossing*, Theoretical Computer Science **560**, 7–11 (2014) (Cited on pages 8 and 57.)

[Ber07] T. Berstermann, T. Auer, H. Kurtze, M. Schwab, D. R. Yakovlev, M. Bayer, J. Wiersig, C. Gies, F. Jahnke, D. Reuter, A. D. Wieck, *Systematic Study of Carrier Correlations in the Electron-Hole Recombination Dynamics of Quantum Dots*, Physical Review B **76**, 165 318 (2007) (Cited on pages 24 and 66.)

[Ber13] T. C. Berkelbach, M. S. Hybertsen, D. R. Reichman, *Theory of Neutral and Charged Excitons in Monolayer Transition Metal Dichalcogenides*, Physical Review B **88**, 045 318 (2013) (Cited on page 31.)

[Beu06] J. Beugnon, M. P. Jones, J. Dingjan, B. Darquié, G. Messin, A. Browaeys, P. Grangier, *Quantum Interference between Two Single Photons Emitted by Independently Trapped Atoms*, Nature **440**, 779–782 (2006) (Cited on page 73.)

[Bhi15] G. R. Bhimanapati, Z. Lin, V. Meunier, Y. Jung, J. Cha, S. Das, D. Xiao, Y. Son, M. S. Strano, V. R. Cooper, L. Liang, S. G. Louie, E. Ringe, W. Zhou, S. S. Kim, R. R. Naik, B. G. Sumpter, H. Terrones, F. Xia, Y. Wang, J. Zhu, D. Akinwande, N. Alem, J. A. Schuller, R. E. Schaak, M. Terrones, J. A. Robinson, *Recent Advances in Two-Dimensional Materials beyond Graphene*, ACS Nano **9**, 11 509–11 539 (2015) (Cited on page 29.)

[Bie23] J. Bienfang, T. Gerrits, P. Kuo, A. Migdall, S. Polyakov, O. T. Slattery, *Single-Photon Sources and Detectors Dictionary*, NIST (2023) (Cited on page 60.)

[Ble11] J. Bleuse, J. Claudon, M. Creasey, Nitin. S. Malik, J.-M. Gérard, I. Maksymov, J.-P. Hugonin, P. Lalanne, *Inhibition, Enhancement, and Control of Spontaneous Emission in Photonic Nanowires*, Physical Review Letters **106**, 103 601 (2011) (Cited on pages 27 and 86.)

[Blu18] D. J. Blumenthal, R. Heideman, D. Geuzebroek, A. Leinse, C. Roeloffzen, *Silicon Nitride in Silicon Photonics*, Proceedings of the IEEE **106**, 2209–2231 (2018) (Cited on page 92.)

[Boo24] K. Boos, F. Sbresny, S. K. Kim, M. Kremser, H. Riedl, F. W. Bopp, W. Rauhaus, B. Scaparra, K. D. Jöns, J. J. Finley, K. Müller, L. Hanschke, *Coherent Swing-Up Excitation for Semiconductor Quantum Dots*, Advanced Quantum Technologies, 2300 359 (2024) (Cited on page 39.)

[Bou97] D. Bouwmeester, J.-W. Pan, K. Mattle, M. Eibl, H. Weinfurter, A. Zeilinger, *Experimental Quantum Teleportation*, Nature **390**, 575–579 (1997) (Cited on page 67.)

[Bou15] S. Bounouar, M. Müller, A. M. Barth, M. Glässl, V. M. Axt, P. Michler, *Phonon-Assisted Robust and Deterministic Two-Photon Biexciton Preparation in a Quantum Dot*, Physical Review B **91**, 161 302 (2015) (Cited on page 47.)

[Bou20] F. Bouchard, A. Sit, Y. Zhang, R. Fickler, F. M. Miatto, Y. Yao, F. Sciarrino, E. Karimi, *Two-Photon Interference: The Hong–Ou–Mandel Effect*, Reports on Progress in Physics **84**, 012 402 (2020) (Cited on page 68.)

[Bra17] A. Branny, S. Kumar, R. Proux, B. D. Gerardot, *Deterministic Strain-Induced Arrays of Quantum Emitters in a Two-Dimensional Semiconductor*, Nature Communications **8**, 15 053 (2017) (Cited on pages 31, 91, and 95.)

[Bra21] T. K. Bracht, M. Cosacchi, T. Seidelmann, M. Cygorek, A. Vagov, V. M. Axt, T. Heindel, D. E. Reiter, *Swing-Up of Quantum Emitter Population Using Detuned Pulses*, PRX Quantum **2**, 040 354 (2021) (Cited on page 39.)

[Bra23] T. K. Bracht, T. Seidelmann, Y. Karli, F. Kappe, V. Remesh, G. Weihs, V. M. Axt, D. E. Reiter, *Dressed-State Analysis of Two-Color Excitation Schemes*, Physical Review B **107**, 035 425 (2023) (Cited on page 39.)

[Bre16] D. Breddermann, D. Heinze, R. Binder, A. Zrenner, S. Schumacher, *All-Optical Tailoring of Single-Photon Spectra in a Quantum-Dot Microcavity System*, Physical Review B **94**, 165 310 (2016) (Cited on page 54.)

[Bre18] D. Breddermann, T. Praschan, D. Heinze, R. Binder, S. Schumacher, *Microscopic Theory of Cavity-Enhanced Single-Photon Emission from Optical Two-Photon Raman Processes*, Physical Review B **97**, 125 303 (2018) (Cited on page 54.)

[Bre20] L. Bremer, K. Weber, S. Fischbach, S. Thiele, M. Schmidt, A. Kaganskiy, S. Rodt, A. Herkommer, M. Sartison, S. L. Portalupi, P. Michler, H. Giessen, S. Reitzenstein, *Quantum Dot Single-Photon Emission Coupled into Single-Mode Fibers with 3D Printed Micro-Objectives*, APL Photonics **5**, 106 101 (2020) (Cited on page 88.)

[Bru94] K. Brunner, G. Abstreiter, G. Böhm, G. Tränkle, G. Weimann, *Sharp-Line Photoluminescence and Two-Photon Absorption of Zero-Dimensional Biexcitons in a GaAs/AlGaAs Structure*, Physical Review Letters **73**, 1138–1141 (1994) (Cited on page 47.)

[Bul14] G. Bulgarini, M. E. Reimer, M. Bouwes Bavinck, K. D. Jöns, D. Dalacu, P. J. Poole, E. P. A. M. Bakkers, V. Zwiller, *Nanowire Waveguides Launching Single Photons in a Gaussian Mode for Ideal Fiber Coupling*, Nano Letters **14**, 4102–4106 (2014) (Cited on pages 28 and 86.)

[Cad16] D. Cadeddu, J. Teissier, F. R. Braakman, N. Gregersen, P. Stepanov, J.-M. Gérard, J. Claudon, R. J. Warburton, M. Poggio, M. Munsch, *A Fiber-Coupled Quantum-Dot on a Photonic Tip*, Applied Physics Letters **108**, 011 112 (2016) (Cited on pages 86 and 94.)

[Cad17] F. Cadiz, E. Courtade, C. Robert, G. Wang, Y. Shen, H. Cai, T. Taniguchi, K. Watanabe, H. Carrere, D. Lagarde, M. Manca, T. Amand, P. Renucci, S. Tongay, X. Marie, B. Urbaszek, *Excitonic Linewidth Approaching the Homogeneous Limit in MoS_2-Based van Der Waals Heterostructures*, Physical Review X **7**, 021 026 (2017) (Cited on page 32.)

[Car11] P. Caroff, J. Bolinsson, J. Johansson, *Crystal Phases in III–V Nanowires: From Random Toward Engineered Polytypism*, IEEE Journal of Selected Topics in Quantum Electronics **17**, 829–846 (2011) (Cited on page 27.)

[Car18] J. C. L. Carreño, E. Z. Casalengua, F. P. Laussy, E. del Valle, *Joint Subnatural-Linewidth and Single-Photon Emission from Resonance Fluorescence*, Quantum Science and Technology **3**, 045 001 (2018) (Cited on pages 65 and 102.)

[Cas14] A. Castellanos-Gomez, M. Buscema, R. Molenaar, V. Singh, L. Janssen, H. S. J. van der Zant, G. A. Steele, *Deterministic Transfer of Two-Dimensional Materials by All-Dry Viscoelastic Stamping*, 2D Materials **1**, 011 002 (2014) (Cited on page 93.)

[Cha17] C. Chakraborty, K. M. Goodfellow, S. Dhara, A. Yoshimura, V. Meunier, A. N. Vamivakas, *Quantum-Confined Stark Effect of Individual Defects in a van Der Waals Heterostructure*, Nano Letters **17**, 2253–2258 (2017) (Cited on page 82.)

[Cha18] C. Chakraborty, L. Qiu, K. Konthasinghe, A. Mukherjee, S. Dhara, N. Vamivakas, *3D Localized Trions in Monolayer WSe_2 in a Charge Tunable van Der Waals Heterostructure*, Nano Letters **18**, 2859–2863 (2018) (Cited on page 82.)

[Cha19a] C. Chakraborty, N. R. Jungwirth, G. D. Fuchs, A. N. Vamivakas, *Electrical Manipulation of the Fine-Structure Splitting of WSe_2 Quantum Emitters*, Physical Review B **99**, 045 308 (2019) (Cited on page 82.)

[Cha19b] C. Chakraborty, N. Vamivakas, D. Englund, *Advances in Quantum Light Emission from 2D Materials*, Nanophotonics **8** (2019) (Cited on pages 9 and 32.)

[Cha23] J. Chang, J. Gao, I. E. Zadeh, A. W. Elshaari, V. Zwiller, *Nanowire-Based Integrated Photonics for Quantum Information and Quantum Sensing*, Nanophotonics **12**, 339–358 (2023) (Cited on page 93.)

[Che10] X. Chew, G. Zhou, H. Yu, F. S. Chau, J. Deng, Y. C. Loke, X. Tang, *An In-Plane Nano-Mechanics Approach to Achieve Reversible Resonance Control of Photonic Crystal Nanocavities*, Optics Express **18**, 22 232–22 244 (2010) (Cited on page 95.)

[Che16] Y. Chen, J. Zhang, M. Zopf, K. Jung, Y. Zhang, R. Keil, F. Ding, O. G. Schmidt, *Wavelength-Tunable Entangled Photons from Silicon-Integrated III–V Quantum Dots*, Nature Communications **7**, 10 387 (2016) (Cited on pages 77 and 78.)

[Che18] Y. Chen, M. Zopf, R. Keil, F. Ding, O. G. Schmidt, *Highly-Efficient Extraction of Entangled Photons from Quantum Dots Using a Broadband Optical Antenna*, Nature Communications **9**, 2994 (2018) (Cited on page 88.)

[Che19] R. Cheng, C.-L. Zou, X. Guo, S. Wang, X. Han, H. X. Tang, *Broadband On-Chip Single-Photon Spectrometer*, Nature Communications **10**, 4104 (2019) (Cited on page 96.)

[Chi19] L. Chirolli, E. Prada, F. Guinea, R. Roldán, P. San-Jose, *Strain-Induced Bound States in Transition-Metal Dichalcogenide Bubbles*, 2D Materials **6**, 025 010 (2019) (Cited on page 31.)

[Cla74] J. F. Clauser, *Experimental Distinction between the Quantum and Classical Field-Theoretic Predictions for the Photoelectric Effect*, Physical Review D **9**, 853–860 (1974) (Cited on page 13.)

[Cla10] J. Claudon, J. Bleuse, N. S. Malik, M. Bazin, P. Jaffrennou, N. Gregersen, C. Sauvan, P. Lalanne, J.-M. Gérard, *A Highly Efficient Single-Photon Source Based on a Quantum Dot in a Photonic Nanowire*, Nature Photonics **4**, 174–177 (2010) (Cited on pages 27 and 86.)

[Cor01] S. Cortez, O. Krebs, P. Voisin, J. M. Gérard, *Polarization of the Interband Optical Dipole in InAs/GaAs Self-Organized Quantum Dots*, Physical Review B **63**, 233 306 (2001) (Cited on page 18.)

[Cra24] A. N. Craddock, Y. Wang, F. Giraldo, R. Sekelsky, M. Flament, M. Namazi, *High-Rate Subgigahertz-Linewidth Bichromatic Entanglement Source for*

Quantum Networking, Physical Review Applied **21**, 034 012 (2024) (Cited on page 15.)

[Cui06] G. Cui, J. M. Hannigan, R. Loeckenhoff, F. M. Matinaga, M. G. Raymer, S. Bhongale, M. Holland, S. Mosor, S. Chatterjee, H. M. Gibbs, G. Khitrova, *A Hemispherical, High-Solid-Angle Optical Micro-Cavity for Cavity-QED Studies*, Optics Express **14**, 2289–2299 (2006) (Cited on page 91.)

[Cur80] J. Curie, P. Curie, *Développement par compression de l'électricité polaire dans les cristaux hémièdres à faces inclinées*, Bulletin de Minéralogie **3**, 90–93 (1880) (Cited on page 77.)

[daS21] S. F. C. da Silva, G. Undeutsch, B. Lehner, S. Manna, T. M. Krieger, M. Reindl, C. Schimpf, R. Trotta, A. Rastelli, *GaAs Quantum Dots Grown by Droplet Etching Epitaxy as Quantum Light Sources*, Applied Physics Letters **119**, 120 502 (2021) (Cited on pages 9 and 26.)

[Dad16] A. C. Dada, T. S. Santana, R. N. E. Malein, A. Koutroumanis, Y. Ma, J. M. Zajac, J. Y. Lim, J. D. Song, B. D. Gerardot, *Indistinguishable Single Photons with Flexible Electronic Triggering*, Optica **3**, 493 (2016) (Cited on pages 46, 66, and 71.)

[Dak70] M. L. Dakss, L. Kuhn, P. F. Heidrich, B. A. Scott, *Grating Coupler for Efficient Excitation of Optical Guided Waves in Thin Films*, Applied Physics Letters **16**, 523–525 (1970) (Cited on page 97.)

[Dal09] D. Dalacu, A. Kam, D. G. Austing, X. Wu, J. Lapointe, G. C. Aers, P. J. Poole, *Selective-Area Vapour–Liquid–Solid Growth of InP Nanowires*, Nanotechnology **20**, 395 602 (2009) (Cited on page 27.)

[Dal12] D. Dalacu, K. Mnaymneh, J. Lapointe, X. Wu, P. J. Poole, G. Bulgarini, V. Zwiller, M. E. Reimer, *Ultraclean Emission from InAsP Quantum Dots in Defect-Free Wurtzite InP Nanowires*, Nano Letters **12**, 5919–5923 (2012) (Cited on page 27.)

[Dar31] C. G. Darwin, *The Diamagnetism of the Free Electron*, Mathematical Proceedings of the Cambridge Philosophical Society **27**, 86–90 (1931) (Cited on page 17.)

[Dav11] M. Davanço, M. T. Rakher, D. Schuh, A. Badolato, K. Srinivasan, *A Circular Dielectric Grating for Vertical Extraction of Single Quantum Dot Emission*, Applied Physics Letters **99**, 041 102 (2011) (Cited on page 90.)

[Dav17] M. Davanco, J. Liu, L. Sapienza, C.-Z. Zhang, J. V. De Miranda Cardoso, V. Verma, R. Mirin, S. W. Nam, L. Liu, K. Srinivasan, *Heterogeneous*

Integration for On-Chip Quantum Photonic Circuits with Single Quantum Dot Devices, Nature Communications **8**, 889 (2017) (Cited on pages 93 and 94.)

[Deb16] S. Debnath, N. M. Linke, C. Figgatt, K. A. Landsman, K. Wright, C. Monroe, *Demonstration of a Small Programmable Quantum Computer with Atomic Qubits*, Nature **536**, 63–66 (2016) (Cited on pages 9 and 14.)

[Din10] F. Ding, R. Singh, J. D. Plumhof, T. Zander, V. Křápek, Y. H. Chen, M. Benyoucef, V. Zwiller, K. Dörr, G. Bester, A. Rastelli, O. G. Schmidt, *Tuning the Exciton Binding Energies in Single Self-Assembled InGaAs/GaAs Quantum Dots by Piezoelectric-Induced Biaxial Stress*, Physical Review Letters **104**, 067 405 (2010) (Cited on page 77.)

[Din23] X. Ding, Y.-P. Guo, M.-C. Xu, R.-Z. Liu, G.-Y. Zou, J.-Y. Zhao, Z.-X. Ge, Q.-H. Zhang, H.-L. Liu, L.-J. Wang, M.-C. Chen, H. Wang, Y.-M. He, Y.-H. Huo, C.-Y. Lu, J.-W. Pan, *High-Efficiency Single-Photon Source above the Loss-Tolerant Threshold for Efficient Linear Optical Quantum Computing*, arXiv:2311.08347 (2023) (Cited on page 91.)

[Dir27] P. A. M. Dirac, N. H. D. Bohr, *The Quantum Theory of the Emission and Absorption of Radiation*, Proceedings of the Royal Society of London. Series A, Containing Papers of a Mathematical and Physical Character **114**, 243–265 (1927) (Cited on page 83.)

[DiV95] D. P. DiVincenzo, *Quantum Computation*, Science **270**, 255–261 (1995) (Cited on page 7.)

[Doh13] M. W. Doherty, N. B. Manson, P. Delaney, F. Jelezko, J. Wrachtrup, L. C. L. Hollenberg, *The Nitrogen-Vacancy Colour Centre in Diamond*, Physics Reports **528**, 1–45 (2013) (Cited on pages 9 and 15.)

[Dou08] A. Dousse, L. Lanco, J. Suffczyński, E. Semenova, A. Miard, A. Lemaître, I. Sagnes, C. Roblin, J. Bloch, P. Senellart, *Controlled Light-Matter Coupling for a Single Quantum Dot Embedded in a Pillar Microcavity Using Far-Field Optical Lithography*, Physical Review Letters **101**, 267 404 (2008) (Cited on page 91.)

[Dou10] A. Dousse, J. Suffczyński, A. Beveratos, O. Krebs, A. Lemaître, I. Sagnes, J. Bloch, P. Voisin, P. Senellart, *Ultrabright Source of Entangled Photon Pairs*, Nature **466**, 217–220 (2010) (Cited on page 89.)

[DR03] H. De Riedmatten, I. Marcikic, W. Tittel, H. Zbinden, N. Gisin, *Quantum Interference with Photon Pairs Created in Spatially Separated Sources*, Physical Review A **67**, 5 (2003) (Cited on pages 9 and 73.)

[Dra23] J.-C. Drawer, V. N. Mitryakhin, H. Shan, S. Stephan, M. Gittinger, L. Lackner, B. Han, G. Leibeling, F. Eilenberger, R. Banerjee, S. Tongay, K. Watanabe, T. Taniguchi, C. Lienau, M. Silies, C. Anton-Solanas, M. Esmann, C. Schneider, *Monolayer-Based Single-Photon Source in a Liquid-Helium-Free Open Cavity Featuring 65% Brightness and Quantum Coherence*, Nano Letters **23**, 8683–8689 (2023) (Cited on page 92.)

[Dud12] Y. O. Dudin, A. Kuzmich, *Strongly Interacting Rydberg Excitations of a Cold Atomic Gas*, Science **336**, 887–889 (2012) (Cited on page 15.)

[Duo18] N. M. H. Duong, Z.-Q. Xu, M. Kianinia, R. Su, Z. Liu, S. Kim, C. Bradac, T. T. Tran, Y. Wan, L.-J. Li, A. Solntsev, J. Liu, I. Aharonovich, *Enhanced Emission from WSe_2 Monolayers Coupled to Circular Bragg Gratings*, ACS Photonics **5**, 3950–3955 (2018) (Cited on pages 32 and 91.)

[Eke91] A. K. Ekert, *Quantum Cryptography Based on Bell's Theorem*, Physical Review Letters **67**, 661–663 (1991) (Cited on pages 8 and 67.)

[Ell18] D. J. P. Ellis, A. J. Bennett, C. Dangel, J. P. Lee, J. P. Griffiths, T. A. Mitchell, T.-K. Paraiso, P. Spencer, D. A. Ritchie, A. J. Shields, *Independent Indistinguishable Quantum Light Sources on a Reconfigurable Photonic Integrated Circuit*, Applied Physics Letters **112**, 211 104 (2018) (Cited on page 96.)

[Els17] A. W. Elshaari, I. E. Zadeh, A. Fognini, M. E. Reimer, D. Dalacu, P. J. Poole, V. Zwiller, K. D. Jöns, *On-Chip Single Photon Filtering and Multiplexing in Hybrid Quantum Photonic Circuits*, Nature Communications **8**, 379 (2017) (Cited on pages 28, 93, 95, and 96.)

[Err20] C. Errando-Herranz, A. Y. Takabayashi, P. Edinger, H. Sattari, K. B. Gylfason, N. Quack, *MEMS for Photonic Integrated Circuits*, IEEE Journal of Selected Topics in Quantum Electronics **26**, 1–16 (2020) (Cited on page 96.)

[Est06] P. Ester, S. Stufler, S. Michaelis de Vasconcellos, M. Bichler, A. Zrenner, *High Resolution Photocurrent-Spectroscopy of a Single Quantum Dot*, physica status solidi c **3**, 3722–3725 (2006) (Cited on page 81.)

[Far07] A. Faraon, D. Englund, I. Fushman, J. Vučković, N. Stoltz, P. Petroff, *Local Quantum Dot Tuning on Photonic Crystal Chips*, Applied Physics Letters **90**, 213 110 (2007) (Cited on page 96.)

[Fey82] R. P. Feynman, *Simulating Physics with Computers*, International Journal of Theoretical Physics **21**, 467–488 (1982) (Cited on page 7.)

[Fis18] K. A. Fischer, R. Trivedi, D. Lukin, *Particle Emission from Open Quantum Systems*, Physical Review A **98**, 023 853 (2018) (Cited on page 72.)

[Fla10] E. B. Flagg, A. Muller, S. V. Polyakov, A. Ling, A. Migdall, G. S. Solomon, *Interference of Single Photons from Two Separate Semiconductor Quantum Dots*, Physical Review Letters **104**, 1–4 (2010) (Cited on pages 73 and 77.)

[Fla18] L. C. Flatten, L. Weng, A. Branny, S. Johnson, P. R. Dolan, A. A. P. Trichet, B. D. Gerardot, J. M. Smith, *Microcavity Enhanced Single Photon Emission from Two-Dimensional WSe_2*, Applied Physics Letters **112**, 191 105 (2018) (Cited on page 92.)

[Fli01] T. Flissikowski, A. Hundt, M. Lowisch, M. Rabe, F. Henneberger, *Photon Beats from a Single Semiconductor Quantum Dot*, Physical Review Letters **86**, 3172–3175 (2001) (Cited on pages 46, 66, and 71.)

[Foc28] V. Fock, *Bemerkung zur Quantelung des harmonischen Oszillators im Magnetfeld*, Zeitschrift für Physik **47**, 446–448 (1928) (Cited on page 17.)

[För03] J. Förstner, C. Weber, J. Danckwerts, A. Knorr, *Phonon-Assisted Damping of Rabi Oscillations in Semiconductor Quantum Dots*, Physical Review Letters **91**, 127 401 (2003) (Cited on page 43.)

[Fox06] A. M. Fox, *Quantum Optics: An Introduction* (OUP Oxford, 2006), ISBN 978-0-19-856672-4 (Cited on pages 42, 58, 60, and 62.)

[Fry00a] P. W. Fry, J. J. Finley, L. R. Wilson, A. Lemaître, D. J. Mowbray, M. S. Skolnick, M. Hopkinson, G. Hill, J. C. Clark, *Electric-Field-Dependent Carrier Capture and Escape in Self-Assembled InAs/GaAs Quantum Dots*, Applied Physics Letters **77**, 4344–4346 (2000) (Cited on page 81.)

[Fry00b] P. W. Fry, I. E. Itskevich, D. J. Mowbray, M. S. Skolnick, J. J. Finley, J. A. Barker, E. P. O'Reilly, L. R. Wilson, I. A. Larkin, P. A. Maksym, M. Hopkinson, M. Al-Khafaji, J. P. R. David, A. G. Cullis, G. Hill, J. C. Clark, *Inverted Electron-Hole Alignment in InAs-GaAs Self-Assembled Quantum Dots*, Physical Review Letters **84**, 733–736 (2000) (Cited on page 79.)

[Gaá22] B. Gaál, M. A. Jacobsen, L. Vannucci, J. Claudon, J.-M. Gérard, N. Gregersen, *Near-Unity Efficiency and Photon Indistinguishability for the "Hourglass" Single-Photon Source Using Suppression of the Background Emission*, Applied Physics Letters **121**, 170 501 (2022) (Cited on page 89.)

[Gay98] B. Gayral, J. M. Gérard, B. Legrand, E. Costard, V. Thierry-Mieg, *Optical Study of GaAs/AlAs Pillar Microcavities with Elliptical Cross Section*, Applied Physics Letters **72**, 1421–1423 (1998) (Cited on page 89.)

[Gaz13] O. Gazzano, S. Michaelis de Vasconcellos, C. Arnold, A. Nowak, E. Galopin, I. Sagnes, L. Lanco, A. Lemaître, P. Senellart, *Bright Solid-State Sources of Indistinguishable Single Photons*, Nature Communications **4**, 1425 (2013) (Cited on page 73.)

[Geh19a] H. Gehring, M. Blaicher, W. Hartmann, P. Varytis, K. Busch, M. Wegener, W. H. P. Pernice, *Low-Loss Fiber-to-Chip Couplers with Ultrawide Optical Bandwidth*, APL Photonics **4**, 010 801 (2019) (Cited on page 97.)

[Geh19b] H. Gehring, A. Eich, C. Schuck, W. H. P. Pernice, *Broadband Out-of-Plane Coupling at Visible Wavelengths*, Optics Letters **44**, 5089–5092 (2019) (Cited on page 97.)

[Ger04] C. Gerry, P. Knight, *Introductory Quantum Optics* (Cambridge University Press, Cambridge, 2004), ISBN 978-0-521-52735-4 (Cited on page 68.)

[Ger07] B. D. Gerardot, S. Seidl, P. A. Dalgarno, R. J. Warburton, D. Granados, J. M. Garcia, K. Kowalik, O. Krebs, K. Karrai, A. Badolato, P. M. Petroff, *Manipulating Exciton Fine Structure in Quantum Dots with a Lateral Electric Field*, Applied Physics Letters **90**, 041 101 (2007) (Cited on page 82.)

[Gha12] M. Ghali, K. Ohtani, Y. Ohno, H. Ohno, *Generation and Control of Polarization-Entangled Photons from GaAs Island Quantum Dots by an Electric Field*, Nature Communications **3**, 661 (2012) (Cited on pages 22, 81, and 82.)

[Gho86] R. Ghosh, C. K. Hong, Z. Y. Ou, L. Mandel, *Interference of Two Photons in Parametric down Conversion*, Physical Review A **34**, 3962–3968 (1986) (Cited on page 69.)

[Gho87] R. Ghosh, L. Mandel, *Observation of Nonclassical Effects in the Interference of Two Photons*, Physical Review Letters **59**, 1903–1905 (1987) (Cited on pages 9 and 69.)

[Gib72] H. M. Gibbs, *Spontaneous Decay of Coherently Excited Rb*, Physical Review Letters **29**, 459–462 (1972) (Cited on page 43.)

[Gib73] H. M. Gibbs, *Incoherent Resonance Fluorescence from a Rb Atomic Beam Excited by a Short Coherent Optical Pulse*, Physical Review A **8**, 446–455 (1973) (Cited on page 43.)

[Gin22] L. Ginés, M. Moczała-Dusanowska, D. Dlaka, R. Hošák, J. R. Gonzales-Ureta, J. Lee, M. Ježek, E. Harbord, R. Oulton, S. Höfling, A. B. Young, C. Schneider, A. Predojević, *High Extraction Efficiency Source of Photon Pairs Based on a Quantum Dot Embedded in a Broadband Micropillar Cavity*, Physical Review Letters **129**, 033 601 (2022) (Cited on page 89.)

[Gla63] R. J. Glauber, *Coherent and Incoherent States of the Radiation Field*, Physical Review **131**, 2766 (1963) (Cited on page 58.)

[Glä13] M. Glässl, A. M. Barth, V. M. Axt, *Proposed Robust and High-Fidelity Preparation of Excitons and Biexcitons in Semiconductor Quantum Dots Making Active Use of Phonons*, Physical Review Letters **110**, 147 401 (2013) (Cited on page 48.)

[Gol85] L. Goldstein, F. Glas, J. Y. Marzin, M. N. Charasse, G. Le Roux, *Growth by Molecular Beam Epitaxy and Characterization of InAs/GaAs Strained-Layer Superlattices*, Applied Physics Letters **47**, 1099–1101 (1985) (Cited on page 16.)

[Gol14] P. Gold, A. Thoma, S. Maier, S. Reitzenstein, C. Schneider, S. Höfling, M. Kamp, *Two-Photon Interference from Remote Quantum Dots with Inhomogeneously Broadened Linewidths*, Physical Review B **89**, 1–7 (2014) (Cited on pages 73 and 76.)

[Gra15] D. Grassani, S. Azzini, M. Liscidini, M. Galli, M. J. Strain, M. Sorel, J. E. Sipe, D. Bajoni, *Micrometer-Scale Integrated Silicon Source of Time-Energy Entangled Photons*, Optica **2**, 88–94 (2015) (Cited on page 95.)

[Gre04] W. M. J. Green, J. Scheuer, G. DeRose, A. Yariv, *Vertically Emitting Annular Bragg Lasers Using Polymer Epitaxial Transfer*, Applied Physics Letters **85**, 3669–3671 (2004) (Cited on page 90.)

[Gre16] N. Gregersen, D. P. S. McCutcheon, J. Mørk, J.-M. Gérard, J. Claudon, *A Broadband Tapered Nanocavity for Efficient Nonclassical Light Emission*, Optics Express **24**, 20 904–20 924 (2016) (Cited on page 89.)

[Gro13] T. Grosjean, M. Mivelle, G. W. Burr, F. I. Baida, *Optical Horn Antennas for Efficiently Transferring Photons from a Quantum Emitter to a Single-Mode Optical Fiber*, Optics Express **21**, 1762–1772 (2013) (Cited on page 84.)

[Grü19] P. Grünwald, *Effective Second-Order Correlation Function and Single-Photon Detection*, New Journal of Physics **21**, 093 003 (2019) (Cited on page 62.)

[Gsc13] M. Gschrey, F. Gericke, A. Schüßler, R. Schmidt, J.-H. Schulze, T. Heindel, S. Rodt, A. Strittmatter, S. Reitzenstein, *In Situ Electron-Beam Lithography of Deterministic Single-Quantum-Dot Mesa-Structures Using Low-Temperature Cathodoluminescence Spectroscopy*, Applied Physics Letters **102**, 251 113 (2013) (Cited on page 91.)

[Gsc15] M. Gschrey, A. Thoma, P. Schnauber, M. Seifried, R. Schmidt, B. Wohlfeil, L. Krüger, J.-H. Schulze, T. Heindel, S. Burger, F. Schmidt, A. Strittmatter, S. Rodt, S. Reitzenstein, *Highly Indistinguishable Photons from Deterministic Quantum-Dot Microlenses Utilizing Three-Dimensional in Situ Electron-Beam Lithography*, Nature Communications **6**, 7662 (2015) (Cited on page 88.)

[Guh90] S. Guha, A. Madhukar, K. C. Rajkumar, *Onset of Incoherency and Defect Introduction in the Initial Stages of Molecular Beam Epitaxical Growth of Highly Strained $In_xGa_{1-x}As$ on GaAs(100)*, Applied Physics Letters **57**, 2110–2112 (1990) (Cited on page 23.)

[Gur19] M. Gurioli, Z. Wang, A. Rastelli, T. Kuroda, S. Sanguinetti, *Droplet Epitaxy of Semiconductor Nanostructures for Quantum Photonic Devices*, Nature Materials **18**, 799–810 (2019) (Cited on pages 9 and 26.)

[Gür21] U. M. Gür, M. Mattes, S. Arslanagić, N. Gregersen, *Elliptical Micropillar Cavity Design for Highly Efficient Polarized Emission of Single Photons*, Applied Physics Letters **118**, 061 101 (2021) (Cited on page 89.)

[Gyg21] S. Gyger, J. Zichi, L. Schweickert, A. W. Elshaari, S. Steinhauer, S. F. Covre da Silva, A. Rastelli, V. Zwiller, K. D. Jöns, C. Errando-Herranz, *Reconfigurable Photonics with On-Chip Single-Photon Detectors*, Nature Communications **12**, 1408 (2021) (Cited on page 96.)

[Haf07] R. Hafenbrak, S. M. Ulrich, P. Michler, L. Wang, A. Rastelli, O. G. Schmidt, *Triggered Polarization-Entangled Photon Pairs from a Single Quantum Dot up to 30 K*, New Journal of Physics **9**, 315 (2007) (Cited on page 22.)

[Han56] R. Hanbury-Brown, R. Q. Twiss, *Correlation between Photons in Two Coherent Beams of Light*, Nature **177**, 27–29 (1956) (Cited on page 62.)

[Han18] L. Hanschke, K. A. Fischer, S. Appel, D. Lukin, J. Wierzbowski, S. Sun, R. Trivedi, J. Vučković, J. J. Finley, K. Müller, *Quantum Dot Single-Photon Sources with Ultra-Low Multi-Photon Probability*, npj Quantum Information **4**, 1–6 (2018) (Cited on pages 48, 65, and 99.)

[Har89] S. Haroche, D. Kleppner, *Cavity Quantum Electrodynamics*, Physics Today **42**, 24–30 (1989) (Cited on page 83.)

[Har14] N. C. Harris, D. Grassani, A. Simbula, M. Pant, M. Galli, T. Baehr-Jones, M. Hochberg, D. Englund, D. Bajoni, C. Galland, *Integrated Source of Spectrally Filtered Correlated Photons for Large-Scale Quantum Photonic Systems*, Physical Review X **4**, 041 047 (2014) (Cited on page 96.)

[He13] Y.-M. He, Y. He, Y.-J. Wei, D. Wu, M. Atatüre, C. Schneider, S. Höfling, M. Kamp, C.-Y. Lu, J.-W. Pan, *On-Demand Semiconductor Single-Photon Source with near-Unity Indistinguishability*, Nature Nanotechnology **8**, 213–217 (2013) (Cited on pages 43, 73, and 84.)

[He14] K. He, N. Kumar, L. Zhao, Z. Wang, K. F. Mak, H. Zhao, J. Shan, *Tightly Bound Excitons in Monolayer WSe_2*, Physical Review Letters **113**, 026 803 (2014) (Cited on page 31.)

[He15] Y. M. He, G. Clark, J. R. Schaibley, Y. He, M. C. Chen, Y. J. Wei, X. Ding, Q. Zhang, W. Yao, X. Xu, C. Y. Lu, J. W. Pan, *Single Quantum Emitters in Monolayer Semiconductors*, Nature Nanotechnology **10**, 497–502 (2015) (Cited on pages 30, 60, and 65.)

[He17] Y. He, X. Ding, Z.-E. Su, H.-L. Huang, J. Qin, C. Wang, S. Unsleber, C. Chen, H. Wang, Y.-M. He, X.-L. Wang, W.-J. Zhang, S.-J. Chen, C. Schneider, M. Kamp, L.-X. You, Z. Wang, S. Höfling, C.-Y. Lu, J.-W. Pan, *Time-Bin-Encoded Boson Sampling with a Single-Photon Device*, Physical Review Letters **118**, 190 501 (2017) (Cited on pages 73 and 89.)

[He19] Y.-M. He, H. Wang, C. Wang, M.-C. Chen, X. Ding, J. Qin, Z.-C. Duan, S. Chen, J.-P. Li, R.-Z. Liu, C. Schneider, M. Atatüre, S. Höfling, C.-Y. Lu, J.-W. Pan, *Coherently Driving a Single Quantum Two-Level System with Dichromatic Laser Pulses*, Nature Physics **15**, 941–946 (2019) (Cited on page 39.)

[Hei10] J. Heinrich, A. Huggenberger, T. Heindel, S. Reitzenstein, S. Höfling, L. Worschech, A. Forchel, *Single Photon Emission from Positioned GaAs/AlGaAs Photonic Nanowires*, Applied Physics Letters **96**, 211 117 (2010) (Cited on page 27.)

[Hei15] D. Heinze, D. Breddermann, A. Zrenner, S. Schumacher, *A Quantum Dot Single-Photon Source with on-the-Fly All-Optical Polarization Control and Timed Emission*, Nature Communications **6**, 8473 (2015) (Cited on pages 52 and 54.)

[Hek23] R. Hekmati, J. P. Hadden, A. Mathew, S. G. Bishop, S. A. Lynch, A. J. Bennett, *Bullseye Dielectric Cavities for Photon Collection from a Surface-Mounted Quantum-Light-Emitter*, Scientific Reports **13**, 5316 (2023) (Cited on page 91.)

[Her13] H. Herrmann, X. Yang, A. Thomas, A. Poppe, W. Sohler, C. Silberhorn, *Post-Selection Free, Integrated Optical Source of Non-Degenerate, Polarization Entangled Photon Pairs*, Optics Express **21**, 27 981–27 991 (2013) (Cited on page 14.)

[Her18] T. Herzog, M. Sartison, S. Kolatschek, S. Hepp, A. Bommer, C. Pauly, F. Muecklich, C. Becher, M. Jetter, S. L. Portalupi, P. Michler, *Pure Single-Photon Emission from InGaAs QDs in a Tunable Fiber-Based External Mirror Microcavity*, Quantum Science and Technology **3**, 034 009 (2018) (Cited on page 91.)

[Hey09] Ch. Heyn, A. Stemmann, W. Hansen, *Dynamics of Self-Assembled Droplet Etching*, Applied Physics Letters **95**, 173 110 (2009) (Cited on page 24.)

[Hey11] C. Heyn, *Kinetic Model of Local Droplet Etching*, Physical Review B **83**, 165 302 (2011) (Cited on page 24.)

[Hig16] D. B. Higginbottom, L. Slodička, G. Araneda, L. Lachman, R. Filip, M. Hennrich, R. Blatt, *Pure Single Photons from a Trapped Atom Source*, New Journal of Physics **18**, 093 038 (2016) (Cited on pages 9, 14, and 60.)

[Hon87] C. K. Hong, Z. Y. Ou, L. Mandel, *Measurement of Subpicosecond Time Intervals between Two Photons by Interference*, Physical Review Letters **59**, 2044–2046 (1987) (Cited on pages 69 and 95.)

[Höt21] A. Hötger, J. Klein, K. Barthelmi, L. Sigl, F. Sigger, W. Männer, S. Gyger, M. Florian, M. Lorke, F. Jahnke, T. Taniguchi, K. Watanabe, K. D. Jöns, U. Wurstbauer, C. Kastl, K. Müller, J. J. Finley, A. W. Holleitner, *Gate-Switchable Arrays of Quantum Light Emitters in Contacted Monolayer MoS_2 van Der Waals Heterodevices*, Nano Letters **21**, 1040–1046 (2021) (Cited on page 82.)

[Hou12] J. Houel, A. V. Kuhlmann, L. Greuter, F. Xue, M. Poggio, B. D. Gerardot, P. A. Dalgarno, A. Badolato, P. M. Petroff, A. Ludwig, D. Reuter, A. D. Wieck, R. J. Warburton, *Probing Single-Charge Fluctuations at a GaAs/AlAs Interface Using Laser Spectroscopy on a Nearby InGaAs Quantum Dot*, Physical Review Letters **108**, 107 401 (2012) (Cited on pages 65 and 73.)

[Hua17] H. Huang, R. Trotta, Y. Huo, T. Lettner, J. S. Wildmann, J. Martín-Sánchez, D. Huber, M. Reindl, J. Zhang, E. Zallo, O. G. Schmidt, A. Rastelli, *Electrically-Pumped Wavelength-Tunable GaAs Quantum Dots Interfaced with Rubidium Atoms*, ACS Photonics **4**, 868–872 (2017) (Cited on pages 9 and 25.)

[Hua21] H. Huang, S. Manna, C. Schimpf, M. Reindl, X. Yuan, Y. Zhang, S. Filipe, A. Rastelli, *Bright Single Photon Emission from Quantum Dots Embedded in a Broadband Planar Optical Antenna*, Advanced Optical Materials **9**, 2001 490 (2021) (Cited on page 84.)

[Hub14] T. Huber, A. Predojević, M. Khoshnegar, D. Dalacu, P. J. Poole, H. Majedi, G. Weihs, *Polarization Entangled Photons from Quantum Dots Embedded in Nanowires*, Nano Letters **14**, 7107–7114 (2014) (Cited on page 28.)

[Hub17] D. Huber, M. Reindl, Y. Huo, H. Huang, J. S. Wildmann, O. G. Schmidt, A. Rastelli, R. Trotta, *Highly Indistinguishable and Strongly Entangled Photons from Symmetric GaAs Quantum Dots*, Nature Communications **8**, 15 506 (2017) (Cited on pages 18 and 26.)

[Hub18] D. Huber, M. Reindl, S. F. Covre da Silva, C. Schimpf, J. Martín-Sánchez, H. Huang, G. Piredda, J. Edlinger, A. Rastelli, R. Trotta, *Strain-Tunable GaAs Quantum Dot: A Nearly Dephasing-Free Source of Entangled Photon Pairs on Demand*, Physical Review Letters **121**, 033 902 (2018) (Cited on page 26.)

[Hub19] D. Huber, B. U. Lehner, D. Csontosová, M. Reindl, S. Schuler, S. F. Covre da Silva, P. Klenovský, A. Rastelli, *Single-Particle-Picture Breakdown in Laterally Weakly Confining GaAs Quantum Dots*, Physical Review B **100**, 235 425 (2019) (Cited on pages 25 and 26.)

[Hud07] A. J. Hudson, R. M. Stevenson, A. J. Bennett, R. J. Young, C. A. Nicoll, P. Atkinson, K. Cooper, D. A. Ritchie, A. J. Shields, *Coherence of an Entangled Exciton-Photon State*, Physical Review Letters **99**, 266 802 (2007) (Cited on page 22.)

[Hun10] D. Hunger, T. Steinmetz, Y. Colombe, C. Deutsch, T. W. Hänsch, J. Reichel, *A Fiber Fabry–Perot Cavity with High Finesse*, New Journal of Physics **12**, 065 038 (2010) (Cited on page 91.)

[Huo13] Y. H. Huo, A. Rastelli, O. G. Schmidt, *Ultra-Small Excitonic Fine Structure Splitting in Highly Symmetric Quantum Dots on GaAs (001) Substrate*, Applied Physics Letters **102**, 152 105 (2013) (Cited on pages 9, 17, 24, and 25.)

[Huo14] Y. H. Huo, B. J. Witek, S. Kumar, J. R. Cardenas, J. X. Zhang, N. Akopian, R. Singh, E. Zallo, R. Grifone, D. Kriegner, R. Trotta, F. Ding, J. Stangl, V. Zwiller, G. Bester, A. Rastelli, O. G. Schmidt, *A Light-Hole Exciton in a Quantum Dot*, Nature Physics **10**, 46–51 (2014) (Cited on page 18.)

[Iff19] O. Iff, D. Tedeschi, J. Martín-Sánchez, M. Moczała-Dusanowska, S. Tongay, K. Yumigeta, J. Taboada-Gutiérrez, M. Savaresi, A. Rastelli, P. Alonso-González, S. Höfling, R. Trotta, C. Schneider, *Strain-Tunable Single Photon Sources in WSe_2 Monolayers*, Nano Letters **19**, 6931–6936 (2019) (Cited on pages 32 and 78.)

[Iff21] O. Iff, Q. Buchinger, M. Moczała-Dusanowska, M. Kamp, S. Betzold, M. Davanco, K. Srinivasan, S. Tongay, C. Antón-Solanas, S. Höfling, C. Schneider, *Purcell-Enhanced Single Photon Source Based on a Deterministically Placed WSe_2 Monolayer Quantum Dot in a Circular Bragg Grating Cavity*, Nano Letters **21**, 4715–4720 (2021) (Cited on pages 32 and 91.)

[Jah15] J.-P. Jahn, M. Munsch, L. Béguin, A. V. Kuhlmann, M. Renggli, Y. Huo, F. Ding, R. Trotta, M. Reindl, O. G. Schmidt, A. Rastelli, P. Treutlein, R. J. Warburton, *An Artificial Rb Atom in a Semiconductor with Lifetime-Limited Linewidth*, Physical Review B **92**, 245 439 (2015) (Cited on page 65.)

[Jea17] M. Jeannin, T. Cremel, T. Häyrynen, N. Gregersen, E. Bellet-Amalric, G. Nogues, K. Kheng, *Enhanced Photon Extraction from a Nanowire Quantum Dot Using a Bottom-Up Photonic Shell*, Physical Review Applied **8**, 054 022 (2017) (Cited on page 18.)

[Jön11] K. D. Jöns, R. Hafenbrak, R. Singh, F. Ding, J. D. Plumhof, A. Rastelli, O. G. Schmidt, G. Bester, P. Michler, *Dependence of the Redshifted and Blueshifted Photoluminescence Spectra of Single $In_xGa_{1-x}As/GaAs$ Quantum Dots on the Applied Uniaxial Stress*, Physical Review Letters **107**, 217 402 (2011) (Cited on page 77.)

[Jön17] K. D. Jöns, L. Schweickert, M. A. Versteegh, D. Dalacu, P. J. Poole, A. Gulinatti, A. Giudice, V. Zwiller, M. E. Reimer, *Bright Nanoscale Source of Deterministic Entangled Photon Pairs Violating Bell's Inequality*, Scientific Reports **7**, 1–11 (2017) (Cited on pages 9 and 28.)

[Jus20] G. Juska, I. Ranjbar Jahromi, F. Mattana, S. Varo, V. Dimastrodonato, E. Pelucchi, *Biexciton Initialization by Two-Photon Excitation in Site-Controlled Quantum Dots: The Complexity of the Antibinding State Case*, Applied Physics Letters **117**, 134 001 (2020) (Cited on pages 19 and 46.)

[Kan11] M. Kaniber, M. F. Huck, K. Müller, E. C. Clark, F. Troiani, M. Bichler, H. J. Krenner, J. J. Finley, *Electrical Control of the Exciton–Biexciton Splitting in Self-Assembled InGaAs Quantum Dots*, Nanotechnology **22**, 325 202 (2011) (Cited on page 82.)

[Kan16] F. Kaneda, K. Garay-Palmett, A. B. U'Ren, P. G. Kwiat, *Heralded Single-Photon Source Utilizing Highly Nondegenerate, Spectrally Factorable Spontaneous Parametric Downconversion*, Optics Express **24**, 10 733–10 747 (2016) (Cited on page 14.)

[Kap24] F. Kappe, Y. Karli, G. Wilbur, R. G. Krämer, S. Ghosh, R. Schwarz, M. Kaiser, T. K. Bracht, D. E. Reiter, S. Nolte, K. C. Hall, G. Weihs,

V. Remesh, *Chirped Pulses Meet Quantum Dots: Innovations, Challenges, and Future Perspectives*, Advanced Quantum Technologies, 2300 352 (2024) (Cited on page 39.)

[Kar22] Y. Karli, F. Kappe, V. Remesh, T. K. Bracht, J. Mu, S. Covre da Silva, T. Seidelmann, V. Martin Axt, A. Rastelli, D. E. Reiter, G. Weihs, *SUPER Scheme in Action: Experimental Demonstration of Red-Detuned Excitation of a Quantum Emitter*, Nano Letters **12**, 13 (2022) (Cited on page 39.)

[Kat18] R. Katsumi, Y. Ota, M. Kakuda, S. Iwamoto, Y. Arakawa, *Transfer-Printed Single-Photon Sources Coupled to Wire Waveguides*, Optica **5**, 691–694 (2018) (Cited on page 93.)

[Kat19] R. Katsumi, Y. Ota, A. Osada, T. Yamaguchi, T. Tajiri, M. Kakuda, S. Iwamoto, H. Akiyama, Y. Arakawa, *Quantum-Dot Single-Photon Source on a CMOS Silicon Photonic Chip Integrated Using Transfer Printing*, APL Photonics **4**, 036 105 (2019) (Cited on pages 93 and 94.)

[Kat20] R. Katsumi, Y. Ota, A. Osada, T. Tajiri, T. Yamaguchi, M. Kakuda, S. Iwamoto, H. Akiyama, Y. Arakawa, *In Situ Wavelength Tuning of Quantum-Dot Single-Photon Sources Integrated on a CMOS-processed Silicon Waveguide*, Applied Physics Letters **116**, 041 103 (2020) (Cited on page 96.)

[Kim77] H. J. Kimble, M. Dagenais, L. Mandel, *Photon Antibunching in Resonance Fluorescence*, Physical Review Letters **39**, 691–695 (1977) (Cited on pages 8, 14, 65, and 67.)

[Kim20] J.-H. Kim, S. Aghaeimeibodi, J. Carolan, D. Englund, E. Waks, *Hybrid Integration Methods for On-Chip Quantum Photonics*, Optica **7**, 291 (2020) (Cited on pages 92 and 93.)

[Kni01] E. Knill, R. Laflamme, G. J. Milburn, *A Scheme for Efficient Quantum Computation with Linear Optics*, Nature **409**, 46 (2001) (Cited on pages 7 and 67.)

[Kol19] S. Kolatschek, S. Hepp, M. Sartison, M. Jetter, P. Michler, S. L. Portalupi, *Deterministic Fabrication of Circular Bragg Gratings Coupled to Single Quantum Emitters via the Combination of* In-Situ *Optical Lithography and Electron-Beam Lithography*, Journal of Applied Physics **125**, 045 701 (2019) (Cited on page 90.)

[Koo21] Z. X. Koong, E. Scerri, ‡. M. Rambach, §. M. Cygorek, M. Brotons-Gisbert, R. Picard, Y. Ma, S. I. Park, J. D. Song, E. M. Gauger, B. D. Gerardot,

Coherent Dynamics in Quantum Emitters under Dichromatic Excitation, Physical Review Letters **126**, 47 403–47 404 (2021) (Cited on page 39.)

[Kop15] M. Koperski, K. Nogajewski, A. Arora, V. Cherkez, P. Mallet, J.-Y. Veuillen, J. Marcus, P. Kossacki, M. Potemski, *Single Photon Emitters in Exfoliated WSe_2 Structures*, Nature Nanotechnology **10**, 503–506 (2015) (Cited on pages 30, 31, 60, and 65.)

[Kor13] M. Korkusinski, P. Hawrylak, *Atomistic Theory of Emission from Dark Excitons in Self-Assembled Quantum Dots*, Physical Review B **87**, 115 310 (2013) (Cited on page 18.)

[Kow05] K. Kowalik, O. Krebs, A. Lemaître, S. Laurent, P. Senellart, P. Voisin, J. A. Gaj, *Influence of an In-Plane Electric Field on Exciton Fine Structure in InAs-GaAs Self-Assembled Quantum Dots*, Applied Physics Letters **86**, 041 907 (2005) (Cited on page 82.)

[Kow07] K. Kowalik, O. Krebs, A. Lemaître, B. Eble, A. Kudelski, P. Voisin, S. Seidl, J. A. Gaj, *Monitoring Electrically Driven Cancellation of Exciton Fine Structure in a Semiconductor Quantum Dot by Optical Orientation*, Applied Physics Letters **91**, 183 104 (2007) (Cited on page 82.)

[Koy99] K. Koyama, M. Yoshita, M. Baba, T. Suemoto, H. Akiyama, *High Collection Efficiency in Fluorescence Microscopy with a Solid Immersion Lens*, Applied Physics Letters **75**, 1667–1669 (1999) (Cited on page 86.)

[Kuh13] A. V. Kuhlmann, J. Houel, A. Ludwig, L. Greuter, D. Reuter, A. D. Wieck, M. Poggio, R. J. Warburton, *Charge Noise and Spin Noise in a Semiconductor Quantum Device*, Nature Physics **9**, 570–575 (2013) (Cited on page 44.)

[Kum11] S. Kumar, R. Trotta, E. Zallo, J. D. Plumhof, P. Atkinson, A. Rastelli, O. G. Schmidt, *Strain-Induced Tuning of the Emission Wavelength of High Quality GaAs/AlGaAs Quantum Dots in the Spectral Range of the ^{87}Rb D_2 Lines*, Applied Physics Letters **99**, 161 118 (2011) (Cited on page 77.)

[Kum12] A. Kumar, P. K. Ahluwalia, *Electronic Structure of Transition Metal Dichalcogenides Monolayers 1H-MX_2 (M = Mo, W; X = S, Se, Te) from Ab-Initio Theory: New Direct Band Gap Semiconductors*, The European Physical Journal B **85**, 186 (2012) (Cited on page 30.)

[Kum15] S. Kumar, A. Kaczmarczyk, B. D. Gerardot, *Strain-Induced Spatial and Spectral Isolation of Quantum Emitters in Mono- and Bilayer WSe_2*, Nano Letters **15**, 7567–7573 (2015) (Cited on pages 31 and 91.)

[Kum16] S. Kumar, M. Brotóns-Gisbert, R. Al-Khuzheyri, A. Branny, G. Ballesteros-Garcia, J. F. Sánchez-Royo, B. D. Gerardot, *Resonant Laser Spectroscopy of Localized Excitons in Monolayer WSe_2*, Optica **3**, 882 (2016) (Cited on pages 30 and 32.)

[Kur00] C. Kurtsiefer, S. Mayer, P. Zarda, H. Weinfurter, *Stable Solid-State Source of Single Photons*, Physical Review Letters **85**, 290–293 (2000) (Cited on pages 15 and 60.)

[Laf23] P. Laferrière, A. Yin, E. Yeung, L. Kusmic, M. Korkusinski, P. Rasekh, D. B. Northeast, S. Haffouz, J. Lapointe, P. J. Poole, R. L. Williams, D. Dalacu, *Approaching Transform-Limited Photons from Nanowire Quantum Dots Using Excitation above the Band Gap*, Physical Review B **107**, 155 422 (2023) (Cited on pages 28 and 66.)

[Lai14] Y. Lai, S. Pirotta, G. Urbinati, D. Gerace, M. Minkov, V. Savona, A. Badolato, M. Galli, *Genetically Designed L3 Photonic Crystal Nanocavities with Measured Quality Factor Exceeding One Million*, Applied Physics Letters **104**, 241 101 (2014) (Cited on page 89.)

[Lan04] W. Langbein, P. Borri, U. Woggon, V. Stavarache, D. Reuter, A. D. Wieck, *Control of Fine-Structure Splitting and Biexciton Binding in $In_xGa_{1-x}As$ Quantum Dots by Annealing*, Physical Review B **69**, 161 301 (2004) (Cited on pages 22 and 76.)

[Lau05] S. Laurent, S. Varoutsis, L. Le Gratiet, A. Lemaître, I. Sagnes, F. Raineri, A. Levenson, I. Robert-Philip, I. Abram, *Indistinguishable Single Photons from a Single-Quantum Dot in a Two-Dimensional Photonic Crystal Cavity*, Applied Physics Letters **87**, 163 107 (2005) (Cited on page 89.)

[Lau09] A. Laucht, F. Hofbauer, N. Hauke, J. Angele, S. Stobbe, M. Kaniber, G. Böhm, P. Lodahl, M.-C. Amann, J. J. Finley, *Electrical Control of Spontaneous Emission and Strong Coupling for a Single Quantum Dot*, New Journal of Physics **11**, 023 034 (2009) (Cited on pages 82 and 91.)

[Lee02] H. Lee, P. Kok, J. P. Dowling, *A Quantum Rosetta Stone for Interferometry*, Journal of Modern Optics **49**, 2325–2338 (2002) (Cited on pages 7 and 68.)

[Leg03] T. Legero, T. Wilk, A. Kuhn, G. Rempe, *Time-Resolved Two-Photon Quantum Interference*, Applied Physics B **77**, 797–802 (2003) (Cited on page 71.)

[Leg04] T. Legero, T. Wilk, M. Hennrich, G. Rempe, A. Kuhn, *Quantum Beat of Two Single Photons*, Physical Review Letters **93**, 070 503 (2004) (Cited on page 71.)

[Leo93] D. Leonard, M. Krishnamurthy, C. M. Reaves, S. P. Denbaars, P. M. Petroff, *Direct Formation of Quantum-Sized Dots from Uniform Coherent Islands of InGaAs on GaAs Surfaces*, Applied Physics Letters **63**, 3203–3205 (1993) (Cited on page 23.)

[Leo94] D. Leonard, K. Pond, P. M. Petroff, *Critical Layer Thickness for Self-Assemled InAs on GaAs*, Physical Review B **50**, 11 687–11 692 (1994) (Cited on page 17.)

[Leo03] K. Leosson, D. Birkedal, I. Magnusdottir, W. Langbein, J. M. Hvam, *Homogeneous Linewidth of Self-Assembled III–V Quantum Dots Observed in Single-Dot Photoluminescence*, Physica E **17**, 1–6 (2003) (Cited on page 40.)

[Let21] T. Lettner, S. Gyger, K. D. Zeuner, L. Schweickert, S. Steinhauer, C. Reuterskiöld Hedlund, S. Stroj, A. Rastelli, M. Hammar, R. Trotta, K. D. Jöns, V. Zwiller, *Strain-Controlled Quantum Dot Fine Structure for Entangled Photon Generation at 1550 nm*, Nano Letters **21**, 10 501–10 506 (2021) (Cited on page 78.)

[Li21] B.-H. Li, Y.-M. Xie, Z. Li, C.-X. Weng, C.-L. Li, H.-L. Yin, Z.-B. Chen, *Long-Distance Twin-Field Quantum Key Distribution with Entangled Sources*, Optics Letters **46**, 5529 (2021) (Cited on pages 32 and 94.)

[LIG16] LIGO Scientific Collaboration and Virgo Collaboration, *Observation of Gravitational Waves from a Binary Black Hole Merger*, Physical Review Letters **116**, 061 102 (2016) (Cited on page 7.)

[Lin12] N. Lindenmann, G. Balthasar, D. Hillerkuss, R. Schmogrow, M. Jordan, J. Leuthold, W. Freude, C. Koos, *Photonic Wire Bonding: A Novel Concept for Chip-Scale Interconnects*, Optics Express **20**, 17 667–17 677 (2012) (Cited on page 97.)

[Lin15] N. Lindenmann, S. Dottermusch, M. L. Goedecke, T. Hoose, M. R. Billah, T. P. Onanuga, A. Hofmann, W. Freude, C. Koos, *Connecting Silicon Photonic Circuits to Multicore Fibers by Photonic Wire Bonding*, Journal of Lightwave Technology **33**, 755–760 (2015) (Cited on page 97.)

[Lin19] L. Linhart, M. Paur, V. Smejkal, J. Burgdörfer, T. Mueller, F. Libisch, *Localized Intervalley Defect Excitons as Single-Photon Emitters in WSe_2*, Physical Review Letters **123**, 146 401 (2019) (Cited on page 31.)

[Lin21] Z. Lin, L. Schweickert, S. Gyger, K. D. Jöns, V. Zwiller, *Efficient and Versatile Toolbox for Analysis of Time-Tagged Measurements*, Journal of Instrumentation **16**, T08 016 (2021) (Cited on page 64.)

[Liu17] J. Liu, M. I. Davanço, L. Sapienza, K. Konthasinghe, J. V. De Miranda Cardoso, J. D. Song, A. Badolato, K. Srinivasan, *Cryogenic Photoluminescence Imaging System for Nanoscale Positioning of Single Quantum Emitters*, Review of Scientific Instruments **88**, 023 116 (2017) (Cited on page 91.)

[Liu18a] F. Liu, A. J. Brash, J. O'Hara, L. M. P. P. Martins, C. L. Phillips, R. J. Coles, B. Royall, E. Clarke, C. Bentham, N. Prtljaga, I. E. Itskevich, L. R. Wilson, M. S. Skolnick, A. M. Fox, *High Purcell Factor Generation of Indistinguishable On-Chip Single Photons*, Nature Nanotechnology **13**, 835–840 (2018) (Cited on pages 82, 89, and 91.)

[Liu18b] J. Liu, K. Konthasinghe, M. Davanço, J. Lawall, V. Anant, V. Verma, R. Mirin, S. W. Nam, J. D. Song, B. Ma, Z. S. Chen, H. Q. Ni, Z. C. Niu, K. Srinivasan, *Single Self-Assembled InAs / GaAs Quantum Dots in Photonic Nanostructures: The Role of Nanofabrication*, Physical Review Applied **9**, 064 019 (2018) (Cited on pages 24 and 66.)

[Liu19] J. Liu, R. Su, Y. Wei, B. Yao, S. F. C. da Silva, Y. Yu, J. Iles-Smith, K. Srinivasan, A. Rastelli, J. Li, X. Wang, *A Solid-State Source of Strongly Entangled Photon Pairs with High Brightness and Indistinguishability*, Nature Nanotechnology **14**, 586–593 (2019) (Cited on page 90.)

[Llo01] S. Lloyd, M. S. Shahriar, J. H. Shapiro, P. R. Hemmer, *Long Distance, Unconditional Teleportation of Atomic States via Complete Bell State Measurements*, Physical Review Letters **87**, 167 903 (2001) (Cited on pages 8, 48, 67, and 102.)

[Lod15] P. Lodahl, S. Mahmoodian, S. Stobbe, *Interfacing Single Photons and Single Quantum Dots with Photonic Nanostructures*, Reviews of Modern Physics **87**, 347–400 (2015) (Cited on pages 82 and 88.)

[Lou00] R. Loudon, *The Quantum Theory of Light* (OUP Oxford, 2000), ISBN 978-0-19-158978-2 (Cited on pages 58 and 61.)

[Ma15] Y. Ma, G. Ballesteros, J. M. Zajac, J. Sun, B. D. Gerardot, *Highly Directional Emission from a Quantum Emitter Embedded in a Hemispherical Cavity*, Optics Letters **40**, 2373–2376 (2015) (Cited on page 88.)

[Mad14] K. H. Madsen, S. Ates, J. Liu, A. Javadi, S. M. Albrecht, I. Yeo, S. Stobbe, P. Lodahl, *Efficient Out-Coupling of High-Purity Single Photons from a Coherent Quantum Dot in a Photonic-Crystal Cavity*, Physical Review B **90**, 155 303 (2014) (Cited on page 89.)

[Mak10] K. F. Mak, C. Lee, J. Hone, J. Shan, T. F. Heinz, *Atomically Thin MoS_2: A New Direct-Gap Semiconductor*, Physical Review Letters **105**, 136 805 (2010) (Cited on pages 30 and 31.)

[Mal97] S. Malik, C. Roberts, R. Murray, M. Pate, *Tuning Self-Assembled InAs Quantum Dots by Rapid Thermal Annealing*, Applied Physics Letters **71**, 1987–1989 (1997) (Cited on page 76.)

[Man66] L. Mandel, *Configuration-Space Photon Number Operators in Quantum Optics*, Physical Review **144**, 1071–1077 (1966) (Cited on page 60.)

[Man90] S. M. Mansfield, G. S. Kino, *Solid Immersion Microscope*, Applied Physics Letters **57**, 2615–2616 (1990) (Cited on page 86.)

[Mar10] S. Marcet, K. Ohtani, H. Ohno, *Vertical Electric Field Tuning of the Exciton Fine Structure Splitting and Photon Correlation Measurements of GaAs Quantum Dot*, Applied Physics Letters **96**, 101 117 (2010) (Cited on pages 81 and 82.)

[Mar17] J. Martín-Sánchez, R. Trotta, A. Mariscal, R. Serna, G. Piredda, S. Stroj, J. Edlinger, C. Schimpf, J. Aberl, T. Lettner, J. Wildmann, H. Huang, X. Yuan, D. Ziss, J. Stangl, A. Rastelli, *Strain-Tuning of the Optical Properties of Semiconductor Nanomaterials by Integration onto Piezoelectric Actuators*, Semiconductor Science and Technology **33**, 013 001 (2017) (Cited on page 78.)

[Mau07] P. Maunz, D. L. Moehring, S. Olmschenk, K. C. Younge, D. N. Matsukevich, C. Monroe, *Quantum Interference of Photon Pairs from Two Remote Trapped Atomic Ions*, Nature Physics **3**, 538–541 (2007) (Cited on page 73.)

[McC92] S. L. McCall, A. F. J. Levi, R. E. Slusher, S. J. Pearton, R. A. Logan, *Whispering-Gallery Mode Microdisk Lasers*, Applied Physics Letters **60**, 289–291 (1992) (Cited on page 88.)

[Mei06] M. A. Meitl, Z.-T. Zhu, V. Kumar, K. J. Lee, X. Feng, Y. Y. Huang, I. Adesida, R. G. Nuzzo, J. A. Rogers, *Transfer Printing by Kinetic Control of Adhesion to an Elastomeric Stamp*, Nature Materials **5**, 33–38 (2006) (Cited on page 94.)

[Men82] E. E. Mendez, G. Bastard, L. L. Chang, L. Esaki, H. Morkoc, R. Fischer, *Effect of an Electric Field on the Luminescence of GaAs Quantum Wells*, Physical Review B **26**, 7101–7104 (1982) (Cited on page 80.)

[Mic87] A. A. Michelson, E. W. Morley, *On the Relative Motion of the Earth and the Luminiferous Ether*, American Journal of Science **s3-34**, 333–345 (1887) (Cited on page 60.)

[Mic00] P. Michler, A. Kiraz, C. Becher, W. V. Schoenfeld, P. M. Petroff, L. Zhang, E. Hu, A. Imamoğlu, *A Quantum Dot Single-Photon Turnstile Device*, Science **290**, 2282–2285 (2000) (Cited on pages 60, 65, and 88.)

[Mic03] P. Michler, *Single Quantum Dots: Fundamentals, Applications and New Concepts* (Springer Science & Business Media, 2003), ISBN 978-3-540-39180-7 (Cited on page 64.)

[Mic18] A. Michaels, E. Yablonovitch, *Inverse Design of near Unity Efficiency Perfectly Vertical Grating Couplers*, Optics Express **26**, 4766–4779 (2018) (Cited on page 97.)

[Mil84] D. A. B. Miller, D. S. Chemla, T. C. Damen, A. C. Gossard, W. Wiegmann, T. H. Wood, C. A. Burrus, *Band-Edge Electroabsorption in Quantum Well Structures: The Quantum-Confined Stark Effect*, Physical Review Letters **53**, 2173–2176 (1984) (Cited on page 80.)

[Mil97] G. J. Milburn, *Schrödinger's Machines: The Quantum Technology Reshaping Everyday Life* (W.H. Freeman Company, 1997) (Cited on page 7.)

[Mna20] K. Mnaymneh, D. Dalacu, J. McKee, J. Lapointe, S. Haffouz, J. F. Weber, D. B. Northeast, P. J. Poole, G. C. Aers, R. L. Williams, *On-Chip Integration of Single Photon Sources via Evanescent Coupling of Tapered Nanowires to SiN Waveguides*, Advanced Quantum Technologies **3**, 1900 021 (2020) (Cited on pages 28 and 94.)

[Moc19] M. Moczała-Dusanowska, Ł. Dusanowski, S. Gerhardt, Y. M. He, M. Reindl, A. Rastelli, R. Trotta, N. Gregersen, S. Höfling, C. Schneider, *Strain-Tunable Single-Photon Source Based on a Quantum Dot–Micropillar System*, ACS Photonics **6**, 2025–2031 (2019) (Cited on page 91.)

[Moc20] M. Moczała-Dusanowska, Ł. Dusanowski, O. Iff, T. Huber, S. Kuhn, T. Czyszanowski, C. Schneider, S. Höfling, *Strain-Tunable Single-Photon Source Based on a Circular Bragg Grating Cavity with Embedded Quantum Dots*, ACS Photonics **7**, 3474–3480 (2020) (Cited on page 91.)

[Moe03] S. Moehl, H. Zhao, B. D. Don, S. Wachter, H. Kalt, *Solid Immersion Lens-Enhanced Nano-Photoluminescence: Principle and Applications*, Journal of Applied Physics **93**, 6265–6272 (2003) (Cited on page 88.)

[Mom11] K. Momma, F. Izumi, *VESTA 3 for Three-Dimensional Visualization of Crystal, Volumetric and Morphology Data*, Journal of Applied Crystallography **44**, 1272–1276 (2011) (Cited on page 29.)

[Mon17] N. Montaut, L. Sansoni, E. Meyer-Scott, R. Ricken, V. Quiring, H. Herrmann, C. Silberhorn, *High-Efficiency Plug-and-Play Source of Heralded Single Photons*, Physical Review Applied **8**, 024 021 (2017) (Cited on page 14.)

[Mor01] E. Moreau, I. Robert, L. Manin, V. Thierry-Mieg, J. M. Gérard, I. Abram, *Quantum Cascade of Photons in Semiconductor Quantum Dots*, Physical Review Letters **87**, 183 601–1–183 601–4 (2001) (Cited on pages 19 and 66.)

[Mor18] S. Morozov, M. Gaio, S. A. Maier, R. Sapienza, *Metal–Dielectric Parabolic Antenna for Directing Single Photons*, Nano Letters **18**, 3060–3065 (2018) (Cited on page 84.)

[Mou15] S. L. Mouradian, T. Schrï¿½der, C. B. Poitras, L. Li, J. Goldstein, E. H. Chen, MichaelWalsh, J. Cardenas, M. L. Markham, D. J. Twitchen, M. Lipson, D. Englund, *Scalable Integration of Long-Lived Quantum Memories into a Photonic Circuit*, Physical Review X **5** (2015) (Cited on page 93.)

[Muk20] A. Mukherjee, A. Widhalm, D. Siebert, S. Krehs, N. Sharma, A. Thiede, D. Reuter, J. Förstner, A. Zrenner, *Electrically Controlled Rapid Adiabatic Passage in a Single Quantum Dot*, Applied Physics Letters **116**, 251 103 (2020) (Cited on page 82.)

[Mul07] A. Muller, E. B. Flagg, P. Bianucci, X. Y. Wang, D. G. Deppe, W. Ma, J. Zhang, G. J. Salamo, M. Xiao, C. K. Shih, *Resonance Fluorescence from a Coherently Driven Semiconductor Quantum Dot in a Cavity*, Physical Review Letters **99**, 187 402 (2007) (Cited on pages 43 and 83.)

[Mul09a] A. Muller, W. Fang, J. Lawall, G. S. Solomon, *Creating Polarization-Entangled Photon Pairs from a Semiconductor Quantum Dot Using the Optical Stark Effect*, Physical Review Letters **103**, 217 402 (2009) (Cited on pages 22 and 77.)

[Mul09b] A. Muller, E. B. Flagg, M. Metcalfe, J. Lawall, G. S. Solomon, *Coupling an Epitaxial Quantum Dot to a Fiber-Based External-Mirror Microcavity*, Applied Physics Letters **95**, 173 101 (2009) (Cited on page 91.)

[Mül14] M. Müller, S. Bounouar, K. D. Jöns, M. Glässl, P. Michler, *On-Demand Generation of Indistinguishable Polarization-Entangled Photon Pairs*, Nature Photonics **8**, 224–228 (2014) (Cited on page 48.)

[Mül17] M. Müller, H. Vural, C. Schneider, A. Rastelli, O. G. G. Schmidt, S. Höfling, P. Michler, *Quantum-Dot Single-Photon Sources for Entanglement Enhanced Interferometry*, Physical Review Letters **118**, 1–6 (2017) (Cited on pages 7 and 68.)

[Mun13] M. Munsch, N. S. Malik, E. Dupuy, A. Delga, J. Bleuse, J.-M. Gérard, J. Claudon, N. Gregersen, J. Mørk, *Dielectric GaAs Antenna Ensuring an Efficient Broadband Coupling between an InAs Quantum Dot and a Gaussian Optical Beam*, Physical Review Letters **110**, 177 402 (2013) (Cited on page 86.)

[Mus20] A. Musiał, K. Żołnacz, N. Srocka, O. Kravets, J. Große, J. Olszewski, K. Poturaj, G. Wójcik, P. Mergo, K. Dybka, M. Dyrkacz, M. Dłubek, K. Lauritsen, A. Bülter, P.-I. Schneider, L. Zschiedrich, S. Burger, S. Rodt, W. Urbańczyk, G. Sęk, S. Reitzenstein, *Plug&Play Fiber-Coupled 73 kHz Single-Photon Source Operating in the Telecom O-Band*, Advanced Quantum Technologies **3**, 2000 018 (2020) (Cited on page 85.)

[Naj15] F. Najafi, J. Mower, N. C. Harris, F. Bellei, A. Dane, C. Lee, X. Hu, P. Kharel, F. Marsili, S. Assefa, K. K. Berggren, D. Englund, *On-Chip Detection of Non-Classical Light by Scalable Integration of Single-Photon Detectors*, Nature Communications **6**, 5873 (2015) (Cited on page 96.)

[Naj19] D. Najer, I. Söllner, P. Sekatski, V. Dolique, M. C. Löbl, D. Riedel, R. Schott, S. Starosielec, S. R. Valentin, A. D. Wieck, N. Sangouard, A. Ludwig, R. J. Warburton, *A Gated Quantum Dot Strongly Coupled to an Optical Microcavity*, Nature **575**, 622–627 (2019) (Cited on page 91.)

[Neu22] S. P. Neumann, A. Buchner, L. Bulla, M. Bohmann, R. Ursin, *Continuous Entanglement Distribution over a Transnational 248 Km Fiber Link*, Nature Communications **13**, 6134 (2022) (Cited on pages 9, 14, and 99.)

[Nov01] L. Novotny, R. D. Grober, K. Karrai, *Reflected Image of a Strongly Focused Spot*, Optics Letters **26**, 789 (2001) (Cited on page 44.)

[Nov04] K. S. Novoselov, A. K. Geim, S. V. Morozov, D. Jiang, Y. Zhang, S. V. Dubonos, I. V. Grigorieva, A. A. Firsov, *Electric Field Effect in Atomically Thin Carbon Films*, Science **306**, 666–669 (2004) (Cited on page 29.)

[Nov05] K. S. Novoselov, D. Jiang, F. Schedin, T. J. Booth, V. V. Khotkevich, S. V. Morozov, A. K. Geim, *Two-Dimensional Atomic Crystals*, Proceedings of the National Academy of Sciences **102**, 10 451–10 453 (2005) (Cited on page 29.)

[Now14] A. K. Nowak, S. L. Portalupi, V. Giesz, O. Gazzano, C. Dal Savio, P.-F. Braun, K. Karrai, C. Arnold, L. Lanco, I. Sagnes, A. Lemaître, P. Senellart, *Deterministic and Electrically Tunable Bright Single-Photon Source*, Nature Communications **5**, 3240 (2014) (Cited on pages 82 and 91.)

[Nus97] P. Nussbaum, R. Völkel, H. P. Herzig, M. Eisner, S. Haselbeck, *Design, Fabrication and Testing of Microlens Arrays for Sensors and Microsystems*, Pure and Applied Optics: Journal of the European Optical Society Part A **6**, 617 (1997) (Cited on page 85.)

[O'B09] J. L. O'Brien, A. Furusawa, J. Vučković, *Photonic Quantum Technologies*, Nature Photonics **3**, 687–695 (2009) (Cited on page 92.)

[Ost19] A. D. Osterkryger, J. Claudon, J.-M. Gérard, N. Gregersen, *Photonic "Hourglass" Design for Efficient Quantum Light Emission*, Optics Letters **44**, 2617–2620 (2019) (Cited on page 89.)

[Ou88] Z. Y. Ou, L. Mandel, *Violation of Bell's Inequality and Classical Probability in a Two-Photon Correlation Experiment*, Physical Review Letters **61**, 50–53 (1988) (Cited on page 14.)

[Pad21] A. Padrón-Brito, J. Lowinski, P. Farrera, K. Theophilo, H. de Riedmatten, *Probing the Indistinguishability of Single Photons Generated by Rydberg Atomic Ensembles*, Physical Review Research **3**, 033 287 (2021) (Cited on page 15.)

[Pal17] C. Palacios-Berraquero, D. M. Kara, A. R.-P. Montblanch, M. Barbone, P. Latawiec, D. Yoon, A. K. Ott, M. Loncar, A. C. Ferrari, M. Atatüre, *Large-Scale Quantum-Emitter Arrays in Atomically Thin Semiconductors*, Nature Communications **8**, 15 093 (2017) (Cited on pages 31, 91, and 95.)

[Pan98] J.-W. Pan, D. Bouwmeester, H. Weinfurter, A. Zeilinger, *Experimental Entanglement Swapping: Entangling Photons That Never Interacted*, Physical Review Letters **80**, 3891–3894 (1998) (Cited on pages 9 and 67.)

[Par22] K. Parto, S. I. Azzam, N. Lewis, S. D. Patel, S. Umezawa, K. Watanabe, T. Taniguchi, G. Moody, *Cavity-Enhanced 2D Material Quantum Emitters Deterministically Integrated with Silicon Nitride Microresonators*, Nano Letters **22**, 9748–9756 (2022) (Cited on pages 29 and 95.)

[Pat10] R. B. Patel, A. J. Bennett, I. Farrer, C. A. Nicoll, D. A. Ritchie, A. J. Shields, *Two-Photon Interference of the Emission from Electrically Tunable Remote Quantum Dots*, Nature Photonics **4**, 632–635 (2010) (Cited on pages 73, 81, and 82.)

[Pau17] M. Paul, F. Olbrich, J. Höschele, S. Schreier, J. Kettler, S. L. Portalupi, M. Jetter, P. Michler, *Single-Photon Emission at 1.55 µm from MOVPE-grown InAs Quantum Dots on InGaAs/GaAs Metamorphic Buffers*, Applied Physics Letters **111**, 033 102 (2017) (Cited on page 76.)

[Paz18] S. Pazzagli, P. Lombardi, D. Martella, M. Colautti, B. Tiribilli, F. S. Cataliotti, C. Toninelli, *Self-Assembled Nanocrystals of Polycyclic Aromatic Hydrocarbons Show Photostable Single-Photon Emission*, ACS Nano **12**, 4295–4303 (2018) (Cited on page 15.)

[Pel22] E. Pelucchi, G. Fagas, I. Aharonovich, D. Englund, E. Figueroa, Q. Gong, H. Hannes, J. Liu, C.-Y. Lu, N. Matsuda, J.-W. Pan, F. Schreck, F. Sciarrino, C. Silberhorn, J. Wang, K. D. Jöns, *The Potential and Global Outlook of Integrated Photonics for Quantum Technologies*, Nature Reviews Physics **4**, 194–208 (2022) (Cited on page 92.)

[Per12] W. H. P. Pernice, C. Schuck, O. Minaeva, M. Li, G. N. Goltsman, A. V. Sergienko, H. X. Tang, *High-Speed and High-Efficiency Travelling Wave Single-Photon Detectors Embedded in Nanophotonic Circuits*, Nature Communications **3**, 1325 (2012) (Cited on page 96.)

[Pey19] F. Peyskens, C. Chakraborty, M. Muneeb, D. Van Thourhout, D. Englund, *Integration of Single Photon Emitters in 2D Layered Materials with a Silicon Nitride Photonic Chip*, Nature Communications **10**, 4435 (2019) (Cited on pages 32 and 94.)

[Plu11] J. D. Plumhof, V. Křápek, F. Ding, K. D. Jöns, R. Hafenbrak, P. Klenovský, A. Herklotz, K. Dörr, P. Michler, A. Rastelli, O. G. Schmidt, *Strain-Induced Anticrossing of Bright Exciton Levels in Single Self-Assembled $GaAs/Al_xGa_{1-x}As$ and $In_yGa_{1-y}As/GaAs$ Quantum Dots*, Physical Review B **83**, 121 302 (2011) (Cited on page 77.)

[Plu13] J. D. Plumhof, R. Trotta, V. Křápek, E. Zallo, P. Atkinson, S. Kumar, A. Rastelli, O. G. Schmidt, *Tuning of the Valence Band Mixing of Excitons Confined in GaAs/AlGaAs Quantum Dots via Piezoelectric-Induced Anisotropic Strain*, Physical Review B **87**, 075 311 (2013) (Cited on pages 18 and 77.)

[Pol09] A. Politi, J. C. Matthews, M. G. Thompson, J. L. O'Brien, *Integrated Quantum Photonics*, IEEE Journal of Selected Topics in Quantum Electronics **15**, 1673–1684 (2009) (Cited on pages 92 and 95.)

[Pre12] J. Preskill, *Quantum Computing and the Entanglement Frontier*, arXiv:1203.5813 (2012) (Cited on page 7.)

[Qi20] Y. Qi, Y. Li, *Integrated Lithium Niobate Photonics*, Nanophotonics **9**, 1287–1320 (2020) (Cited on page 92.)

[Qui15] J. H. Quilter, A. J. Brash, F. Liu, M. Glässl, A. M. Barth, V. M. Axt, A. J. Ramsay, M. S. Skolnick, A. M. Fox, *Phonon-Assisted Population Inversion*

of a Single InGaAs/GaAs Quantum Dot by Pulsed Laser Excitation, Physical Review Letters **114**, 1–5 (2015) (Cited on page 47.)

[Raj17] A. Raja, A. Chaves, J. Yu, G. Arefe, H. M. Hill, A. F. Rigosi, T. C. Berkelbach, P. Nagler, C. Schüller, T. Korn, C. Nuckolls, J. Hone, L. E. Brus, T. F. Heinz, D. R. Reichman, A. Chernikov, *Coulomb Engineering of the Bandgap and Excitons in Two-Dimensional Materials*, Nature Communications **8**, 15 251 (2017) (Cited on page 31.)

[Rak08] M. T. Rakher, N. G. Stoltz, L. A. Coldren, P. M. Petroff, D. Bouwmeester, *Polarization-Switchable Single Photon Source Using the Stark Effect*, Applied Physics Letters **93**, 091 118 (2008) (Cited on page 82.)

[Ram10] A. J. Ramsay, A. V. Gopal, E. M. Gauger, A. Nazir, B. W. Lovett, A. M. Fox, M. S. Skolnick, *Damping of Exciton Rabi Rotations by Acoustic Phonons in Optically Excited InGaAs/GaAs Quantum Dots*, Physical Review Letters **104**, 20–23 (2010) (Cited on page 43.)

[Ram13] S. Ramelow, A. Mech, M. Giustina, S. Gröblacher, W. Wieczorek, J. Beyer, A. Lita, B. Calkins, T. Gerrits, S. W. Nam, A. Zeilinger, R. Ursin, *Highly Efficient Heralding of Entangled Single Photons*, Optics Express **21**, 6707–6717 (2013) (Cited on page 14.)

[Ray98] S. Raymond, J. P. Reynolds, J. L. Merz, S. Fafard, Y. Feng, S. Charbonneau, *Asymmetric Stark Shift in $Al_xIn_{1-x}As$/ $Al_yGa_{1-y}As$ Self-Assembled Dots*, Physical Review B **58**, R13 415–R13 418 (1998) (Cited on page 80.)

[Ree86] M. A. Reed, *Spatial Quantization in GaAs–AlGaAs Multiple Quantum Dots*, Journal of Vacuum Science & Technology B: Microelectronics and Nanometer Structures **4**, 358 (1986) (Cited on page 16.)

[Rei04] J. P. Reithmaier, G. Sęk, A. Löffler, C. Hofmann, S. Kuhn, S. Reitzenstein, L. V. Keldysh, V. D. Kulakovskii, T. L. Reinecke, A. Forchel, *Strong Coupling in a Single Quantum Dot-Semiconductor Microcavity System*, Nature **432**, 197–200 (2004) (Cited on page 91.)

[Rei11] M. E. Reimer, M. P. van Kouwen, A. W. Hidma, M. H. M. van Weert, E. P. A. M. Bakkers, L. P. Kouwenhoven, V. Zwiller, *Electric Field Induced Removal of the Biexciton Binding Energy in a Single Quantum Dot*, Nano Letters **11**, 645–650 (2011) (Cited on page 82.)

[Rei12] M. E. Reimer, G. Bulgarini, N. Akopian, M. Hocevar, M. B. Bavinck, M. A. Verheijen, E. P. A. M. Bakkers, L. P. Kouwenhoven, V. Zwiller, *Bright Single-Photon Sources in Bottom-up Tailored Nanowires*, Nature Communications **3**, 737 (2012) (Cited on page 27.)

[Rei13] G. Reithmaier, S. Lichtmannecker, T. Reichert, P. Hasch, K. Müller, M. Bichler, R. Gross, J. J. Finley, *On-Chip Time Resolved Detection of Quantum Dot Emission Using Integrated Superconducting Single Photon Detectors*, Scientific Reports **3**, 1–6 (2013) (Cited on page 96.)

[Rei16] M. E. Reimer, G. Bulgarini, A. Fognini, R. W. Heeres, B. J. Witek, M. A. M. Versteegh, A. Rubino, T. Braun, M. Kamp, S. Höfling, D. Dalacu, J. Lapointe, P. J. Poole, V. Zwiller, *Overcoming Power Broadening of the Quantum Dot Emission in a Pure Wurtzite Nanowire*, Physical Review B **93**, 195 316 (2016) (Cited on page 28.)

[Rei17] M. Reindl, K. D. Jöns, D. Huber, C. Schimpf, Y. Huo, V. Zwiller, A. Rastelli, R. Trotta, *Phonon-Assisted Two-Photon Interference from Remote Quantum Emitters*, Nano Letters **17**, 4090–4095 (2017) (Cited on pages 48, 66, 73, and 77.)

[Rei18] M. Reindl, D. Huber, C. Schimpf, S. F. C. da Silva, M. B. Rota, H. Huang, V. Zwiller, K. D. Jöns, A. Rastelli, R. Trotta, *All-Photonic Quantum Teleportation Using on-Demand Solid-State Quantum Emitters*, Science Advances **4**, 1255 (2018) (Cited on pages 26, 48, and 73.)

[Rei19] M. Reindl, J. H. Weber, D. Huber, C. Schimpf, S. F. Covre da Silva, S. L. Portalupi, R. Trotta, P. Michler, A. Rastelli, *Highly Indistinguishable Single Photons from Incoherently Excited Quantum Dots*, Physical Review B **100**, 155 420 (2019) (Cited on pages 26, 39, and 66.)

[Rez19] M. Rezai, J. Wrachtrup, I. Gerhardt, *Polarization-Entangled Photon Pairs from a Single Molecule*, Optica **6**, 34–40 (2019) (Cited on pages 9 and 15.)

[Rin96] R. Rinaldi, P. V. Giugno, R. Cingolani, H. Lipsanen, M. Sopanen, J. Tulkki, J. Ahopelto, *Zeeman Effect in Parabolic Quantum Dots*, Physical Review Letters **77**, 342–345 (1996) (Cited on page 77.)

[Rip18] F. Ripka, H. Kübler, R. Löw, T. Pfau, *A Room-Temperature Single-Photon Source Based on Strongly Interacting Rydberg Atoms*, Science **362**, 446–449 (2018) (Cited on page 15.)

[Roe07] G. Roelkens, D. V. Thourhout, R. Baets, *High Efficiency Grating Coupler between Silicon-on-Insulator Waveguides and Perfectly Vertical Optical Fibers*, Optics Letters **32**, 1495–1497 (2007) (Cited on page 97.)

[Rot22] M. B. Rota, T. M. Krieger, Q. Buchinger, M. Beccaceci, J. Neuwirth, H. Huet, N. Horová, G. Lovicu, G. Ronco, S. F. C. da Silva, G. Pettinari, M. Moczała-Dusanowska, C. Kohlberger, S. Manna, S. Stroj, J. Freund,

X. Yuan, C. Schneider, M. Ježek, S. Höfling, F. B. Basset, T. Huber-Loyola, A. Rastelli, R. Trotta, *A Source of Entangled Photons Based on a Cavity-Enhanced and Strain-Tuned GaAs Quantum Dot*, arXiv:2212.12506 (2022) (Cited on pages 90 and 91.)

[Sac17] W. D. Sacher, J. C. Mikkelsen, P. Dumais, J. Jiang, D. Goodwill, X. Luo, Y. Huang, Y. Yang, A. Bois, P. G.-Q. Lo, E. Bernier, J. K. S. Poon, *Tri-Layer Silicon Nitride-on-Silicon Photonic Platform for Ultra-Low-Loss Crossings and Interlayer Transitions*, Optics Express **25**, 30 862–30 875 (2017) (Cited on page 93.)

[San02] C. Santori, D. Fattal, J. Vučković, G. S. Solomon, Y. Yamamoto, *Indistinguishable Photons from a Single-Photon Device*, Nature **419**, 594–597 (2002) (Cited on pages 72 and 89.)

[San04] C. Santori, D. Fattal, J. Vuckovic, G. S. Solomon, Y. Yamamoto, *Single-Photon Generation with InAs Quantum Dots*, New Journal of Physics **6**, 1–16 (2004) (Cited on page 72.)

[Sap15] L. Sapienza, M. Davanço, A. Badolato, K. Srinivasan, *Nanoscale Optical Positioning of Single Quantum Dots for Bright and Pure Single-Photon Emission*, Nature Communications **6**, 7833 (2015) (Cited on page 91.)

[Sar17] M. Sartison, S. L. Portalupi, T. Gissibl, M. Jetter, H. Giessen, P. Michler, *Combining In-Situ Lithography with 3D Printed Solid Immersion Lenses for Single Quantum Dot Spectroscopy*, Scientific Reports **7**, 39 916 (2017) (Cited on page 88.)

[Sar21] M. Sartison, K. Weber, S. Thiele, L. Bremer, S. Fischbach, T. Herzog, S. Kolatschek, M. Jetter, S. Reitzenstein, A. Herkommer, P. Michler, S. L. Portalupi, H. Giessen, *3D Printed Micro-Optics for Quantum Technology: Optimised Coupling of Single Quantum Dot Emission into a Single-Mode Fibre*, Light: Advanced Manufacturing **2**, 103–119 (2021) (Cited on page 88.)

[Sch11a] A. W. Schell, G. Kewes, T. Schröder, J. Wolters, T. Aichele, O. Benson, *A Scanning Probe-Based Pick-and-Place Procedure for Assembly of Integrated Quantum Optical Hybrid Devices*, Review of Scientific Instruments **82**, 073 709 (2011) (Cited on page 94.)

[Sch11b] T. Schröder, F. Gädeke, M. J. Banholzer, O. Benson, *Ultrabright and Efficient Single-Photon Generation Based on Nitrogen-Vacancy Centres in Nanodiamonds on a Solid Immersion Lens*, New Journal of Physics **13**, 055 017 (2011) (Cited on pages 15 and 60.)

[Sch18a] M. Schwartz, E. Schmidt, U. Rengstl, F. Hornung, S. Hepp, S. L. Portalupi, K. llin, M. Jetter, M. Siegel, P. Michler, *Fully On-Chip Single-Photon Hanbury-Brown and Twiss Experiment on a Monolithic Semiconductor–Superconductor Platform*, Nano Letters **18**, 6892–6897 (2018) (Cited on page 96.)

[Sch18b] L. Schweickert, K. D. Jöns, K. D. Zeuner, S. F. Covre da Silva, H. Huang, T. Lettner, M. Reindl, J. Zichi, R. Trotta, A. Rastelli, V. Zwiller, *On-Demand Generation of Background-Free Single Photons from a Solid-State Source*, Applied Physics Letters **112**, 093 106 (2018) (Cited on pages 9, 16, 26, 48, 60, 65, and 99.)

[Seg05] R. Seguin, A. Schliwa, S. Rodt, K. Pötschke, U. W. Pohl, D. Bimberg, *Size-Dependent Fine-Structure Splitting in Self-Organized InAs/GaAs Quantum Dots*, Physical Review Letters **95**, 257 402 (2005) (Cited on page 24.)

[Sei06] S. Seidl, M. Kroner, A. Högele, K. Karrai, R. J. Warburton, A. Badolato, P. M. Petroff, *Effect of Uniaxial Stress on Excitons in a Self-Assembled Quantum Dot*, Applied Physics Letters **88**, 203 113 (2006) (Cited on pages 22 and 77.)

[Sha17] P. R. Sharapova, K. H. Luo, H. Herrmann, M. Reichelt, T. Meier, C. Silberhorn, *Toolbox for the Design of LiNbO3-based Passive and Active Integrated Quantum Circuits*, New Journal of Physics **19**, 123 009 (2017) (Cited on page 96.)

[She95] C. J. R. Sheppard, *Approximate Calculation of the Reflection Coefficient from a Stratified Medium*, Pure and Applied Optics: Journal of the European Optical Society Part A **4**, 665 (1995) (Cited on page 83.)

[She17] G. D. Shepard, O. A. Ajayi, X. Li, X.-Y. Zhu, J. Hone, S. Strauf, *Nanobubble Induced Formation of Quantum Emitters in Monolayer Semiconductors*, 2D Materials **4**, 021 019 (2017) (Cited on page 31.)

[Sho97] P. W. Shor, *Polynomial-Time Algorithms for Prime Factorization and Discrete Logarithms on a Quantum Computer*, SIAM Journal on Computing **26**, 1484–1509 (1997) (Cited on page 8.)

[Sie21] S. Y. Siew, B. Li, F. Gao, H. Y. Zheng, W. Zhang, P. Guo, S. W. Xie, A. Song, B. Dong, L. W. Luo, C. Li, X. Luo, G.-Q. Lo, *Review of Silicon Photonics Technology and Platform Development*, Journal of Lightwave Technology **39**, 4374–4389 (2021) (Cited on page 92.)

[Sil16] J. W. Silverstone, D. Bonneau, J. L. O'Brien, M. G. Thompson, *Silicon Quantum Photonics*, IEEE Journal of Selected Topics in Quantum Electronics **22**, 390–402 (2016) (Cited on page 92.)

[Sim05] C. Simon, J.-P. P. Poizat, *Creating Single Time-Bin-Entangled Photon Pairs*, Physical Review Letters **94**, 030 502 (2005) (Cited on page 48.)

[Sin83] S. Singh, *Antibunching, Sub-Poissonian Photon Statistics and Finite Bandwidth Effects in Resonance Fluorescence*, Optics Communications **44**, 254–258 (1983) (Cited on page 62.)

[Sin09] R. Singh, G. Bester, *Nanowire Quantum Dots as an Ideal Source of Entangled Photon Pairs*, Physical Review Letters **103**, 1–4 (2009) (Cited on page 28.)

[Sin10] R. Singh, G. Bester, *Lower Bound for the Excitonic Fine Structure Splitting in Self-Assembled Quantum Dots*, Physical Review Letters **104**, 196 803 (2010) (Cited on page 77.)

[Sny91] C. W. Snyder, B. G. Orr, D. Kessler, L. M. Sander, *Effect of Strain on Surface Morphology in Highly Strained InGaAs Films*, Physical Review Letters **66**, 3032–3035 (1991) (Cited on page 23.)

[Som16] N. Somaschi, V. Giesz, L. De Santis, J. C. Loredo, M. P. Almeida, G. Hornecker, S. L. Portalupi, T. Grange, C. Antón, J. Demory, C. Gómez, I. Sagnes, N. D. Lanzillotti-Kimura, A. Lemaítre, A. Auffeves, A. G. White, L. Lanco, P. Senellart, *Near-Optimal Single-Photon Sources in the Solid State*, Nature Photonics **10** (2016) (Cited on pages 73, 82, 89, and 91.)

[Son18] G. Son, S. Han, J. Park, K. Kwon, K. Yu, *High-Efficiency Broadband Light Coupling between Optical Fibers and Photonic Integrated Circuits*, Nanophotonics **7**, 1845–1864 (2018) (Cited on pages 54 and 97.)

[Ste06a] T. Steinmetz, Y. Colombe, D. Hunger, T. W. Hänsch, A. Balocchi, R. J. Warburton, J. Reichel, *Stable Fiber-Based Fabry-Pérot Cavity*, Applied Physics Letters **89**, 111 110 (2006) (Cited on page 91.)

[Ste06b] R. M. Stevenson, R. J. Young, P. See, D. G. Gevaux, K. Cooper, P. Atkinson, I. Farrer, D. A. Ritchie, A. J. Shields, *Magnetic-Field-Induced Reduction of the Exciton Polarization Splitting in InAs Quantum Dots*, Physical Review B **73**, 033 306 (2006) (Cited on pages 22 and 77.)

[Ste08a] A. Stemmann, Ch. Heyn, T. Köppen, T. Kipp, W. Hansen, *Local Droplet Etching of Nanoholes and Rings on GaAs and AlGaAs Surfaces*, Applied Physics Letters **93**, 123 108 (2008) (Cited on page 24.)

[Ste08b] R. M. Stevenson, A. J. Hudson, A. J. Bennett, R. J. Young, C. A. Nicoll, D. A. Ritchie, A. J. Shields, *Evolution of Entanglement Between Distinguishable Light States*, Physical Review Letters **101**, 170 501 (2008) (Cited on pages 22 and 46.)

[Ste15] P. Stepanov, A. Delga, N. Gregersen, E. Peinke, M. Munsch, J. Teissier, J. Mørk, M. Richard, J. Bleuse, J.-M. Gérard, J. Claudon, *Highly Directive and Gaussian Far-Field Emission from "Giant" Photonic Trumpets*, Applied Physics Letters **107**, 141 106 (2015) (Cited on page 86.)

[Str37] I. N. Stranski, L. Krastanow, *Zur Theorie der orientierten Ausscheidung von Ionenkristallen aufeinander*, Monatshefte für Chemie und verwandte Teile anderer Wissenschaften **71**, 351–364 (1937) (Cited on page 23.)

[Sue13] I. Suemune, H. Nakajima, X. Liu, S. Odashima, T. Asano, H. Iijima, J.-H. Huh, Y. Idutsu, H. Sasakura, H. Kumano, *Metal-Coated Semiconductor Nanostructures and Simulation of Photon Extraction and Coupling to Optical Fibers for a Solid-State Single-Photon Source*, Nanotechnology **24**, 455 205 (2013) (Cited on page 84.)

[Tak07] K. Takemoto, M. Takatsu, S. Hirose, N. Yokoyama, Y. Sakuma, T. Usuki, T. Miyazawa, Y. Arakawa, *An Optical Horn Structure for Single-Photon Source Using Quantum Dots at Telecommunication Wavelength*, Journal of Applied Physics **101**, 081 720 (2007) (Cited on page 84.)

[Tar04] A. I. Tartakovskii, M. N. Makhonin, I. R. Sellers, J. Cahill, A. D. Andreev, D. M. Whittaker, J.-P. R. Wells, A. M. Fox, D. J. Mowbray, M. S. Skolnick, K. M. Groom, M. J. Steer, H. Y. Liu, M. Hopkinson, *Effect of Thermal Annealing and Strain Engineering on the Fine Structure of Quantum Dot Excitons*, Physical Review B **70**, 193 303 (2004) (Cited on pages 22 and 76.)

[Tho16] A. Thoma, P. Schnauber, M. Gschrey, M. Seifried, J. Wolters, J.-H. Schulze, A. Strittmatter, S. Rodt, A. Carmele, A. Knorr, T. Heindel, S. Reitzenstein, *Exploring Dephasing of a Solid-State Quantum Emitter via Time- and Temperature-Dependent Hong-Ou-Mandel Experiments*, Physical Review Letters **116**, 033 601 (2016) (Cited on pages 65, 73, and 76.)

[Tom21] N. Tomm, A. Javadi, N. O. Antoniadis, D. Najer, M. C. Löbl, A. R. Korsch, R. Schott, S. R. Valentin, A. D. Wieck, A. Ludwig, R. J. Warburton, *A Bright and Fast Source of Coherent Single Photons*, Nature Nanotechnology **16**, 1–5 (2021) (Cited on pages 26, 43, 73, 91, and 102.)

[Ton15] P. Tonndorf, R. Schmidt, R. Schneider, J. Kern, M. Buscema, G. A. Steele, A. Castellanos-Gomez, H. S. J. van der Zant, S. Michaelis de Vasconcellos,

R. Bratschitsch, *Single-Photon Emission from Localized Excitons in an Atomically Thin Semiconductor*, Optica **2**, 347 (2015) (Cited on pages 30, 31, 60, and 65.)

[Ton17] P. Tonndorf, O. Del Pozo-Zamudio, N. Gruhler, J. Kern, R. Schmidt, A. I. Dmitriev, A. P. Bakhtinov, A. I. Tartakovskii, W. Pernice, S. Michaelis De Vasconcellos, R. Bratschitsch, *On-Chip Waveguide Coupling of a Layered Semiconductor Single-Photon Source*, Nano Letters **17**, 5446–5451 (2017) (Cited on page 94.)

[Tro14] R. Trotta, J. S. Wildmann, E. Zallo, O. G. Schmidt, A. Rastelli, *Highly Entangled Photons from Hybrid Piezoelectric-Semiconductor Quantum Dot Devices*, Nano Letters **14**, 3439–3444 (2014) (Cited on page 78.)

[Tro15] R. Trotta, J. Martín-Sánchez, I. Daruka, C. Ortix, A. Rastelli, *Energy-Tunable Sources of Entangled Photons: A Viable Concept for Solid-State-Based Quantum Relays*, Physical Review Letters **114**, 150 502 (2015) (Cited on pages 22 and 78.)

[Tro16] R. Trotta, J. Martín-Sánchez, J. S. Wildmann, G. Piredda, M. Reindl, C. Schimpf, E. Zallo, S. Stroj, J. Edlinger, A. Rastelli, *Wavelength-Tunable Sources of Entangled Photons Interfaced with Atomic Vapours*, Nature Communications **7**, 10 375 (2016) (Cited on page 77.)

[Usk01] A. V. Uskov, I. Magnusdottir, B. Tromborg, J. Mo/rk, R. Lang, *Line Broadening Caused by Coulomb Carrier–Carrier Correlations and Dynamics of Carrier Capture and Emission in Quantum Dots*, Applied Physics Letters **79**, 1679–1681 (2001) (Cited on page 40.)

[Vag07] A. Vagov, M. D. Croitoru, V. M. Axt, T. Kuhn, F. M. Peeters, *Nonmonotonic Field Dependence of Damping and Reappearance of Rabi Oscillations in Quantum Dots*, Physical Review Letters **98**, 227 403 (2007) (Cited on page 102.)

[van90] H. W. van Kesteren, E. C. Cosman, W. A. J. A. van der Poel, C. T. Foxon, *Fine Structure of Excitons in Type-II GaAs/AlAs Quantum Wells*, Physical Review B **41**, 5283–5292 (1990) (Cited on page 21.)

[Van23] L. Vannucci, N. Gregersen, *Highly Efficient and Indistinguishable Single-Photon Sources via Phonon-Decoupled Two-Color Excitation*, Physical Review B **107**, 195 306 (2023) (Cited on page 39.)

[Ver14] M. A. M. Versteegh, M. E. Reimer, K. D. Jöns, D. Dalacu, P. J. Poole, A. Gulinatti, A. Giudice, V. Zwiller, *Observation of Strongly Entangled*

Photon Pairs from a Nanowire Quantum Dot, Nature Communications **5**, 5298 (2014) (Cited on page 28.)

[Vog07] M. M. Vogel, S. M. Ulrich, R. Hafenbrak, P. Michler, L. Wang, A. Rastelli, O. G. Schmidt, *Influence of Lateral Electric Fields on Multiexcitonic Transitions and Fine Structure of Single Quantum Dots*, Applied Physics Letters **91**, 051 904 (2007) (Cited on page 82.)

[Wan07] Zh. M. Wang, B. L. Liang, K. A. Sablon, G. J. Salamo, *Nanoholes Fabricated by Self-Assembled Gallium Nanodrill on GaAs(100)*, Applied Physics Letters **90**, 113 120 (2007) (Cited on page 24.)

[Wan12a] J. Wang, M. Gong, G.-C. Guo, L. He, *Eliminating the Fine Structure Splitting of Excitons in Self-Assembled InAs/GaAs Quantum Dots via Combined Stresses*, Applied Physics Letters **101**, 063 114 (2012) (Cited on page 78.)

[Wan12b] X. Wang, W. Shi, H. Yun, S. Grist, N. A. F. Jaeger, L. Chrostowski, *Narrow-Band Waveguide Bragg Gratings on SOI Wafers with CMOS-compatible Fabrication Process*, Optics Express **20**, 15 547–15 558 (2012) (Cited on page 95.)

[Wan16] X.-L. Wang, L.-K. Chen, W. Li, H.-L. Huang, C. Liu, C. Chen, Y.-H. Luo, Z.-E. Su, D. Wu, Z.-D. Li, H. Lu, Y. Hu, X. Jiang, C.-Z. Peng, L. Li, N.-L. Liu, Y.-A. Chen, C.-Y. Lu, J.-W. Pan, *Experimental Ten-Photon Entanglement*, Physical Review Letters **117**, 210 502 (2016) (Cited on page 14.)

[Wan19a] H. Wang, Y.-M. He, T.-H. Chung, H. Hu, Y. Yu, S. Chen, X. Ding, M.-C. Chen, J. Qin, X. Yang, R.-Z. Liu, Z.-C. Duan, J.-P. Li, S. Gerhardt, K. Winkler, J. Jurkat, L.-J. Wang, N. Gregersen, Y.-H. Huo, Q. Dai, S. Yu, S. Höfling, C.-Y. Lu, J.-W. Pan, *Towards Optimal Single-Photon Sources from Polarized Microcavities*, Nature Photonics **13**, 770–775 (2019) (Cited on pages 89 and 90.)

[Wan19b] H. Wang, J. Qin, X. Ding, M.-C. Chen, S. Chen, X. You, Y.-M. He, X. Jiang, Z. Wang, L. You, J. J. Renema, S. Hoefling, C.-Y. Lu, J.-W. Pan, *Boson Sampling with 20 Input Photons in 60-Mode Interferometers at* 10^{14} *State Spaces*, Physical Review Letters **123**, 250 503 (2019) (Cited on page 90.)

[Wan20a] N. H. Wan, T.-J. Lu, K. C. Chen, M. P. Walsh, M. E. Trusheim, L. De Santis, E. A. Bersin, I. B. Harris, S. L. Mouradian, I. R. Christen, E. S. Bielejec, D. Englund, *Large-Scale Integration of Artificial Atoms in Hybrid Photonic Circuits*, Nature **583**, 226–231 (2020) (Cited on page 93.)

[Wan20b] J. Wang, F. Sciarrino, A. Laing, M. G. Thompson, *Integrated Photonic Quantum Technologies*, Nature Photonics **14**, 273–284 (2020) (Cited on page 92.)

[Wan21] B.-Y. Wang, T. Häyrynen, L. Vannucci, M. A. Jacobsen, C.-Y. Lu, N. Gregersen, *Suppression of Background Emission for Efficient Single-Photon Generation in Micropillar Cavities*, Applied Physics Letters **118**, 114 003 (2021) (Cited on page 90.)

[Wei14] Y.-J. Wei, Y.-M. He, M.-C. Chen, Y.-N. Hu, Y. He, D. Wu, C. Schneider, M. Kamp, S. Höfling, C.-Y. Lu, J.-W. Pan, *Deterministic and Robust Generation of Single Photons from a Single Quantum Dot with 99.5% Indistinguishability Using Adiabatic Rapid Passage*, Nano Letters **14**, 6515–6519 (2014) (Cited on page 39.)

[Wid18] A. Widhalm, A. Mukherjee, S. Krehs, N. Sharma, P. Kölling, A. Thiede, D. Reuter, J. Förstner, A. Zrenner, *Ultrafast Electric Phase Control of a Single Exciton Qubit*, Applied Physics Letters **112**, 111 105 (2018) (Cited on page 82.)

[Wid21] A. Widhalm, S. Krehs, D. Siebert, N. L. Sharma, T. Langer, B. Jonas, D. Reuter, A. Thiede, J. Förstner, A. Zrenner, *Optoelectronic Sampling of Ultrafast Electric Transients with Single Quantum Dots*, Applied Physics Letters **119**, 181 109 (2021) (Cited on page 82.)

[Wie17] J. Wierzbowski, J. Klein, F. Sigger, C. Straubinger, M. Kremser, T. Taniguchi, K. Watanabe, U. Wurstbauer, A. W. Holleitner, M. Kaniber, K. Müller, J. J. Finley, *Direct Exciton Emission from Atomically Thin Transition Metal Dichalcogenide Heterostructures near the Lifetime Limit*, Scientific Reports **7**, 12 383 (2017) (Cited on page 32.)

[Win17] R. Winik, D. Cogan, Y. Don, I. Schwartz, L. Gantz, E. R. Schmidgall, N. Livneh, R. Rapaport, E. Buks, D. Gershoni, *On-Demand Source of Maximally Entangled Photon Pairs Using the Biexciton-Exciton Radiative Cascade*, Physical Review B (2017) (Cited on page 22.)

[Woo00] E. Wooten, K. Kissa, A. Yi-Yan, E. Murphy, D. Lafaw, P. Hallemeier, D. Maack, D. Attanasio, D. Fritz, G. McBrien, D. Bossi, *A Review of Lithium Niobate Modulators for Fiber-Optic Communications Systems*, IEEE Journal of Selected Topics in Quantum Electronics **6**, 69–82 (2000) (Cited on page 96.)

[Wu99] Q. Wu, G. D. Feke, R. D. Grober, L. P. Ghislain, *Realization of Numerical Aperture 2.0 Using a Gallium Phosphide Solid Immersion Lens*, Applied Physics Letters **75**, 4064–4066 (1999) (Cited on page 86.)

[Wu00] Q. Wu, R. D. Grober, D. Gammon, D. S. Katzer, *Excitons, Biexcitons, and Electron-Hole Plasma in a Narrow 2.8-nm GaAs/$Al_xGa_{1-x}As$ Quantum Well*, Physical Review B **62**, 13 022–13 027 (2000) (Cited on page 86.)

[Yab87] E. Yablonovitch, *Inhibited Spontaneous Emission in Solid-State Physics and Electronics*, Physical Review Letters **58**, 2059–2062 (1987) (Cited on page 88.)

[Yin20] J. Yin, Y.-H. Li, S.-K. Liao, M. Yang, Y. Cao, L. Zhang, J.-G. Ren, W.-Q. Cai, W.-Y. Liu, S.-L. Li, R. Shu, Y.-M. Huang, L. Deng, L. Li, Q. Zhang, N.-L. Liu, Y.-A. Chen, C.-Y. Lu, X.-B. Wang, F. Xu, J.-Y. Wang, C.-Z. Peng, A. K. Ekert, J.-W. Pan, *Entanglement-Based Secure Quantum Cryptography over 1,120 Kilometres*, Nature **582**, 501–505 (2020) (Cited on pages 9, 14, and 99.)

[You15] Y. You, X.-X. Zhang, T. C. Berkelbach, M. S. Hybertsen, D. R. Reichman, T. F. Heinz, *Observation of Biexcitons in Monolayer WSe_2*, Nature Physics **11**, 477–481 (2015) (Cited on page 31.)

[You21] X. You, M.-Y. Zheng, S. Chen, R.-Z. Liu, J. Qin, M. C. Xu, Z. X. Ge, T. H. Chung, Y. K. Qiao, Y. F. Jiang, H. S. Zhong, M. C. Chen, H. Wang, Y. M. He, X. P. Xie, H. Li, L. X. You, C. Schneider, J. Yin, T. Y. Chen, M. Benyoucef, Y.-H. Huo, S. Hoefling, Q. Zhang, C.-Y. Lu, J.-W. Pan, *Quantum Interference between Independent Solid-State Single-Photon Sources Separated by 300 Km Fiber*, arXiv:2106.15545 (2021) (Cited on page 73.)

[Yu21] P. Yu, H. Qiu, T. Dai, R. Cheng, B. Lian, W. Li, H. Yu, J. Yang, *Ultracompact Channel Add-Drop Filter Based on Single Multimode Nanobeam Photonic Crystal Cavity*, Journal of Lightwave Technology **39**, 162–166 (2021) (Cited on page 95.)

[Zad16] I. E. Zadeh, A. W. Elshaari, K. D. Jöns, A. Fognini, D. Dalacu, P. J. Poole, M. E. Reimer, V. Zwiller, *Deterministic Integration of Single Photon Sources in Silicon Based Photonic Circuits*, Nano Letters **16**, 2289–2294 (2016) (Cited on pages 9, 28, and 94.)

[Zai00] A. M. Zaitsev, *Vibronic Spectra of Impurity-Related Optical Centers in Diamond*, Physical Review B **61**, 12 909–12 922 (2000) (Cited on page 15.)

[Zeu18] K. D. Zeuner, M. Paul, T. Lettner, C. Reuterskiöld Hedlund, L. Schweickert, S. Steinhauer, L. Yang, J. Zichi, M. Hammar, K. D. Jöns, V. Zwiller, *A Stable Wavelength-Tunable Triggered Source of Single Photons and Cascaded Photon Pairs at the Telecom C-band*, Applied Physics Letters **112**, 173 102 (2018) (Cited on page 79.)

[Zeu21] K. D. Zeuner, K. D. Jöns, L. Schweickert, C. R. Hedlund, C. N. Lobato, T. Lettner, K. Wang, S. Gyger, E. Schöll, S. Steinhauer, M. Hammar, V. Zwiller, *On-Demand Generation of Entangled Photon Pairs in the Telecom C-Band with InAs Quantum Dots*, ACS Photonics **8**, 2337–2344 (2021) (Cited on page 22.)

[Zha20] L. Zhai, M. C. Löbl, G. N. Nguyen, J. Ritzmann, A. Javadi, C. Spinnler, A. D. Wieck, A. Ludwig, R. J. Warburton, *Low-Noise GaAs Quantum Dots for Quantum Photonics*, Nature Communications **11**, 4745 (2020) (Cited on pages 26 and 101.)

[Zha22] L. Zhai, G. N. Nguyen, C. Spinnler, J. Ritzmann, M. C. Löbl, A. D. Wieck, A. Ludwig, A. Javadi, R. J. Warburton, *Quantum Interference of Identical Photons from Remote GaAs Quantum Dots*, Nature Nanotechnology **17**, 829–833 (2022) (Cited on pages 9, 16, 26, 73, 82, and 102.)

[Zhe19] Y. J. Zheng, Y. Chen, Y. L. Huang, P. K. Gogoi, M.-Y. Li, L.-J. Li, P. E. Trevisanutto, Q. Wang, S. J. Pennycook, A. T. S. Wee, S. Y. Quek, *Point Defects and Localized Excitons in 2D WSe_2*, ACS Nano **13**, 6050–6059 (2019) (Cited on page 31.)

[Zho20] H.-S. Zhong, H. Wang, Y.-H. Deng, M.-C. Chen, L.-C. Peng, Y.-H. Luo, J. Qin, D. Wu, X. Ding, Y. Hu, P. Hu, X.-Y. Yang, W.-J. Zhang, H. Li, Y. Li, X. Jiang, L. Gan, G. Yang, L. You, Z. Wang, L. Li, N.-L. Liu, C.-Y. Lu, J.-W. Pan, *Quantum Computational Advantage Using Photons*, Science **370**, 1460–1463 (2020) (Cited on page 7.)

[Zhu21] D. Zhu, L. Shao, M. Yu, R. Cheng, B. Desiatov, C. J. Xin, Y. Hu, J. Holzgrafe, S. Ghosh, A. Shams-Ansari, E. Puma, N. Sinclair, C. Reimer, M. Zhang, M. Lončar, *Integrated Photonics on Thin-Film Lithium Niobate*, Advances in Optics and Photonics **13**, 242–352 (2021) (Cited on page 92.)

[Zis17] D. Ziss, J. Martín-Sánchez, T. Lettner, A. Halilovic, G. Trevisi, R. Trotta, A. Rastelli, J. Stangl, *Comparison of Different Bonding Techniques for Efficient Strain Transfer Using Piezoelectric Actuators*, Journal of Applied Physics **121**, 135 303 (2017) (Cited on pages 78 and 85.)

[Zop19] M. Zopf, R. Keil, Y. Chen, J. Yang, D. Chen, F. Ding, O. G. Schmidt, *Entanglement Swapping with Semiconductor-Generated Photons Violates Bell's Inequality*, Physical Review Letters **123**, 160 502 (2019) (Cited on pages 26, 48, and 73.)

[Zou90] X. T. Zou, L. Mandel, *Photon-Antibunching and Sub-Poissonian Photon Statistics*, Physical Review A **41**, 475–476 (1990) (Cited on page 62.)

[Zre02] A. Zrenner, E. Beham, S. Stufler, F. Findeis, M. Bichler, G. Abstreiter, *Coherent Properties of a Two-Level System Based on a Quantum-Dot Photodiode*, Nature **418**, 612–614 (2002) (Cited on pages 43 and 81.)

[Zwi02] V. Zwiller, G. Björk, *Improved Light Extraction from Emitters in High Refractive Index Materials Using Solid Immersion Lenses*, Journal of Applied Physics **92**, 660–665 (2002) (Cited on page 87.)

Selbstständigkeitserklärung

Ich versichere, dass ich die Arbeit ohne fremde Hilfe und ohne Benutzung anderer als der angegebenen Quellen angefertigt habe und dass die Arbeit in gleicher oder ähnlicher Form noch keiner anderen Prüfungsbehörde vorgelegen hat und von dieser als Teil einer Prüfungsleistung angenommen worden ist. Alle Ausführungen, die wörtlich oder sinngemäß übernommen worden sind, sind als solche gekennzeichnet.

Ort, Datum

Unterschrift